CHEMICAL REVIEWS

pubs.acs.org/CR

Review

Operando Scanning Electrochemical Probe Microscopy during Electrocatalysis

Published as part of the Chemical Reviews virtual special issue "Operando and In Situ Studies in Catalysis and Electrocatalysis".

Carla Santana Santos,[#] Bright Nsolebna Jaato,[#] Ignacio Sanjuán,[#] Wolfgang Schuhmann,* and Corina Andronescu*

Cite This: *Chem. Rev.* 2023, 123, 4972−5019

Read Online

ACCESS | Metrics & More | Article Recommendations

ABSTRACT: Scanning electrochemical probe microscopy (SEPM) techniques can disclose the local electrochemical reactivity of interfaces in single-entity and sub-entity studies. Operando SEPM measurements consist of using a SEPM tip to investigate the performance of electrocatalysts, while the reactivity of the interface is simultaneously modulated. This powerful combination can correlate electrochemical activity with changes in surface properties, e.g., topography and structure, as well as provide insight into reaction mechanisms. The focus of this review is to reveal the recent progress in local SEPM measurements of the catalytic activity of a surface toward the reduction and evolution of O_2 and H_2 and electrochemical conversion of CO_2. The capabilities of SEPMs are showcased, and the possibility of coupling other techniques to SEPMs is presented. Emphasis is given to scanning electrochemical microscopy (SECM), scanning ion conductance microscopy (SICM), electrochemical scanning tunneling microscopy (EC-STM), and scanning electrochemical cell microscopy (SECCM).

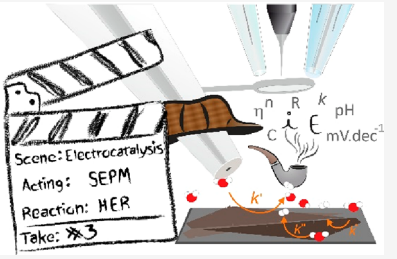

CONTENTS

Received: November 3, 2022
Published: March 27, 2023

https://doi.org/10.1021/acs.chemrev.2c00766
Chem. Rev. 2023, 123, 4972−5019

1. INTRODUCTION

Today, electrocatalysis plays a key role in achieving defossilization in minimizing carbon emission and hence in supporting the ambitious goals necessary to fight climate change. The electrochemical conversion of abundant small molecules like H_2O, N_2, O_2, and CO_2 into chemical feedstocks or energy carriers using renewable electricity is considered a promising approach to the global supply of sustainable energy.[1−6] Consequently, the development of (electro)-catalysts that can maximize the rates of reaction and minimize the overpotentials of these conversions is crucial for the large-scale industrialization of this green technology.[7,8] To enable a rational design of electrocatalysts, an in-depth understanding of the complex chemical occurrences at the electrochemical interface during a reaction (e.g., adsorption and desorption, charge and electron transfer, solvation and desolvation, and electrostatic interactions) is of high importance and the basis for engineering and optimizing electrocatalytic systems.[2,7,9−11]

A holistic study of the interfacial processes demands measuring kinetic and thermodynamic parameters.[12] One strategy to enhance the selectivity and to investigate the interfacial electrode−electrolyte composition is to couple methods for real-time analysis, enabling so-called operando measurements. The goal of most operando measurements is to gain in-depth insight into the mechanism of a reaction. To this end, working under operando conditions has been proposed as a method that bridges experimental gaps in measurement conditions between instrumental requirements and realistic electrocatalytic reactions.[13] This approach combines techniques for simultaneously recording independent signals, where one technique is employed as an actuator for altering the interface properties (e.g., structure, morphology, activity, mechanism), while a second technique acts as a spectator to monitor the resulting changes.[14] General aspects of operando measurements are illustrated in Scheme 1. As such, changes in chemical or structural compositions are typically monitored using spectroscopic methods while controlling the reactivity of the surface with e.g., electrochemical methods. Most applied operando characterization methods including transmission electron microscopy (TEM), X-ray absorption spectroscopy (XAS), X-ray photoelectron spectroscopy (XPS), X-ray diffraction (XRD), Raman spectroscopy, infrared (IR) spectroscopy, mass spectroscopy, online inductively coupled plasma mass spectrometry (ICP-MS), among others, have been developed to study electrocatalysts under realistic reaction conditions.[15−17] However, each approach shows its advantages and limitations. For instance, operando XAS is sensitive to the local coordination structure and oxidation state of elements in the catalysts, but it is a bulk technique failing to reflect detailed information on reactions occurring at the catalyst surface.[18] While operando XRD has been well-developed, it is often challenging to detect amorphous structures at the surface of a reconstructed OER electrocatalyst.[19] Considering the advantages and disadvantages, local investigation of exclusively the catalytically active interface is one important key to obtain a complete picture of the reaction. In this regard, scanning electrochemical probe microscopy (SEPM) has been largely explored in electrocatalysis to shed light on the mechanism of a catalytic reaction and on the activity of the catalyst.[13,18,20] Besides the advantage of its inherent high lateral resolution, the use of micro-nano-electrochemistry in SEPM studies of electrocatalytic activity circumvents the limiting mass transport condition of conventional/traditional techniques due to the hemispherical diffusion conditions.[10,21−23]

Scheme 1. Diagram Exemplifying a General Operando Measurement Which Involves a Spectator and an Actuator Method Performed Simultaneously, with the Spectator Response Depending on the Actuator Modulation in Real-Time

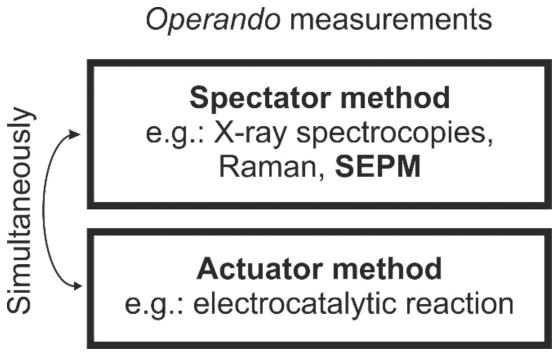

Although "operando" is not a typical wording used in the majority of SEPM investigations, the combination of measurements to invoke kinetics changes on a surface while monitoring the subsequent effect is a common aspect in many in situ SEPM analyses. Hence, to clarify this, we here refer to operando SEPM for SEPM experiments when simultaneously: (i) an actuator measurement is applied to tailor changes at the investigated surface, and (ii) the SEPM tip is employed as a spectator to monitor local changes at the investigated surface by measuring processes directly or indirectly related to the surface reaction. In the general case of operando SEPM, two electrochemical reactions are controlled independently and simultaneously, where the reaction of interest is invoked at the sample surface and the SEPM response depends in real-time on the modulation of the response at the sample surface. In contrast with macroscopic techniques, the use of operando SEPM can help to disclose the interfacial dynamics that influence electrode kinetics and reaction mechanisms. Moreover, the correlation of intrinsic electrochemical reactivity with the physical and chemical properties of an electrocatalyst is possible by SEPM mapping or coupling with other techniques.

The literature is replete with review papers on applications of SEPM for imaging electrochemical processes at interfaces locally.[24−26] Hence, the focus of this review is on the advances made thus far using SEPM techniques in the field of electrocatalysis however exclusively concerning operando measurements, i.e., the simultaneous readout of an actuator process and a spectator process usually at the tip of the SEPM method. The discussed SEPM methods comprise scanning electrochemical microscopy (SECM), scanning ion conductance microscopy (SICM), scanning electrochemical cell microscopy (SECCM), and electrochemical scanning tunneling microscopy (EC-STM).

https://doi.org/10.1021/acs.chemrev.2c00766
Chem. Rev. 2023, 123, 4972−5019

Table 1. General Aspects of Scanning Electrochemical Probe Microscopy (More Details Are Discussed in Each SEPM Technique Section)

SEPM (resolution)	set point for the feedback position	main application	main limitation	operation modes and hybrid techniques
SECM[54,78] (sub-μm)	The set point is typically achieved at the distance range where the diffusion layer (faradaic process) or electrical double layer of the tip is disturbed physically or chemically by the investigated surface. The range of the set point distance is wide, and the tip current depends on electrochemical processes and the difference in surface topography.	SECM is applied for the investigation of local electron-transfer processes at interfaces (liquid/solid, liquid/gas, liquid/liquid). It is the most adaptable SEPM technique covered in this review. Because the sample can be independently polarized, investigation with good chemical specificity is achievable.	Imaging is typically done at a constant distance. However, the distance between the tip and the sample can vary with changes in the sample topography. The user should use a hybrid SECM technique to decouple the topographic effect from electroactivity. The complexity associated with the fabrication of smaller tips limits the resolution achievable in SECM measurements. Besides that, SECM tips of few nm was already reported (>3 nm).[79,80] Hybrid techniques should be coupled to deconvolute the topographic contribution on the tip response.	The option to use a large variability of different SECM tips such as modified electrodes surfaces, potentiometric tips, or ion-selective electrodes makes SECM a versatile tool. Modes: feedback (FB), tip collector/substrate generator (TC-SG) and substrate collector/tip generator (SC-TG), redox competition (RC), AC-SECM (or local EIS), direct mode, and surface interrogation (SI). Hybrid techniques: SECM/SICM, SECM/Raman, SECM/SPR, SECM/FTIR, SECM/AFM, SECM/EQCM, SECM/SVET, SPECM.
SICM[73] (few nm)	The set point is defined by a distance at which the ion current is disturbed by the underlying surface. The ion current is caused by the movement of ions through the pipette aperture.	SICM is used to acquire topographical images of soft surfaces such as biological samples. In contrast to STM, the tip never touches the sample surface.	SICM has low chemical specificity, which can be rectified by coupling the SICM to other SEPM techniques like SECM (SECM-SICM) or by using ion current rectification (ICR).	Modes: DC and AC (oscillating) modes, and ICR. Hybrid techniques: SICM/SECM, SICM/AFM, SICM/potentiometric sensor.
EC-STM[76,81] (sub-nm, atomic resolution)	The tunneling current is used as set point, and the feedback signal is reached when the sharp tip is positioned at some atomic distances to the sample surface. A potential is applied between the tip and sample surface to generate the tunneling current.	EC-STM is the technique with the highest resolution (atomic resolution) and is used to simultaneously probe the electrochemical activity and topography of surfaces.	The main limitations are the inability to follow rough surfaces, prolonged scanning times, and the restriction to cover large areas.	Modes: constant current and constant height. Hybrid techniques: EC-STM/SECM, EC-STM/DEMS
SECCM[74,82] (few nm)	SECCM pipette confines the electrochemical cell size to the contact of the hanging droplet with the surface. The set point is reached when the meniscus of the droplet touches the surface. Typically, a potential is applied between the surface and the QRCE inserted inside the pipette.	SECCM is used to record both topographical and electrochemical activity, at the same time. It exhibits high lateral resolution and yields high-throughput information.	Its is hard to control the integrity of the droplet at the SECCM tip. Additionally, because the set point is defined when the droplet touches the surface, and experimentation begins when the surface is polarized, coupling with other techniques is limited.	Modes: SECCM is a direct method to probe the surface because the desired electrochemical reaction occurs at the sample surface. Single- or double-barrel pipettes are used to interrogate the surface. Hybrid techniques: SECCM/optical methods.

https://doi.org/10.1021/acs.chemrev.2c00766
Chem. Rev. 2023, 123, 4972−5019

Scheme 2. Typical Electrochemical Cell Configuration for the Operation of SEPM Techniques[a]

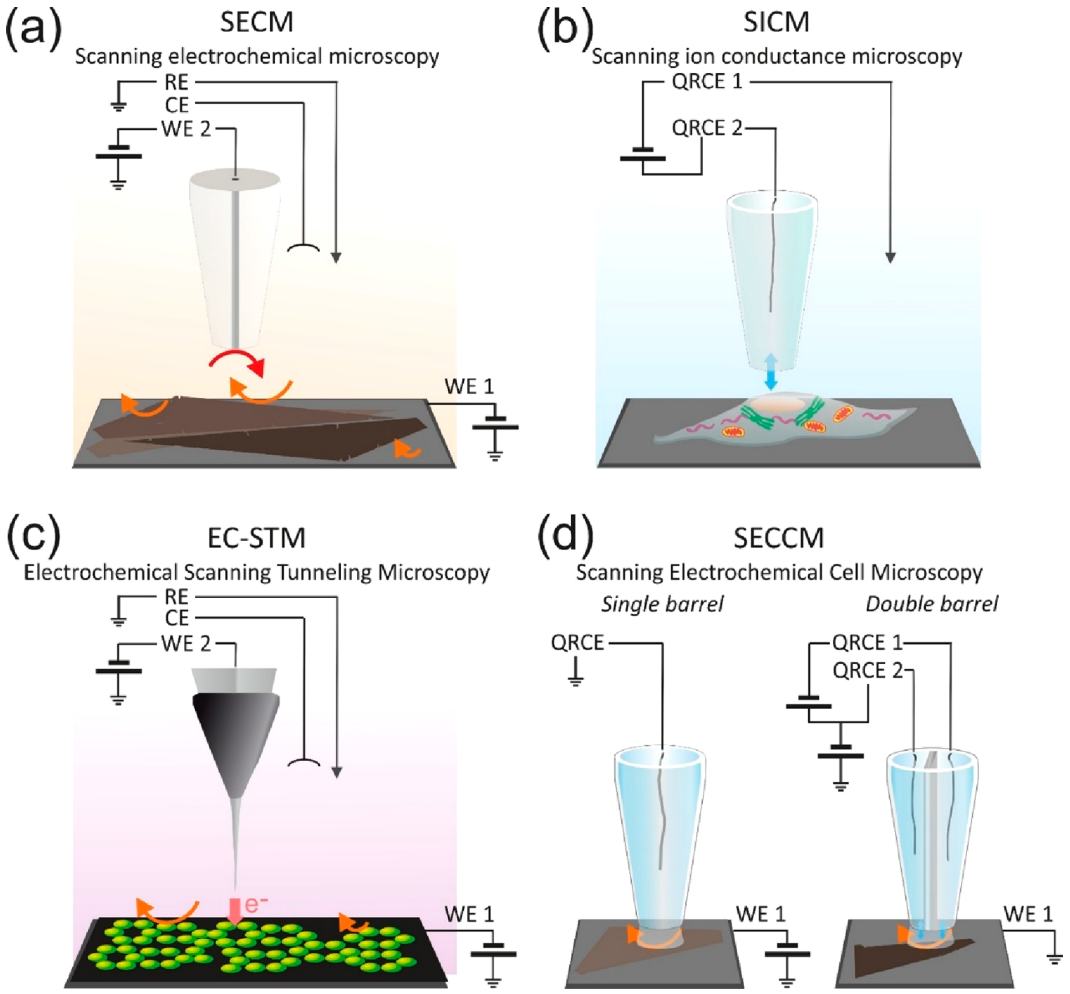

[a]WE, working electrode; RE, reference electrode; CE, counter electrode; QRCE, quasi reference-counter electrode; colored curved arrows indicate an electron-transfer reaction recorded at the WE 1 (orange arrows) and WE 2 (red arrows). (a) Four-electrode SECM cell, where a disk-shaped micro/nanoelectrode is the SECM tip (WE 2). An electron-transfer reaction at the tip generates the SECM tip current, which is modulated by the underlying surface (WE 1). (b) SICM two-electrode configuration, in which one QRCE is inserted inside the filled nanopipette (SICM tip), while the other QRCE is immersed in the sample solution. A potential is applied between the QRCEs, and the SICM tip current is related to the ion flux through the aperture of the capillary. (c) A sharp EC-STM tip is employed as working electrode (WE 2) in a four-electrode cell configuration. The tunneling current is the set point for the EC-STM, due to the electron-transfer tunneling between the surface (WE 1) and the tip. (d) In the case of SECCM, the electron-transfer reaction occurs directly on the investigated surface (WE 1). A single-barrel or double-barrel pipette is filled with the electrolyte, and a QRCE is inserted in each channel. The SECCM tip droplet confines the electrochemical cell. In the double-barrel configuration, a potential is applied between the two QRCEs to achieve the set point, while the sample potential is applied between the sample and the QRCEs.

The review is organized in two sections considering the preknowledge of potentially interested readers. In the first section, each SEPM method is presented with respect to principles and modes of operation as well as potential applicability. This is complemented by a description of the prerequisites for operando SEPM measurement conditions with examples to enable the reader to appreciate the potential and current limitations of each technique. Moreover, the diversity of the applicability of the different SEPM techniques is covered to provide an overview of the limitations of each technique for the evaluation of interfacial processes. The second section focuses on the progress in operando SEPM for electrocatalysis. Measurements as applied to monitor electrocatalytic processes such as the oxygen reduction reaction (ORR), the hydrogen evolution reaction (HER), the oxygen evolution reaction (OER), and the CO_2 reduction reaction (CO_2RR) are comprehensively discussed.

2. BACKSTAGE: PRINCIPLES AND APPLICABILITY OF OPERANDO SEPM

SEPM represents a family of techniques that use an electrochemical tip or probe to investigate the local properties of an interface.[27] The tip interacts with the surface under investigation and physical quantities such as current or potential are determined. SEPM has been employed for electrochemical studies in corrosion,[28−31] single-cells,[32−41] batteries,[42−48] bioelectrocatalysis,[49−51] and electrocatalysis.[52,53] Generally, the working principle of all SEPM techniques hinges on the precise positioning of a localized probe (the SEPM tip) to interact with a surface under interrogation, allowing one to image and manipulate the surface with submicron, nanometer and/or atomic scale precision.[54−56] To this end, the SEPM tip plays a central role in SEPM measurements because its properties (size and shape) define the resolution and applicability of the particular

https://doi.org/10.1021/acs.chemrev.2c00766
Chem. Rev. 2023, 123, 4972−5019

SEPM technique.[54] Note, millimeter resolution and non-scanning techniques such as the scanning vibrating electrode technique (SVET)[57−59] and single nanoparticle electrochemical impact (SNEI) measurements,[60−63] which, although powerful tools used to investigate corrosion and electron-transfer processes, are not included in this review.

SEPM tips can be divided into solid and pipette-based probes. For instance, tips used for EC-STM measurements consist of a very-sharp metal or an alloy that allows resolutions down to the atomic level.[64−67] Likewise, SECM tips are solid-based and predominantly made of platinum, gold, and carbon-based disk-shaped electrodes allowing resolutions in the micrometer to nanometer range. Surface-modified micro/nanoelectrodes are also employed in SECM to increase selectivity during amperometric or potentiometric measurements.[26,54,68−72] Electrolyte-filled pipettes are employed in SICM and SECCM in which case the resolution (which reaches the nanometer range) depends on the aperture of the pipette.[73,74] In coupled SEPM techniques (e.g., SECM-SICM), solid- and pipette-based probes are merged into a single tip.[75] Besides the SEPM tip, the positioning unit which enables precise control of tip movement in the *x*-, *y*-, and *z*-directions relative to the investigated surface is of high importance.[54,68,76] The positioned tip monitors signals whose magnitude corresponds to the tip-to-surface distance, which need to be compared with a reference value, known as the set point or feedback signal. For image generation the set point needs to be established, and as the tip scans the surface of interest, a feedback loop compares the measured signals (i.e., faradaic or capacitive signals for SECM and SECCM, ion current for SICM, and tunneling current for EC-STM) with the set point.[54,68,73−77]

The main goal is to demonstrate the general principles and the limitations associated with the use of operando SEPM. Table 1 and Scheme 2 resume the general aspects and cell configurations of each SEPM technique discussed in this review. The intention is to present a snapshot of the general principles and to give the reader an overview of the capability of each SEPM technique for performing in situ measurements as well as the possibility of simultaneously coupling independent techniques to achieve operando conditions. The applicability of operando SEPM is exemplified also with studies not addressing specifically electrocatalysis to give the reader a general overview of principle operando capabilities, while examples of operando SEPM electrocatalysis are covered in the next section.

2.1. Scanning Electrochemical Microscopy

SECM was first reported in 1989[54,78] and has since become a robust and largely explored SEPM technique for electrochemical investigations. The SECM technique uses a micro/nanoelectrode as a probe, typically a metallic disk-shaped electrode encased in an insulating body. Scheme 2a shows a SECM electrochemical cell in which WE1 and WE2 are controlled independently. The principle of SECM is to register the electrochemical conversion of free-diffusing species under diffusion-limited conditions, such that the current recorded at the tip during the lateral and vertical interrogation of the interfacial region is invariable with time. The SECM tip current results either from a faradaic process or a non-faradaic process that occurs at the tip surface and is dependent on the distance between the tip and the sample.[54] Thus, one of the limitations of SECM is that when the tip scans laterally (*x*- and *y*-directions) over the surface at a constant height without variations in the *z*-position of the tip, the recorded current contains contributions from the sample topography. Deconvolution of these two contributions is the primary motivation for coupling SECM with other techniques to independently adjust the working distance and obtain a constant distance mapping condition. The tip−sample interaction condition occurs when the polarized microelectrode is positioned very close to the sample surface such that the diffusion layer of the tip is modulated by the presence of the sample. The sample, on the one hand, acts as a physical barrier to the diffusion of species to the tip. Furthermore, the sample can locally perturb the composition/flux of species reaching the tip by consuming or releasing material. Under this condition, the sample surface can be unbiased or polarized (WE2) simultaneously with the tip, ensuring that the operando condition is intrinsically achieved as the tip and surface are modulated independently. The analytical aspects of SECM,[83] its versatility for nanoscale studies,[84] applications in heterogeneous electron transfer,[23,26] and biological processes have been reviewed.[85,86] The operation of SECM modes depends on the electrochemical processes occurring at the tip and the sample surface. In the ensuing sections, the main SECM modes and hybrid techniques are described. We also highlight the conditions that qualify a particular mode as an operando measurement, where the SECM tip acts as a spectator while the WE1 is employed as an actuator (Scheme 1).

2.1.1. Feedback SECM Mode. The feedback mode (FB) is the most commonly used operational mode of SECM, where due to the feedback effect, the sample does not necessarily require polarization to enable the local biased tip-to-sample electron-transfer kinetics.[68,87] The tip current depends on faradaic processes involving electroactive species like freely diffusing reversible redox couples (redox mediators) in the electrolyte. In the bulk solution, when a disk-shaped microelectrode is polarized at a potential, at which the mass transport is limited by diffusion of the species, then the current follows the equation for hemispherical diffusion:[54]

$$i_{\text{bulk}} = 4nFDCr \tag{1}$$

where i_{bulk} is the measured current at the tip at positions far from the sample surface, n is the number of transferred electrons involved in the electrochemical reaction, F is the Faraday constant ($\text{s}\cdot\text{A}\cdot\text{mol}^{-1}$), D is the diffusion coefficient of the electroactive species ($\text{m}^2\cdot\text{s}^{-1}$), C is the concentration of the electroactive species in the bulk ($\text{mol}\cdot\text{m}^{-3}$), and r is the radius of the electroactive surface of probe/tip/microelectrode (m).

When the SECM tip is moved toward the sample surface, the species generated at the tip during the electrochemical process diffuse to the surface of the sample. Once the species of the reversible redox couple are confined within a thin layer, a small overpotential is generated, sufficiently high to facilitate electrochemical reactions at the surface of a conductive sample. This phenomenon is called positive feedback, as countless cycles occur between the tip and the conductive surface, leading to a higher SECM tip current in comparison to the value measured at far working distance.[54,78] The extension of the feedback effect depends on the kinetics of the electrochemical conversion on the conductive surface and can be calculated.[68,88,89] When the substrate is an insulator or the tip reaction yields a non-electroactive species, the SECM tip current decreases as it approaches the substrate, because the diffusion of the electroactive species is hindered by the

https://doi.org/10.1021/acs.chemrev.2c00766
Chem. Rev. 2023, 123, 4972−5019

insulating walls of the SECM tip and the sample surface. This effect is known as hindered diffusion or negative feedback and is entirely dependent on the size of the microelectrode.[54,90] The negative feedback is used to map topographical features, while the positive feedback mode is used to assess the electron-transfer ability of the sample surface.[54]

As the FB mode does not necessarily require that the sample is polarized, an external or additional method/technique must be incorporated simultaneously to conduct operando measurements. As an example, operando FB mode was used to follow the growth of the insulating character of the solid-electrolyte interphase on battery materials.[91] The SECM tip was positioned at a working distance using the feedback effect on an anatase TiO_2 paste, and the oxidation of ferrocene was performed at the tip while the potential at the battery surface was scanned to invoke the formation of the solid-electrolyte interphase. The potential at which the electrochemical processes on the TiO_2 paste occurred to generate the insulating film, were monitored by the drastic changes of the feedback current at the tip.[91]

2.1.2. Generation−Collection SECM Modes: Substrate Generation−Tip Collection and Tip Generation/Substrate Collection Modes. The generation−collection (G-C)[87,92,93] mode of SECM is carried out in a four-electrode electrochemical cell or with two separate electrochemical cells. The principle of the G-C mode relies on the generation of an electroactive species at a biased substrate (or tip), which diffuses and gets detected or collected electrochemically by a simultaneously polarized tip (or substrate). Thus, the G-C mode is, in principle, considered operando, even though the SECM community rarely used this term. During the substrate generation−tip collection (SG-TC) mode experiments, the SECM tip is polarized at a defined potential to collect substrate-generated species while the potential at the substrate is scanned.[93]

The SG-TC mode was explored extensively to map the local electron transfer at electrode surfaces.[94,95] Interfacial processes during the OER on irradiated semiconductor materials for photoelectrochemical cell applications have been studied via the SG-TC mode to screen n-type W-doped $BiVO_4$, and to determine the effective heterogeneous electron-transfer constant of semiconductor materials.[96,97] Moreover, the SECM tip can also be employed as a local generator in the TG-SC mode, and most of the species generated at the small tip are collected by the polarized sample surface. Under this condition, the collection efficiency is about 1, which is a difficult value to be reached with conventional rotating ring-disk electrodes.[98−102] The SG-TC-SECM mode has also been used to monitor the activity of biological samples like cells and enzymes,[103,104] although the increased complexity associated with modulating the activity of the biological samples makes it difficult to meet the operando condition.

2.1.3. Redox Competition SECM Mode. Although previously reported in the context of numerical simulation at a heptode SECM tip,[105] the feasibility of the RC-SECM mode was first employed experimentally to locally visualize the catalytic activity of surface-confined noble metal catalysts toward the ORR.[106] In the RC mode both the SECM tip and the substrate compete for the same electroactive species present in the electrolyte.[106−109] The RC mode, like the two G-C modes, is an "intrinsic" operando measurement because two independent signals are employed to modulate the reaction on the substrate and the SECM tip simultaneously. The RC mode was used to study corrosion processes,[110,111] enzyme activity,[112−114] ORR activity of catalysts,[115−117] and to evaluate the rates of respiration in cells and biological entities.[36−38,118−120] In a particular study, local oxygen consumption rates calculated by SECM measurements via the RC mode showed that the reproductive organ of *C. elegans* was responsible for the observed oxygen consumption, indicating the high energy demand of reproduction for adult worms.[37] A similar approach was used to follow oxygen consumption due to mitochondrial activity.[38] Specific mitochondria inhibitors were added to the electrolyte containing the cells and the measured SECM tip current showed a variation in the oxygen consumption rate by the cells.

2.1.4. AC-SECM or Local Electrochemical Impedance Spectroscopy (LEIS). In the AC-SECM mode, a sine potential wave (AC) is applied to the SECM tip enabling the acquisition of localized electrochemical impedance spectra as a function of spatial position.[121−125] The tip response in the AC-SECM mode also depends on the working distance between the electrode and the sample surface. During AC-SECM, when the tip is brought closer to an insulating surface, the electric field lines are blocked by the tip leading to a significant increase in the measured impedance. Conversely, when the tip is moved toward a conducting surface, the field lines can pass through the conducting sample to the counter electrode thereby reducing the measured impedance. The observed effect depends on the properties of the conducting surface and the resistance of the solution. In the case of low salt concentration, the pathway of lowest resistance for charge transfer is through the conducting surface, especially at high frequencies. Consequently, the measured impedance at the tip decreases as a function of the working distance. In any case, adequate fitting to equivalent circuits is necessary to extract quantitative and physically meaningful information. An advantage of the AC-SECM is that, unlike the FB mode, no redox mediator is required to map the topography of the sample.[123,126] Hence, AC-SECM measurements can be used to decouple topographical effects during kinetic evaluations of surfaces.

2.1.5. Surface Interrogation SECM Mode and Direct Mode of SECM. The surface interrogation (SI) mode was first described in 2008 to quantify surface-adsorbed species at the substrate electrode.[127] The technique involves first the generation of a surface intermediate on the substrate by biasing the substrate, followed by a switch of the substrate to open circuit potential and finally the polarization of the tip to generate a redox pair which then reacts with the surface-adsorbed species.[128−130] The SECM tip follows a positive feedback effect due to the diverse redox cycles occurring between the tip-generated species and the adsorbed species. The SI-SECM mode can quantify an interfacial modification when the redox cycle is complete or when the depletion of adsorbed species on the sample surface occurs.[131] The SI-SECM mode was applied to quantify adsorbed CO,[132,133] hydroxyl radicals during water oxidation,[134,135] and other molecules.[136−138]

The direct mode of SECM is used to pattern surfaces and also acquire topographic images.[139−142] In this mode, the SECM tip works as a counter electrode while the substrate is employed as the working electrode. The reaction taking place at the tip locally modifies the sample surface, making the direct mode an ideal strategy for constructing microstructures on films or surfaces.[143−145] To the best of our knowledge, no

https://doi.org/10.1021/acs.chemrev.2c00766
Chem. Rev. 2023, 123, 4972−5019

operando studies with SI and direct SECM modes have been reported.

2.1.6. SECM Hybrid Techniques. SECM is a dynamic technique and coupling it to other techniques allows the acquisition of a plethora of information in a single experiment. Complementary SECM techniques can be applied to correlate an additional property (structural or chemical information) to the electrochemical property. Contrary to the use of several techniques in sequence to analyze the interface, we focused here on the coupling of a technique with SECM to perform operando measurements. As explained before, SECM is normally coupled with other independent methods to deconvolute the topographic contribution of the SECM tip response during mapping. AFM, SICM, and shear force positioning have been coupled with SECM to overcome this bottleneck.[75,146−166] Such approaches have been essential in the study of biological materials.[167−169] Strategies to deconvolute SECM tip topographic contribution from the electrochemical activity are still hot topics under discussion.[170,171] Although the clear advantage of coupling methods to deconvolute the topographic contribution, the independent additional method is mostly performed in a sequence of measurements with the SECM and not simultaneously, therefore the measurement is not intrinsically an operando method. The coupling of SECM with potentiometric sensors and double-barrel electrodes, SECM tips have been employed to control the tip positioning while mapping local information with the tip. Local information such as pH, magnesium ions, potassium ions or metal ions concentrations has been mapped using this approach.[172−174] Recently, a multibarrel SECM tip containing a pH sensor and a Mg^{2+} ion-selective electrode was employed to map the spontaneous corrosion process at the interface of a magnesium alloy.[175]

A combination of SECM and quartz crystal microbalance (EQCM) was proposed as an operando approach to correlate the changes in mass with the local electrochemical activity.[176−179] Copper ions were monitored using the SECM tip positioned in the vicinity of an aluminum alloy interface, while a cyclic voltammogram was performed at the substrate and the EQCM results were correlated to the corrosion rate.[180] A similar strategy was adopted to monitor the evolution of iron pitting corrosion.[181,182]

SECM was also coupled to Raman spectroscopy to analyze the changes in chemical properties while modulating electrochemical processes on the surface.[183−186] The operando SECM-Raman analysis was recently applied to interrogate a self-assembled monolayer with high structural-pH sensitivity.[185] The local pH was modulated by the HER on the SECM tip and the Raman analysis registered changes of the protonated state of a modified self-assembled monolayer on the surface. Additionally, SECM was combined with optical techniques, such as surface plasmon resonance (SPR)[187−189] and infrared,[190,191] fluorescence, and chemiluminescence spectroscopies[192−195] to study molecular changes on surfaces, electrodeposition processes, or film thickness changes.

Strategies to modify the tip functionality were also used to derive information with an enhancement in selectivity. In scanning photoelectrochemical microscopy (SPECM) a focalized light source is coupled to locally illuminate the SECM analysis.[196−201] For instance, photocurrents of an irradiated $BiVO_4$/FTO semiconductor surface were monitored while the SECM tip measured the local photoelectrocatalytic activity through the oxygen evolved from the semiconductor surface.[196]

The above discussions show how SECM/hybrid techniques can be employed to correlate interfacial processes to local electroactivity.

2.2. Scanning Ion Conductance Microscopy (SICM)

SICM was introduced by Hansma and colleagues in 1989, as a high-resolution and noncontact imaging SEPM technique for the investigation of samples.[73] The technique uses an electrolyte-filled nanopipette as a scanning probe and relies on the flow of ionic current between an electrode inside the nanopipette and a second electrode immersed in the bulk solution or electrochemical cell to create a surface-sensitive feedback signal. Topographical information on the sample is obtained by scanning the nanopipette or probe over the interface in the *x*- and *y*-directions. Fluctuations in the flow of ionic current are used to monitor the position of the tip relative to the substrate surface.[73]

During operation, a DC or an AC potential is applied between two wires: one wire, typically Ag/AgCl, is inserted into the SICM pipette and the other wire is immersed into the electrolyte of the electrochemical cell outside of the nanopipette channel. Scheme 2b illustrates the SICM tip and the two wires as QRCE, with the blue arrow representing the ions movement and no electron-transfer reaction occurring at the pipette aperture. The resulting current is caused by the movement of ions through the SICM tip aperture, which serves as a resistor to the ionic flux.[202] Once the pipette is moved toward a surface, the ion flux is physically blocked when the aperture is some nanometers close to the substrate. At this point, the monitored ion current decreases due to the increased resistance and this variation defines the set point for controlling the SICM tip position.[203,204] SICM topographic maps are obtained by correcting the tip height (*z*-direction) to reach the set point. In contrast to SECM microelectrodes, the simple SICM pipette fabrication allows the preparation of nanometer-sized tips. For this reason, SICM is a high-resolution technique, capable of measuring the topography of nonconductive surfaces,[205] and mapping activities of soft samples such as cells,[205−210] in contrast to AFM.[211]

2.2.1. SICM Modes of Operation. In addition to the DC or AC modulation of the ion flux into the SICM tip strategies are employed to allow imaging beyond highly resolved topographic maps. The capability to map the topography of highly ordered porous silicon functionalized with lipid membranes was shown using noncontact DC-SICM including the manipulation of the soft membranes.[212] Due to drifts encountered using the DC-SICM current response, the positioning stability can be increased by employing AC-SICM. During AC modulation, the set point is reached when a small variation of the tip response is detected. Typically the AC modulation is imposed using an AC potential signal or a physical tip vibration in the vertical direction.[203,213,214] The variation in AC is coupled to topographic acquisition while the variation of the DC ion current is related to the charge transfer property of the surface. As an example, vibrations in the vertical direction were used to record topographic images of pores on polymeric membranes while the DC ion current was correlated to the transport of KCl through the pores.[215] Instrumental advances have made it possible to carry out electrochemical impedance experiments to image the local capacitance and topography of a gold nanoparticle.[216]

https://doi.org/10.1021/acs.chemrev.2c00766
Chem. Rev. 2023, 123, 4972−5019

Advances in DC-SICM and pulse-mode SICM have been proposed as routes to improve the SICM mapping and applied to monitor volume changes in cells.[217,218] In parallel, modified nanopipettes were developed to record the ion current rectification (ICR).[219−223] With this approach, the SICM sensitivity is increased due to specific ion interaction with the modified aperture.[219−223] The correlation of changes in the ion current of functionalized nanopipette pores to the presence of ions was demonstrated by measuring variations in ICR due to a KCl concentration gradient[224] and at different pH conditions.[225] Moreover, a modified lipid bilayer SICM pore was reported and used to map the diffusion of β-cyclodextrin through a glass micropore.[226] Furthermore, the possibility to set up an SICM experiment in a configuration similar to the patch-clamp technique paves the way for SICM to be largely explored in the biophysical analysis of cells.[227−231] Recently, SICM tips were inserted into a macrophage cell, and intracellular events such as nanoparticles and vesicle collisions were monitored.[232]

Although the high capability of SICM to record topography with high resolution is widely explored, the correlation of electrochemical activity to surface properties is complex using SICM alone. A strategy adopted to overcome this is to conduct the measurement in a low ionic strength electrolyte, allowing the double layer of the SICM tip to interact with the charged substrate.[220,233] This way, the SICM tip response can then be correlated to surface reactivity.

The use of surface charge mapping was demonstrated on living cells,[234−238] films,[239,240] and electrode surfaces.[241−243] Recently, operando SICM was employed to simultaneously map the surface charge, reactivity and topography of a carbon fiber microelectrode surface.[242] In this operando SICM case, the SICM tip is employed as the spectator while the surface activity is modulated by an electrochemical method (Scheme 1). Moreover, Unwin's group showed that electroosmotic flow controls the flux of uncharged molecules within the SICM tip, in contrast to the flux of charged molecules, which is easily controlled through the migration effect. The role of a biased underlying surface on the ion current was also interrogated and the mass transport and flow rate of species were quantified using simulation tools. This work showed that besides voltage, pipette wall charge, and working distance, the ion flux through the SICM tip also depends on the substrate surface charge.[242] Besides the richness on the information on charge mapping, the exploration of using operando SICM during modulation of the surface was not extended to any electrocatalysis study.

2.2.2. SICM Hybrid Techniques. As pointed out before, SICM is a great tool to provide stable and great control of the tip positioning. Due to this unique functionality, SICM was coupled with other techniques like SECM, as this compensates for the lack of selectivity of the SICM measurements, and also serves as a strategy to deconvolute the topographic contributions from the SECM tip response.[75,157,244] As discussed in the SECM section 2.1, to adjust the tip height by means of the SICM response and acquisition of the electrochemical information by SECM response is commonly performed sequentially (not operando).

The same hybrid strategy was used by coupling a potentiometric sensor to the SICM tip,[245,246] and in a typical example, a dual function tip was used to record the local pH value and the topography: one channel of the double-barrel electrode was modified with a potentiometric iridium oxide sensor to record the pH map, while the SICM tip channel corrected the working distance over a calcite microcrystal.[247]

SICM hybrid techniques were also employed to image living cells by coupling SICM to near-field optical microscopy[248] and confocal microscopy.[249−254] The confocal microscopy SICM approach was used to target fluorescing molecules and to correlate changes in the topography of cells. A hybrid confocal microscopy SICM was applied to monitor the topographical changes due to a virus-like particle assembly on a cellular membrane.[255] A protein that induces the formation of a virus-like particle was labeled with fluorescent molecules. The topographic changes were correlated to the virus-like particle growth mechanism, as well as the release event. The obtained results were an important step in the elucidation of the replication mechanism of the virus.

2.3. Electrochemical Scanning Tunneling Microscopy (EC-STM)

Scanning tunneling microscopy (STM) was proposed by Binnig and Rohrer at the beginning of 1980 as a technique for imaging the topography of samples with atomic resolution.[76] For that, a sharp metallic tip is slightly polarized against the underlying conductive sample, and when the distance between the very end of the STM tip and the surface reaches a distance in the atomic range, electrons can flow due to the tunneling effect.[256,257] The electron flow initiates a tunneling current which is adopted as the set point to control the working distance. The STM technique can image surfaces with atomic resolution because of the very sensitive interaction between atoms of the STM tip and the sample surface.[258] Advances in STM have enabled measurements in aqueous solution, making it possible to monitor structural changes due to surface polarization.[81,259] This condition is called electrochemical STM (EC-STM or ESTM) and it was proposed to monitor redox processes on surfaces by adding a high-impedance reference electrode in a four-electrode cell configuration (2 WE, 1 CE, 1 RE) and illustrated in Scheme 2c.[260−263] In this configuration, the potential can be applied independently at the conductive surface and the STM tip, in a similar manner as in the G-C mode of the SECM. One limitation of the EC-STM is the difficulty to deconvolute the tunneling current from the faradaic process at the tip. A strategy frequently used to offset this challenge is to partially coat the body of the EC-STM probe (but not the tip) with an insulating layer, such as nail varnish or Apiezon wax,[154,264] to reduce the area exposed to the electrolyte. The insulating layer is illustrated as a black cover on the EC-STM tip in the Scheme 2c). As faradaic and double-layer charge−discharge currents depend on the surface area, this approach is adopted to minimize such currents with respect to the tunneling current.[265,266] Another strategy is to keep the tip at the same position while the potential on the surface is scanned. The scanning tunneling spectroscopy (STS) is a deviation of EC-STM, where the applied potentials on the sample are interpreted as energy levels and scanned to obtain an electronic spectrogram. This strategy was widely utilized to study electron-transfer reactions on Au substrates, where the enhancement of the tunneling current was correlated to the reactivity of the surface.[267−271]

2.3.1. EC-STM Modes of Operation. The typical operation of EC-STM is based on approaching the STM tip toward the surface until a tunneling current is detected and used as the set point. The main feature of STM is to acquire the morphology of the investigated surface with atomic

https://doi.org/10.1021/acs.chemrev.2c00766
Chem. Rev. 2023, 123, 4972−5019

resolution.[272] The STM map is built by adjusting the STM position in the vertical direction (z-axis) to reach the same set point value. In contrast, the STM image can also be recorded by keeping the vertical distance (z-axis) constant and recording the tunneling current at each $x-y$-position. This strategy reduces the image acquisition time, however, the surface morphology should not be rough. Most of the EC-STM measurements are done by using the constant tunneling current mode, which is a powerful tool for investigating electrochemical processes like adsorption,[273−275] passivation,[276−278] and corrosion[279] of surfaces. One of the limitations of EC-STM is the slow scanning process, which makes it difficult to couple measurements simultaneously for operando studies. For this reason, in situ analysis is often used to evaluate morphological changes on surfaces, such as to investigate protein/enzyme covered surfaces,[280−284] metallic crystalline interfaces,[272,285] electrocatalysts,[286−288] and battery materials.[289,290] EC-STM was employed to study the topographical changes on highly oriented pyrolytic graphite (HOPG), that was polarized to invoke intercalation of Li ions.[289,290] The results indicated that the exfoliation process took place at the HOPG edges instead of at the basal planes. Recently, Wan and Wang used the approach of sequentially polarizing the surface and intermittently acquiring EC-STM images to study the mechanisms of CO_2RR and ORR on an adlayer of a cobalt-phthalocyanine catalyst on a gold surface.[291,292] In parallel, Itaya's group used EC-STM to investigate the correlation between the morphology and applied potentials in the formation of regularly patterned adlayers of Zn(II)-phthalocyanine and a zinc metalloporphyrin on the crystalline surfaces of Au(111) or Au(100).[293] It was shown that the assembly of fullerene molecules was dependent on the packing arrangement of the adlayer, which is also influenced by the crystallographic orientation of Au. Another interesting study used in situ EC-STM to follow the changes in the HOPG morphology during the solid-electrolyte interphase (SEI) formation.[294] The topographical changes during electrolyte reduction and film deposition were monitored, as well as the intercalation processes of Li ions and solvent molecules into the resulting surface. Moreover, the operando conditions employed allowed for the concurrent acquisition of STM images and potential programs on the HOPG surface. The overlay of the STM image with the potential scans showed a clear potential dependence of the surface processes, such as material deposition and surface morphological changes. After sequentially scanning the potential of the surface, a potential limit was found where the changes in surface processes became irreversible, which was attributed to the reduction process of the electrolyte anion.

These studies demonstrated the capability of the EC-STM to correlate morphological changes to the electrochemical activity of interrogated surfaces.

2.3.2. EC-STM Hybrid Techniques. One of the limitations of EC-STM is the convolution of the tunneling current with the faradaic processes occurring at the EC-STM tip. Consequently, EC-STM has been coupled with SECM to overcome this bottleneck.[295] In this case, a single tip is employed with a dual function of acting as an EC-STM tip to image the surface morphology and as an SECM tip to register the local electroactivity of the surface. After the positioning step, the tip is retracted to a working distance where there is no tunneling effect but is still in the range of the SECM set point. The applicability of SECM/EC-STM to image the topography and reactivity was demonstrated on a self-assembled monolayer (SAM) on gold by the feedback effect.[295] Soriaga's group employed a hybrid EC-STM/DEMS technique to follow changes on a polycrystalline Cu surface in basic medium and under an applied potential to promote CO reduction.[296] The products of the reduction reaction were detected by differential electrochemical mass spectrometry (DEMS). The hybrid EC-STM/DEMS analysis was used to correlate the observed low activity of ethanol generation to the ordering process of the Cu(100) lattice over Cu(110), in comparison to the Cu(110) on the polycrystalline surface.[296]

2.4. Scanning Electrochemical Cell Microscopy

Scanning electrochemical cell microscopy (SECCM), sometimes also called scanning micropipette contact method (SMCM), is a pipette-based tip technique capable of imaging surfaces with a lateral resolution in the nanometer ranges. As a result, SECCM has become a powerful tool for investigating electrochemical properties in single entity/sub-entity studies.[297−299] The principle of the technique is to confine the electrochemical cell in a droplet (protruding from the end of the nanopipette aperture), which is brought in contact with the interrogated surface. In contrast to SECM, SICM, and EC-STM, SECCM operates in air or an immiscible solution. Hence, the sample is not entirely immersed in the electrolyte before the local measurement is made. The colored background in Scheme 2a−c represents the electrolyte, indicating the absence of an electrolyte covering the sample in the case of SECCM (Scheme 2d). The electrochemical processes in SECCM take place exclusively on the probed surface providing direct electrochemical activity imaging. The SECCM tip is typically a single-barrel micro- or nanopipette containing the electrolyte and a quasi-reference counter electrode (QRCE). During measurements, a potential is applied between the QRCE and the conductor/semiconductor surface under interrogation. The set point is reached with the flow of a non-faradaic current caused by the contact of the hanging droplet to the surface (note: the pipette tip never touches the surface). Like in the SICM, an AC-modulated current caused by tip vibration is implemented in SECCM measurement for tip positioning. In this configuration, a double-barrel pipette (theta capillary) is used as SECCM tip with QRCEs inserted in each channel (see Scheme 2d). A potential is applied between the QRCEs, and the modulated ion current is then used as a set point. Before the contact between the hanging droplet and the surface is achieved, the modulated ion current is constant, and once there is contact, the ion current changes in its magnitude and oscillates with the same frequency as the tip vibration due to the droplet deformation. The magnitude of the resulting AC current is used to control the tip-to-surface distance. In the case that the interrogated surface is a semiconductor/conductor, an additional (floating) potential can be applied between the QRCEs and the sample. By adjusting this potential, the electrochemical processes occurring at the sample surface, which is wetted by the droplet, can be measured. Details of SECCM instrumentation have been reviewed.[74,299,300] Scanning is performed either in a constant distance mode by adjusting the magnitude of the ion current signal with the SECCM tip position, or in a hopping scanning mode where the tip is withdrawn far from the surface and reapproached at each $x-y$-position. The latter is essential for single-barrel SECCM configurations because it prevents tip crash on rough surfaces.[301]

https://doi.org/10.1021/acs.chemrev.2c00766
Chem. Rev. 2023, 123, 4972−5019

The general limitations of all SPEMs such as long scanning time and noise level in single-entity studies are also present in SECCM. The use of smaller SECCM tips leads to a reduction in the noise level because such tips wet smaller electrochemical areas, which increase the signal-to-noise ratio. This approach was explored to record the electron-transfer reaction on nanoparticles[82,302,303] and events of single nanoparticle electrochemical impacts (SNEI).[304,305] A strategy of coupling optical microscopy to SECCM to follow events during electrochemical measurements was proposed by Hill et al.[306,307] for reducing the typical extended scanning time. The optical image was employed to visualize Au nanorods on a transparent electrode surface, i.e., indium tin oxide (ITO). By using a LABVIEW program, the electrochemical measurements were performed just where a particle was visualized. The strategy reduced the scanning time and improved the sample throughput compared to the typical scanning-tip approach.[306]

Developments in SECCM are still in progress, and the power of the technique is enhanced when local electrochemical data in tandem with data treatment and simulations are used to calculate intrinsic properties. In addition, some technical and instrumental improvements are still under discussion. For example, recently strategies were shown to measure electrochemical impedance spectra,[308] acquire high-speed images,[309] and use amplified signals to achieve high temporal resolution.[310] Moreover, effects of experimental parameters such as the impact of the ohmic drop on the applied potential[311] or the possibility of contamination from the Ag-QRCE[312] were described.

2.4.1. SECCM Operation Modes and Applicability. During SECCM measurement, the tip performs a direct electrochemical interrogation of electron or charge transfer reactions on the sample surface in a single electrochemical cell configuration (see Scheme 2d). This is in contrast to SECM, SICM, and EC-STM, where the SEPM tip works generally as a spectator to probe the surface properties. The intrinsic operation of SECCM complicates the possibility of combining it with other techniques to perform operando measurements (Scheme 1). Although SECCM, hitherto, has not been coupled with other electrochemical method for operando measurements, the use of optical probes to modulate surface activity was suggested as actuator method. In this approach, the sample surface is irradiated to induce changes in surface activity while the SECCM tip acts as a spectator. The operando optical/SECCM approach was explored for studying the photoelectrochemical activity of semiconductors. Differences in the photoelectrochemical activity of TiO_2 and transition metal dichalcogenides such as MoS_2 were evaluated by performing measurements in dark and light conditions in the presence of a redox mediator.[313−315] The lack of operando SECCM is most likely due to the high complexity of the experimental design of coupling techniques.

It is worth noting that its applicability has been extensively demonstrated to directly probe electrochemical processes on surfaces at high resolution.[316] The electrochemical activity was probed using reversible redox species (e.g., hexaammineruthenium(III), ferrocenium, ferrocene trimethylammonium) to establish the structure−activity relationship in single entity studies.[317] SECCM was extensively used to acquire high spatial resolution maps to elucidate differences in electrochemical activity between phases and grain boundaries of many polycrystalline materials such as platinum,[318,319] palladium,[320] gold,[321−323] copper,[28] or boron-doped diamond[324−327] surfaces. SECCM in tandem with simulations was used to spatially map electron-transfer kinetics parameters, like the Tafel slope and the heterogeneous electron-transfer rate constant.[328−330] The sensitivity of the SECCM for local activity measurement was demonstrated and used to differentiate the surface activities of glassy carbon[331] and graphite.[332−335] Two-dimensional materials, such as graphene,[336−339] MoS_2,[340,341] and other transition metal dichalcogenides[341,342] were also investigated by SECCM. The studies demonstrated the presence of heterogeneous activity at different sites such as defects, edges, and basal planes. The results further showed that the local activity depends on the number of layers of the 2D material. These findings reveal the capability of SECCM to disclose the role of surface conditions on the activity of materials.

Moreover, SECCM is a powerful technique for monitoring the activity of electrocatalysts, allowing the correlation of topography/structure with electrocatalytic activity. The high-throughput characterization potential of SECCM helps to study the intrinsic activity and the kinetic of electron-transfer processes. Catalyst materials for the HER that have been interrogated include transition metal dichalcogenides,[323,331,341−345] bimetallic materials such as FeNi,[346] Au,[323,347,348] Pt,[303,349−354] Zn,[355] ITO, doped graphene,[339,356] boron-doped diamond,[326] and low-carbon steel.[357] SECCM has also been used to study the ORR,[28,82,323,326,358−361] the OER,[309,362−364] and the CO_2RR.[321,322,365,366]

In addition to decreasing the probed area, SECCM tip droplets can also be employed as a tool to modify surfaces with high spatial precision. Such strategies have been used for local deposition,[367,368] etching,[369,370] as well as to fabricate thin film metal oxides[371,372] and polymers.[373−375] The small area confined by the SECCM tip droplet is an important feature that allows high mass transport rates of materials coming from the pipette aperture to the interrogated surface. For this reason, SECCM is used to study slow kinetic processes, such as charge transfer on lithium-ion battery materials.[302,376−382] Adaptations of the experimental conditions of SECCM are in progress to enable further studies for lithium-ion batteries materials. Recently, SECCM studies were carried out in an argon-filled glovebox,[383] and using aprotic electrolytes.[384] Moreover, SECCM was also employed to monitor corrosion processes by recording polarization curves and revealing the susceptibility of crystallographic phases to the corrosion of polycrystalline low-carbon steel.[355,385−389]

3. OPERANDO SEPM APPLICATIONS IN ELECTROCATALYSIS

In this section, we discuss the application of operando SEPMs during electrocatalysis (ORR, OER, HER, CO_2RR, and other important reactions). In selecting the papers that have been reviewed, particular attention was given to those in which operando conditions, as delineated in the introductory and earlier sections of this paper, are met. These studies comprise an actuator measurement or potential, which is applied to stimulate changes at the investigated surface or substrate, while a ***simultaneously*** biased SEPM tip is employed as a spectator to detect or monitor local changes on the investigated surface.

Overall, SECM is the most explored SEPM technique for operando investigation of local electrocatalytic activity and interfacial electron-transfer processes during the ORR, OER, HER, and CO_2RR. This extended utility stems from the versatility of SECM due to its unique ability to characterize a

https://doi.org/10.1021/acs.chemrev.2c00766
Chem. Rev. 2023, 123, 4972−5019

wide variety of samples for various applications, adapt with other SEPMs (to improve and augment the information available for SECM only) and employ amperometric, potentiometric, as well as multifunctional probes during investigations. Furthermore, compared to the other SEPMs, which require coupling to other techniques to perform operando studies, the intrinsic operational modes of the SECM (SG-TC, TG-SC, and RC) are by default operando measurements.

3.1. Investigation of ORR Activity at the Sample Surface

The electrochemical reduction of molecular oxygen (ORR) has been extensively investigated because of its central role in fuel cells, metal-air batteries, sealed storage batteries, corrosion, and industrial electrocatalytic processes.[390,391] Generally, depending on the cathode material, electrode potential, and electrolyte composition,[392] it is believed (though debatable) that ORR proceeds in either of two pathways:[391,392] a highly efficient four-electron pathway in one step to generate H_2O or OH^- or a sluggish peroxide-intermediate-based two-electron pathway in two steps to form H_2O_2. ORR reaction pathways have been extensively reviewed.[393−398] The ORR follows either a direct four-electron pathway, or a two-electron-transfer pathway with hydrogen peroxide as intermediate.[391,392]

ORR investigations are typically performed using Pt-based electrocatalysts because Pt can reduce both O_2 and H_2O_2 to H_2O, and more importantly, it avoids the formation of H_2O_2 and/or other aggressive oxygenated species.[399] The high cost, scarcity, and easy poisoning associated with Pt-based materials discourage their use as ORR electrocatalysts on a large scale.[399] Addressing these challenges has triggered an intensive search for active electrocatalysts that are less expensive, earth-abundant, poisoning-tolerant, and can achieve ORR overpotentials in the range of that of Pt-based materials.[400] Some advances made in this direction include the alloying of Pt with less expensive metals, use of non-platinum metal combinations, transition metal oxides, chalcogenides, inorganic and organometallic complexes, and enzyme electrodes for ORR.[400] Despite these research leaps, the detailed mechanism of the ORR process, even on Pt, remains elusive.[400] Besides the difficulty encountered in O_2 activation, and O−O bond cleavage, which results in the observed sluggish kinetics,[401] the pronounced irreversibility of the cathodic reaction, the different possible reaction pathways and the possible generation of a wide spectrum of oxygenated intermediates, are considered as factors that make the detailed study of ORR mechanism an arduous task. Furthermore, the dependence of the reaction rate on the state of the electrode surface, coupled with the lack of a rational approach to the design of new electrocatalysts that can strictly follow the direct four-electron reduction pathway makes studying ORR even more difficult.[99,400] As an alternative to traditional macroscopic RDE and RRDE measurements, operando SEPMs, particularly SECM, have been employed to study the ORR (Scheme 3). Maps of chemical reactivity and topographic images were obtained.[99] Furthermore, the coupling of SECM with other analytical methods was proposed already by Hillier and Bard in 2003 as an effective approach for studying the ORR and screening of electrocatalysts.[99] The general principle for probing the ORR with operando SEPM involves biasing the substrate of interest to invoke the ORR while a simultaneously polarized SEPM tip is used to locally monitor the substrate-generated species, such as H_2O_2, HO_2^-, or OH^- (SG-TC, TG-SC, and EC-STM in Scheme 3) or compete (RC-SECM on the Scheme 3) with the substrate for O_2 in the gap between them. Kinetic parameters, such as the heterogeneous electron-transfer rate, can then be extracted by fitting the experimental tip approach curves to developed quantitative theories for the different operational modes in the case of SECM techniques.[23,68,93] In the ensuing paragraphs, the advances made thus far in ORR investigations with SEPMs are recounted, highlighting the operando conditions and the uniqueness of SEPMs as qualitative and/or quantitative electroanalytical characterization tools during ORR electrocatalysis.

Scheme 3. Schematic Drawing Representing the Main Operando SEPM Configurations for ORR Interrogation[a]

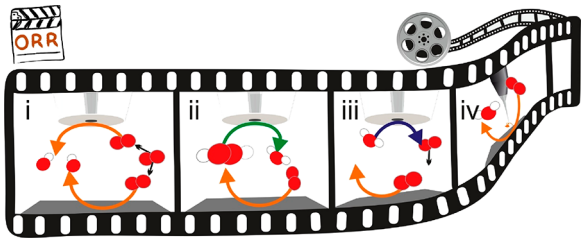

[a]The SEPM tip acts as the spectator while a modulation occurs on the electrocatalyst's activity by an actuator method. The SEPM tip can be polarized to (i) reduce oxygen (orange arrows) in RC-SECM; (ii) reduce (green arrow) H_2O_2, an ORR product when $n = 2$, in SG-TC-SECM; (iii) oxidize H_2O_2 in TG-SC-SECM; (iv) map with high-resolution SEPM, EC-STM.

One of the pioneering studies of ORR with the SECM was performed by Liu and Bard[402] under operando conditions using the FB operational mode (Figure 1a) to estimate the rate constant of the ORR on a Pt electrode in alkaline solution. A Au UME was employed as SECM tip which was polarized to 1.2 V vs $Hg/HgSO_4$ (i.e., at the diffusion limiting potential for OH^- oxidation). The polarized tip was then moved toward the surface of the Pt substrate which was simultaneously held at different potentials to obtain the SECM approach curves (Figure 1b). The Tafel slope and rate constant agreed with previously reported values derived from RDE and other electrochemical techniques. However, the operation of this technique was limited to a short pH range (9−12), where OH^- oxidation at the tip could be used. As such, the study of ORR in acid or neutral media is impossible with the FB mode because the feedback diffusion of the tip reactant (H_2O) does not induce modulations in the tip current.[93,396] Perhaps this observation explains why the FB mode was less explored in operando ORR SECM studies. The Bard group in 2003 proposed the TG-SC mode (Figure 1c) as an alternative to the FB mode to analyze and compare the electrocatalytic activity of an array of finely dispersed catalyst spots of Pt, Ru, and Au for the ORR in acidic medium (0.5 M H_2SO_4).[99] In this mode, the substrate (Pt, Ru, and Au catalyst spots) was polarized to a potential (<1.23 V vs $Hg/HgSO_4$) to facilitate the reduction of O_2 to H_2O while an oxidation current (between 10 and 220 nA) was applied to the Pt SECM tip to oxidize H_2O to O_2 and ensure a constant flow and diffusion of tip-generated O_2 to the substrate. Figure 1d represents an ORR image obtained in the TG-SC mode of an array of Pt and Ru spots on glassy carbon (GC). The main advantage of the TG-SC mode is that it assumes no feedback contribution and hence allows for the study of reactions inaccessible to the FB mode. Additionally, working in the TG-SC mode allows for studies in solutions

https://doi.org/10.1021/acs.chemrev.2c00766
Chem. Rev. 2023, 123, 4972−5019

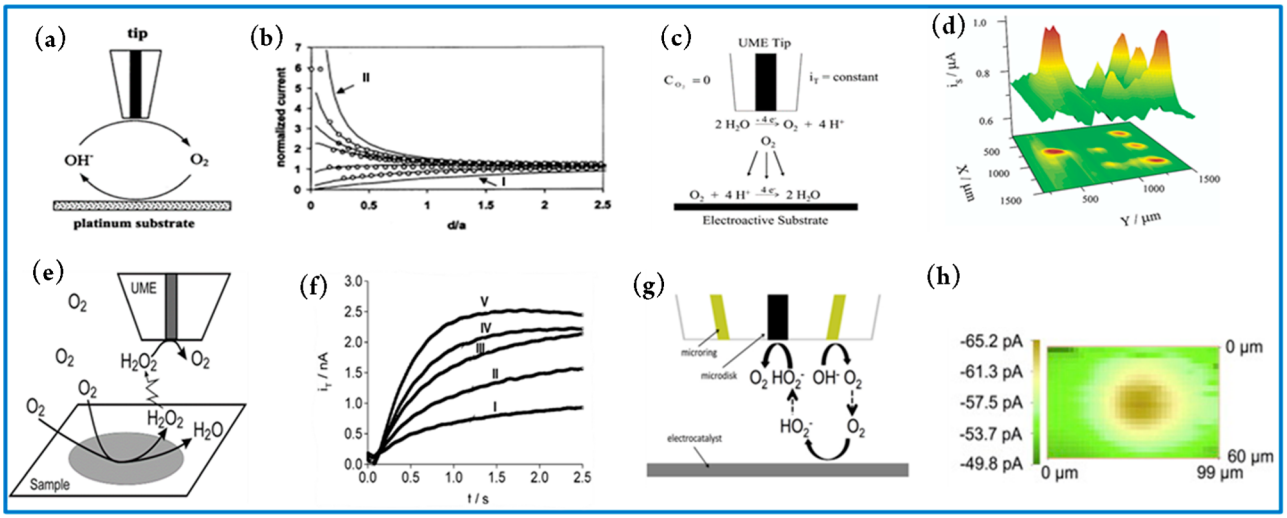

Figure 1. (a) Feedback mode SECM used in the study of O_2 reduction in alkaline solution. (b) SECM approach curves: solid lines "a" and "b" are theoretical approach curves at conducting and insulating substrates, respectively. Circular symbols are experimental approach curves, and solid lines are theoretical curves at a Pt substrate with its potential held at, from top to bottom, −0.9, −0.8, −0.7, −0.6, and −0.5 V vs $Hg/HgSO_4$. Reproduced from ref 402. Copyright 2002 American Chemical Society. (c) Scheme of the modified TG-SC mode for the study of the ORR in acidic medium. (d) ORR images obtained by the TG-SC mode of an array of Pt (left spot and right row) and Ru (middle row) spots supported on glassy carbon. Reproduced from ref 99. Copyright 2003 American Chemical Society. (e) Schematic illustration of the SECM operation in the pulsed SG-TC mode. (f) UME transient currents at E_T = 1.1 V for the collection of H_2O_2 produced during ORR at a Au electrode. The potential of the Au substrate was stepped from +0.4 V to (I) +0.1, (II) +0.05, (III) 0, (IV) −0.05, and (V) −0.1 V. Reproduced from ref 399. Copyright 2008 American Chemical Society. (g) "Tip generation−substrate collection−tip collection" mode SECM using a microring-disk SECM tip for simultaneous ORR electrocatalyst screening and HO_2^- detection. (h) SECM image recorded at the microring-disk SECM tip (held at 0.2 V to oxidize HO_2^-) while scanned over the Au substrate polarized at −0.5 V vs Ag/AgCl. Reproduced with permission from ref 100. Copyright 2012 Elsevier Ltd.

with varying concentrations as opposed to the stringent conditions needed in the FB mode to reach diffusion control at the UME tip. As an added advantage, TG-SC is ideal for the rapid screening of large arrays of multicomponent electrocatalysts.[99,400] The TG-SC mode was later used to study and screen the electrocatalytic activity of binary and ternary combinations of Pd, Au, Ag, and Co (or Cu) deposited on GC as substrates for the ORR in acidic medium using Pt as SECM tip.[400] A drawback of the TG-SC mode lies in the inability to precisely quantify the products/intermediates formed during the ORR.[100,399] The detection and quantification of H_2O_2, for instance, is very important because its formation has been associated with undesirable processes like membrane degradations, corrosion of metals, polymer fittings, and carbon materials, as well as a reduction in the efficiencies of fuel cells.[399] Hence there is a need for methods that can directly investigate the formation of H_2O_2. In 2008, Shen et al.[399] proposed and used a transient SG-TC mode to detect H_2O_2 produced during the ORR at Au, Pt, and PdCo alloy-modified GC electrodes in acidic medium using a Pt-UME as amperometric H_2O_2 sensor. Figure 1e shows the principle of the transient SG-TC mode: the substrate is first stepped from a potential where no faradaic processes happen, to a value within the limiting-current region of the ORR, while the tip is kept at a fixed potential of 1.1 V vs Ag/AgCl (Figure 1f) to detect and oxidize H_2O_2.[399] Sánchez-Sánchez and co-workers demonstrated a new approach to quantify reaction intermediates based on the SG-TC mode but using smaller substrates (≤200 μm diameter) to induce stationary-state reaction conditions.[403] As a demonstration, they employed the technique to quantify H_2O_2 during ORR at a Hg on Au substrate (100 μm) electrode in acidic media using Pt or Au as SECM tips. The use of smaller substrate electrodes (100 μm diameter) allowed a relatively high collection efficiency at the SECM tip, making it possible to detect and quantify the substrate generated H_2O_2 as well as to estimate the number of transferred electrons (n) during the ORR. The value of n was in the range of 2.12 to 2.19, and thus the two-electron pathway was clearly revealed as the predominant reaction pathway.[404] Bard and co-workers employed SG-TC-SECM in a fundamental study of the ORR mechanism at a Pt SECM tip in alkaline media. Operando SG-TC-SECM was capable to estimate n = 2 when the ORR occurred at NaOH concentration <2 M, and n = 1 in the case of concentrations >6 M with formation of $O_2^{\bullet-}$.[405] Related ORR studies with the SG-TC mode were reported for different electrocatalysts including Hg, Au, Ag, Cu, Pt, Pd, $Pd_{80}Co_{20}$, $Au_{60}Cu_{40}$,[403] Pt and Pd nano/microstructures embedded in multilayer polyelectrolyte films,[406] different Fe porphyrins on GC,[407] nanoporous Au and flat Au substrates,[408] and cobalt metalloids (Co_xB and Co_xP) in a nitrogen-doped carbon matrix.[409] Johnson and Walsh suggested a novel "tip generation−substrate collection−tip collection" (TG-SC-TC) sequence for screening the activity of ORR catalysts while detecting H_2O_2 simultaneously with the aid of a microring-disk SECM tip (Figure 1g).[100] As a proof of concept, the technique was employed to measure the activity of a Au electrocatalyst toward the ORR in alkaline media, while simultaneously monitoring the formation of H_2O_2. Oxygen is generated at the microring of the SECM tip at a constant current, the O_2 generated at the microring diffuses to the substrate (which is polarized at −0.5 V vs Ag/AgCl) to reduce oxygen to HO_2^-. The substrate-generated HO_2^- then diffuses to the microdisk (which is biased at a sufficiently anodic potential of 0.2 V vs Ag/AgCl) and HO_2^- gets oxidized to O_2. Figure 1h is an SECM image recorded when the substrate was polarized at −0.50 V vs Ag/AgCl. The advantage of this method lies in the

https://doi.org/10.1021/acs.chemrev.2c00766
Chem. Rev. 2023, 123, 4972−5019

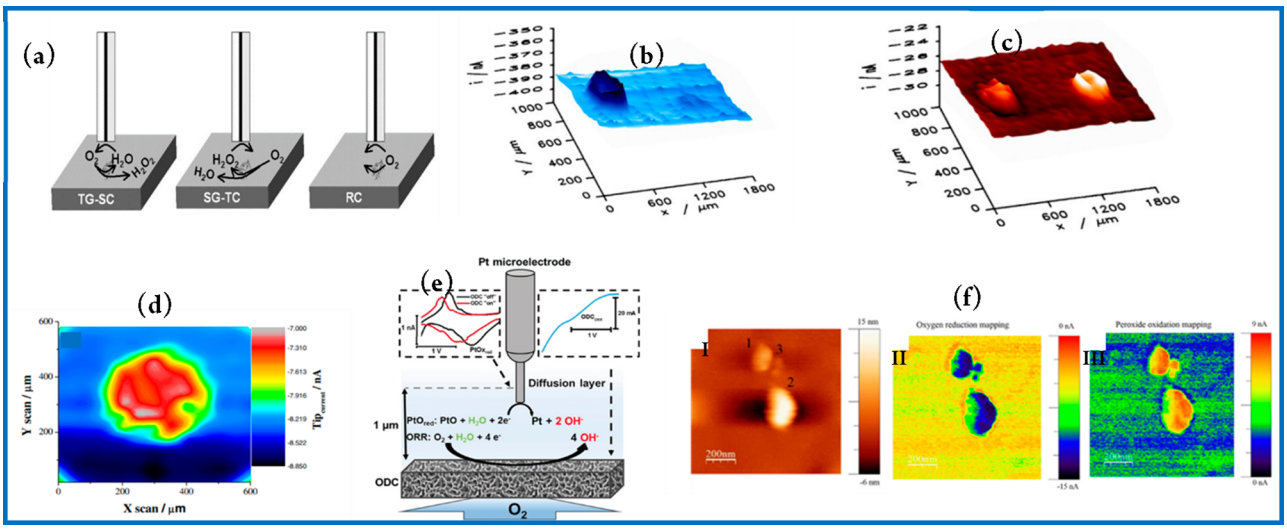

Figure 2. (a) Schematic representations of different detection modes in SECM. (I) Tip generation−sample collection (TG-SC) mode. The scanning microtip oxidizes water to produce O_2. The O_2 reduction current at the sample is the analytical signal. (II) Sample generation−tip collection (SG-TC) mode. The sample is polarized to reduce O_2. The tip oxidizes H_2O_2 which may be formed as a byproduct at the sample. The analytical signal is the peroxide oxidation current detected at the tip. (III) Redox competition mode (RC-SECM). The O_2 reduction current is detected at the tip. Depletion of this current is correlated to a locally diminished oxygen concentration caused by a competing O_2-reducing catalyst site of the sample, 3D false color representations of the obtained SECM images when the substrate was polarized at −400 V. (b) Reduction current at the tip due to competition for oxygen. Darker shaded blue areas correspond to a diminished current flow due to competition for the available O_2 with active sites of the substrate. (c) Oxidation current of H_2O_2 at the tip concurrently registered. Reproduced with permission from ref 115. Copyright 2007 Elsevier Ltd. (d) Tip generation−redox competition−SECM images for O_2 reduction on FeN_4/rGO modified microelectrode. Color contrasts correspond to the measured cathodic tip current. Reproduced with permission from ref 420. Copyright 2016 Springer Nature. (e) Monitoring local ion activity changes in the water and hydroxide diffusion layer of an operating GDE and in dependence of its ORR rate is realized by voltammetric detection of the PtO reduction peak at a positioned Pt microelectrode. Reproduced with permission from ref 422. Copyright 2018 John Wiley & Sons, Ltd. (f) AFM/SECM mapping on Pt NPs performed using a Au-c-Pt tip: (I) topography, (II) oxygen reduction currents, and (III) peroxide oxidation currents recorded in N_2-saturated on HOPG. Reproduced with permission from ref 423. Copyright 2019 John Wiley & Sons, Ltd.

fact that no potential programming of tip or substrate is needed. Furthermore, taking continuous SECM tip scans of the substrate generates maps that correlate to activity and reaction mechanism.

In a quest to further improve the lateral resolution of the SECM the feasibility of a transient RC mode, which was mentioned in an earlier heptode SECM tip simulation study,[410] was introduced. In the RC mode, local catalytic information at the substrate is transduced through a current measured at the tip while simultaneously avoiding the need to apply potential pulses to the substrate. The technique was applied to qualitatively monitor the lateral activity of Pt-spots on a GC support during the ORR using a Pt-UME as SECM tip. During the study, both tip and substrate were biased to a reductive potential (e.g., −0.60 V vs Ag/AgCl/3 M KCl) to compete for O_2 in the gap between them. Since the diffusion of bulk O_2 to the gap between the tip and substrate is hindered during measurement, a predefined potential pulse (1.4 V vs Ag/AgCl/3 M KCl) is applied to the tip to avoid complete depletion of O_2. The activity of catalyst spots with different Pt loadings within a single spot was successfully visualized. The inability to extract quantitative kinetic conclusions was reported as an inherent limitation of the RC mode that needed to be addressed to enable the detection of H_2O_2. Furthermore, it was suggested that by combining the RC-mode with the shearforce-based constant distance mode of SECM, the chronoamperometric features of the RC mode can provide a detailed insight into the catalytic activity at tip-to-substrate distances below 100 nm.[106] Regardless of the noted drawbacks, the transient RC mode was successfully used to visualize the local ORR catalytic activity of Pt−Ag nanoparticles with different Ag content,[411] patterned carbon nanotubes decorated with Pt nanoparticles,[412] undoped and nitrogen-doped CNTs,[413] metal nanoclusters (Pt, Au, Ru, and Rh and their co-deposits), CoS_2,[414] and lanthanide-based oxides ($La_{0.6}M_{0.4}Ni_{0.6}Cu_{0.4}O_3$, M = Ag, Ba, Ce).[415]

In 2007, Eckhard and Schuhmann suggested a sequential dual imaging mode of SECM making it possible not only to monitor local activity but also to determine the selectivity of electrocatalysts concurrently. The principle as depicted in Figure 2a involves combining three different SECM modes (TG-SC, SG-TC, and RC) and applying a sequential pulse program. Thus, two images are obtained in parallel; one gives information about the activity of the catalyst while the other monitors H_2O_2 (if any) produced during the ORR (see Figure 2b,c). The local activity and selectivity of Pt and Au spots for ORR were visualized using a Pt-UME as SECM tip. The RC mode enabled effective visualization of the local activity of substrates and the SG-TC mode allowed H_2O_2 detection and a better understanding of the branching between the two-electron and four-electron pathway of ORR at a given potential.[115] The same technique was employed to visualize the catalytic activity and selectivity of different electro-polymerized metalloporphyrins,[416] tetratolyl porphyrins (with Mn, Fe, and Co as central metal ions),[108] to screen Pd−Pt and Pd−Au co-deposits for H_2O_2 reduction,[417] bifunctional catalysts based on cobalt and nickel oxides embedded in nitrogen-doped carbon (Co_xO_y/NC, Ni_xO_y/NC), bifunctional catalyst materials (mixed $Ni_{0.9}Co_{0.1}Fe_2O_4$ oxide) in alkaline media,[418] multiwalled carbon nanotubes (MWCNTs), cobalt

https://doi.org/10.1021/acs.chemrev.2c00766
Chem. Rev. 2023, 123, 4972−5019

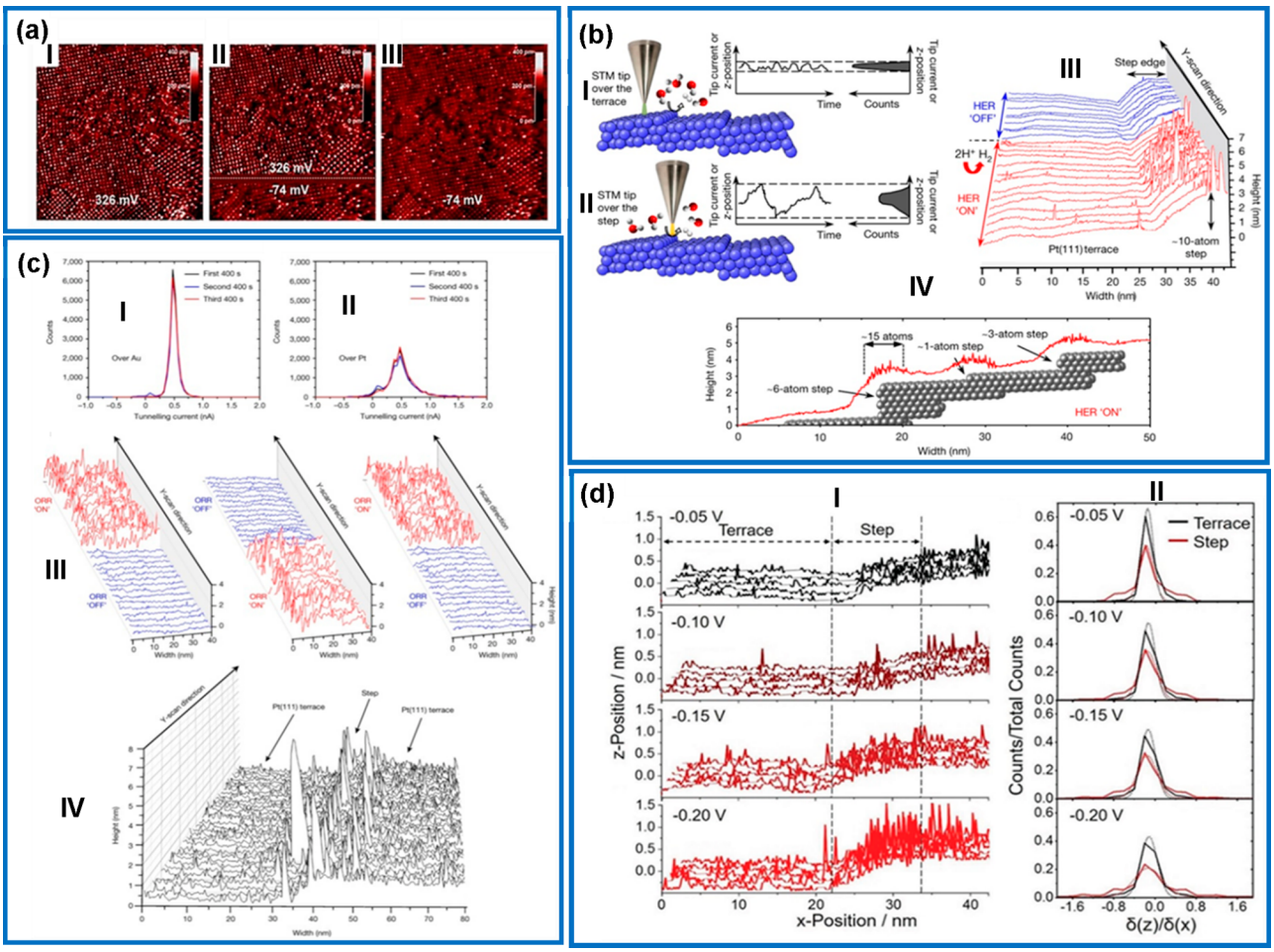

Figure 3. (a) Sequential STM images of a CoTPP monolayer on Au(111) in 0.1 M $HClO_4$ saturated with oxygen at different potentials. Reproduced with permission from ref 426. Copyright 2016 John Wiley & Sons, Ltd. (b) Scheme explaining the concept. When the local environment between the STM tip and the sample changes (in this case, when the tip is over a terrace (I) versus a step (II)), the tunneling barrier also changes in a way that is driven by the changes in approaching and departing reactants and products. In this scenario, increased tunneling-current noise is likely to appear when the tip is over a step edge, which is more active than the terrace sites. If the STM is operated in constant-current mode, then the noise is revealed in the measured *z*-position (the height of the STM tip over the sample). (III) STM line scans (constant-current mode) obtained over a Pt(111) surface in 0.1 M $HClO_4$ when the potential of the sample is either sufficiently negative or too positive to initiate the HER (which is therefore either "ON" or "OFF"). (IV) Typical STM line scan over the Pt(111) surface in 0.1 M $HClO_4$ under HER conditions. (c) Histograms of the tunneling-current noise over a polycrystalline Au surface (I) and corresponding histograms obtained over a polycrystalline Pt surface (II), results of repetitive ORR "ON" and "OFF" STM noise experiments at the same terrace of a Pt(111) sample (III), STM line scans at the surface of a Pt(111) electrode under ORR conditions, where both terraces and steps can be visualized (IV). Reproduced with permission from ref 427. Copyright 2017 Springer Nature. (d) n-EC-STM measurement of a Pt(111) step and adjacent terraces. With decreasing potential, the overall noise level increases. For data evaluation, the terrace data (on the left) are used for calibration for the relation between noise level and activity on this sample (I), histograms after separating the data for terrace (black) and step (red). At every applied sample potential, the step shows a higher noise level relative to the terrace, as evident from the broader and less intense distribution. All potentials given are referred to the Pt quasi-reference electrode (II). Reproduced with permission from ref 428. Copyright 2021 John Wiley & Sons, Ltd.

protoporphyrin (CoP) and their composite (MWCNTs/CoP) in neutral solution[419] during ORR.

Silva and colleagues, employed a TG-RC mode to map the activity of iron(III) tetra(*N*-methyl-4-pyridyl)porphyrin/reduced graphene oxide composite (FeN_4/rGO) toward the ORR using a Pt-UME as SECM tip.[420] The tip was first polarized at 1.25 V vs Ag/AgCl to generate O_2 in the substrate−tip gap followed by an immediate polarization of both tip and substrate at sufficiently cathodic potentials to consume the O_2 generated. Figure 2d shows the SECM image obtained for the ORR when the substrate was polarized at −0.50 V vs Ag/AgCl.[420] Schulte and co-workers used the RC mode combined with shearforce-based constant distance positioning (4D-SF/SECM) to examine the topography and activity of gas diffusion electrodes toward the ORR.[421] Botz and colleagues developed a method to monitor the activity of other redox species in parallel with the ORR (Figure 2(e)) which they implemented to visualize the changes in the local activities of OH^- ions and H_2O on the surface of an oxygen-depolarized cathode during the ORR in high alkaline medium.[422] The substrate was polarized to induce the ORR consuming O_2 and H_2O and producing OH^- while recording CV scans at a Pt-UME SECM tip for the detection of the OH^- and H_2O activities. The reduction of PtO on the surface of the tip was used to quantify local OH^- and H_2O activities which is a relevant information for the properties of high-current-density GDEs.[422]

https://doi.org/10.1021/acs.chemrev.2c00766
Chem. Rev. 2023, 123, 4972−5019

Table 2. Summary of Experimental Conditions for ORR Studies with SEPMs

SEPM	mode	substrate for ORR	tip	tip reaction	ref
SECM	FB	Pt	Au disk UME (Ø, 25 μm)	OER	402
SECM	TG-SC	Pt, Ru, and Au	Pt disk UME (Ø, 25 μm)	H_2O oxidation	99
SECM	TG-SC	binary and tertiary combinations of Pd, Au, Ag, and Co (or Cu) on GC	W or Au disk UME (Ø, 25 μm)	H_2O oxidation	400
SECM	SG-TC	Au, Pt, and PdCo alloy-modified GC	Pt disk UME (Ø, 25 μm)	H_2O oxidation	399
SECM	SG-TC	Hg on Au	Pt or Au disk UME (Ø, 25 or 50 μm)	H_2O_2 oxidation	404
SECM	SG-TC	Hg, Au, Ag, Cu, Pt, Pd, $Pd_{80}Co_{20}$, and $Au_{60}Cu_{40}$	Pt disk UME (Ø, 25 μm)	H_2O_2 oxidation	403
SECM	SG-TC	Pt and Pd nano/microstructure	Pt disk UME (Ø, 25 μm)	H_2O_2 oxidation	406
SECM	SG-TC	Fe porphyrins on GC	Au disk UME (Ø, 25 μm)	FeIII(OO_2^-) oxidation	407[a]
SECM	SG-TC	nanoporous Au and flat Au substrates	Pt disk UME (Ø, 25 μm)	H_2O_2 oxidation	408
SECM	TG-SC-TC	Au microdisk	microring-disk (ring Au thickness 750 nm, disk Pt Ø, 1 μm)	HO_2^- oxidation	100
SECM	RC	Pt spots on GC	Pt disk UME (Ø, 10 μm)	ORR	106
SECM	RC	Pt−Ag NPs (varying Ag content)	Pt disk UME (Ø, 25 μm)	ORR	411
SECM	RC	patterned CNTs decorated with Pt NPs	Pt disk UME (Ø, 25 μm)	ORR, H_2O oxidation	412
SECM	RC	undoped and N-doped CNTs	Pt disk UME (Ø, 25 μm)	ORR	413
SECM	RC	Pt, Au, Ru, and Rh and their co-deposits	Pt disk UME (Ø, 25 or 50 μm)	ORR, H_2O oxidation	432
SECM	RC	CoS_2	Pt disk UME (Ø, 10 μm)	ORR	414[a]
SECM	RC	$La_{0.6}M_{0.4}Ni_{0.6}Cu_{0.4}O_3$ (M = Ag, Ba, Ce)	Pt disk UME (Ø, 10 μm)	ORR	415[a]
SECM	RC	tetratolyl porphyrins (containing Mn, Fe, and Co as central metals)	Pt disk UME (Ø, 25 μm)	ORR	108
SECM	RC, SG-TC	Pd−Pt and Pd−Au electrodeposits on graphite	Pt disk UME (Ø, 25 μm)	H_2O_2 oxidation	417
SECM	TG-SC, SG-TC, RC	Pt and Au on GC	Pt disk UME	ORR	115
SECM	RC, SG-TC	Co_xO_y/NC and Ni_xO_y/NC	Pt disk UME (Ø, 25 μm)	H_2O_2 oxidation	433
SECM	RC	$Ni_{0.9}Co_{0.1}Fe_2O_4$ mixed oxide	Pt disk UME (Ø, 25 μm)	ORR	418
SECM	RC	MWCNTs, CoP, and MWCNTs/CoP	Pt disk UME (Ø, 25 μm)	ORR	419
SECM	TG-RC	FeN_4/rGO	Pt disk UME (Ø, 10 μm)	ORR	420
SECM	RC (4D-SF/SECM)	GDEs	Pt disk UME (Ø, ∼1.8 μm)	ORR	421
SECM	4D-SF/SECM	GDEs	Pt disk UME (Ø, ∼1 μm)	PtO reduction	422[a]
SECM/SICM	SG-TC, hopping	Au NPs	Theta pipette filled with (aperture Ø, ∼200 nm)	H_2O_2 oxidation	425
AFM/SECM	noncontact	HOPG and isolated Pt particles	Au-coated SiO_2 Pt (edge size 100 nm)	H_2O_2 oxidation	423[a]
EC-STM	noncontact	cobalt(II) and copper(II) phthalocyanines	W coated with nail polish	ORR tunneling current	429
EC-STM	constant current	iron octaethyiporphyrin,	W coated with nail polish	ORR tunneling current	430
EC-STM	noncontact	iron phthalocyanine	W coated with nail polish	ORR tunneling current	287
EC-STM		CoTPP on Au	W coated with nail polish	ORR tunneling current	426
n-EC-STM	constant current	Pt on Au	W coated with nail polish	ORR noise	427
n-EC-STM	noncontact	Pt_5Gd and Pt_5Pr	ripped Pt/Ir alloy wire insulated with Apiezon	ORR noise	52[a]
n-EC-STM	noncontact	Pt(111)-based surfaces	ripped Pt/Ir alloy wire insulated with Apiezon	ORR noise	431[a]
n-EC-STM	noncontact	Pt(111)	Pt/Ir alloy wire insulated with Apiezon	ORR noise	428[a]

[a]Works published in the last 5 years.

Besides the use of shear force-based systems,[421,424] SECM was hyphenated with other probe techniques to minimize the effect of sample topography on the measured tip current during ORR measurements. O'Connell et al. coupled SECM and SICM (SECM-SICM) to study localized H_2O_2 generation at individual Au nanoparticles (AuNPs) within ensemble electrodes during the ORR.[425] They fabricated a theta (double-barrel) pipette which they used as the imaging probe and employed the SG-TC-SECM mode to detect H_2O_2 during the ORR at individual AuNPs. The potential of the substrate was varied to induce ORR while the SECM tip was biased at +1 V vs RHE to oxidize H_2O_2. The SICM hoping mode was employed to yield topographical information about the substrate.[425] AFM-SECM operating in the noncontact mode was used to simultaneously map topography, oxygen reduction and detect peroxide intermediates on a bare highly oriented pyrolytic graphite (HOPG) surface and isolated Pt particles during ORR, using a Au-coated SiO_2/Pt tip.[423] During AFM-SECM image acquisition (Figure 2(f)) the substrate was polarized at 0.7 V vs SHE (for the ORR) and

https://doi.org/10.1021/acs.chemrev.2c00766
Chem. Rev. 2023, 123, 4972−5019

tip at 0.98 V vs SHE (for H_2O_2 oxidation), and it was concluded that the ORR on isolated Pt particles proceeds selectively via the two-electron pathway.[423]

Following the first successful application of the STM in the study of an electrode/electrolyte interface,[81] EC-STM has found a wide range of applications in electrode processes during ORR electrocatalysis. In situ EC-STM (operated in constant-current mode with tungsten STM tips) was used to successfully investigate the effect on ORR of adlayer structures of metal porphyrin and phthalocyanine substrates including cobalt(II) and copper(II) phthalocyanines,[429] iron octaethylporphyrin,[430] iron phthalocyanine,[287] and 5,10,15,20-tetraphenyl-21*H*,23*H*-porphine cobalt(II).[426] Cai and colleagues used EC-STM operated under in situ conditions enabling them to monitor the interfacial reactions on the adlayer of metal porphyrins (CoTPP) on a Au(111) single-crystal electrode in gas-saturated (O_2, N_2 and air) 0.1 M $HClO_4$ solution.[426] During the ORR, the substrate was kept at 0.326 V vs SCE (to hinder the ORR) resulting in the formation of high-contrast adsorbed species in oxygen saturated electrolyte (suspected to be CoTPP-O_2 complexes) before invoking ORR (by switching the potential to −0.074 V vs SCE). They observed that the final shift to the cathodic potential (invoking ORR) resulted in a shift from CoTPP adsorbates the initial high-contrast CoTPP adsorbates to low contrast, as shown in Figure 3a. This particular study demonstrates the ability of EC-STM to provide direct evidence of the catalytic role of metal porphyrins toward the ORR at the molecular level, information essential for designing such catalysts.[426] It is known that when EC-STM is carried out under reaction conditions, the recorded analytical signal shows higher fluctuations (noise) at active sites compared to nonactive sites, which has been suggested as a valid tool to identify the location of active sites.[81]

In 2017, Pfisterer proposed and demonstrated a method to readily map and quantitatively distinguish the catalytic activity of active sites on electrocatalysts with high spatial resolution by monitoring relative changes in the tunneling current noise.[427] The monitoring of noise in EC-STM (n-EC-STM) allowed them to directly evaluate the significance and relative contribution of different defects and sites to the overall catalyst activity of materials toward ORR and HER. Figure 3b is a sketch of the concept. To probe the performance of the STM noise measurement approach in mapping local catalytic activity during ORR, the authors deposited catalytically active platinum nanoparticles on less-active polycrystalline gold which they used as the substrate in 0.1 M $HClO_4$. In the noise measurement, tunneling currents were recorded during the ORR on the pure Pt part as well as on the pure Au part by adjusting potentials to either induce ORR (ON) or hinder ORR (OFF), as shown in Figure 3c. This work portrays the superb ability of STM noise analysis in locating active sites even under the demanding conditions associated with electrochemical interfaces, although the results obtained were only qualitative.[427] n-EC-STM has recently been applied to monitor and distinguish the activity levels to link structure to the ORR activity of Pt_5Gd and Pt_5Pr in acidic medium,[52] and Pt(111)-based surfaces in different electrolytes.[431] Haid and colleagues showed in 2020 that the hitherto qualitative n-EC-STM method could be extended to obtain quantitative information on the local activity. They demonstrated this by using the well-studied Pt(111) as an ORR catalyst in acidic media as model system. During the n-EC-STM measurements, the potential of the sample was set such that ORR occurred at the Pt(111) surface and the tip potential was gradually increased, from −0.05 V to −0.20 V vs Pt causing faradaic reactions at the tip. The authors were able to link the recorded noise, from ORR at a well-defined active site on the Pt(111) surface to the corresponding TOF estimated from the current recorded at the substrate, thus establishing a direct link between the variations in the STM signal or noise over an active site and the activity levels or rate of the reaction (Figure 3d).[428]

3.2. Investigation of OER Activity at the Substrate Surface

The oxygen evolution reaction is another of the most studied reactions in electrochemistry. OER is involved in the generation process of many energy vectors which are considered promising for sustainable energy supply as well as in other industrial electrochemical processes such as cathodic protection, and metal recovery.[434] For example, the OER represents a bottleneck in the production of hydrogen gas through electrochemical water splitting as it limits the overall efficiency of the process.[435] The reason lies in the fact that this reaction has a complex mechanism based on four coupled electron−proton transfer steps, which results in sluggish kinetics and high overpotentials. The general mechanism pathways as proposed in the literature for the OER in different electrolyte media evidence the complexity of the process with multiple chemical and electrochemical steps and intermediates.[436,437]

The development of OER catalysts is of great importance for the future of eco-friendly power generation technologies. The state-of-the-art electrocatalysts for OER are noble metal-based materials like RuO_2 and IrO_2, but their scarcity and cost definitively hinder their large-scale application.[438] Transition-metal oxide-based electrocatalysts (TMOs) are promising alternatives with comparable OER activity and robustness while being inexpensive and earth-abundant.[439,440]

Considerable progress has been attained in preparing OER catalysts, as materials science has been able to prepare an extensive variety of electrocatalysts in terms of compositions, structures, and morphologies.[441] Nevertheless, the rational design of OER active materials is still challenging owing to the lack of knowledge about the mechanisms and the correlation between structure and catalytic performance.[442] Electrocatalytic surfaces often present nonuniform properties which lead to high complexity for characterization and benchmarking as their activity depends on many parameters such as the preparative conditions, the aging, the used precursors, and their processing.[443] Despite exhaustive work has been done on this matter, one can find a lot of contradictions in the published data; probably due to the variability in experimental conditions.[15] Moreover, the structures and surface chemical properties of TMO-based electrocatalysts inherently change during the OER, whose intermediate states play an important role in the process.[443] This highlights the need for studies in operando conditions which can provide information about the structure−activity relationship during the OER.[442] As already discussed, information about the intrinsic activity of the active centers and their distribution across the surface is vital for catalyst optimization. SEPM techniques are powerful tools to shed light on the characterization of heterogeneous surfaces and the analysis of local electrochemical activity. In this section, we will in-depth gather and review the works that report operando mode SEPM techniques for the study of the OER along with the strategies to achieve an ever more accurate

https://doi.org/10.1021/acs.chemrev.2c00766
Chem. Rev. 2023, 123, 4972−5019

data acquisition. Among the SEPM techniques, SECM was definitively the most employed for the study of OER, possibly due to the same reasons stated in the ORR section (Scheme 4). Even though several modes are available, the SG-TC is by

Scheme 4. Schematic Drawing Representing the Main Operando SEPM Configurations for OER Interrogation[a]

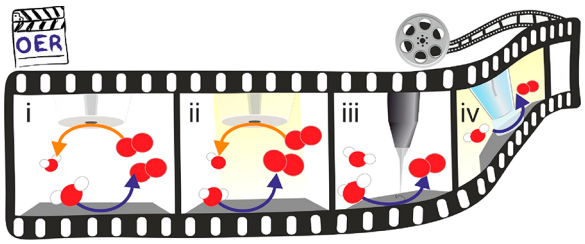

[a]The SEPM tip acts as the spectator and the electrocatalyst's activity is tailored by an actuator method. The SEPM tip can employed for (i) collecting the OER products formed at the sample in SG-TC-SECM (ORR at the tip, orange arrows); (ii) selectively collecting the OER product when the sample surface is locally irradiated in SPECM; (iii) atomic-resolution mapping of crystalline surfaces; (iv) evaluating the electroactivity of semiconductors with SECCM coupled with light source.

far the most employed in OER studies, which is by default an operando method. Scheme 4i–iv summarizes the operando SEPM configuration for OER evaluation, where the reaction products (O_2 and H_2O_2) are collected at the SEPM tip. Since the reactant in OER is water (or OH^- in alkaline conditions), which is already present in the solution, other SECM modes such as FB, TG-SC, and RC were not largely explored for studying the OER. A typical experiment in the SG-TC mode is based on the polarization of the catalyst-modified substrate to drive the OER reaction while the tip scans the catalyst surface. The tip is simultaneously polarized to continuously detect the formed products, generally O_2. Figure 4a displays a scheme representing the working principle of an SECM experiment in operando SG-TC mode for the OER.[444]

One of the first works in which OER is studied by SECM in the SG-TC mode was published in the early 2000s. Fushimi et al.[445] studied the anodic oxidation of a titanium electrode in acidic media and measured the simultaneously produced O_2 by conducting ORR at the SECM tip, a 10 μm diameter Pt UME. They found that OER preferentially takes place on Ti grains covered by a thin oxide film. Also, they could observe that the oxide film of twin grains is easily broken, becoming an active site. Some years later, in 2007, Kang and co-workers studied the oxidation process on a Ni electrode surface in alkaline electrolyte using SECM in the SG-TC mode, gaining insight into Ni surface transformations prior to the OER.[446] The tip was not polarized to directly collect the O_2 and the oxidation/reduction voltammetric profile of a Pt UME was used to determine the local pH changes near the Ni surface as a result of the electron-transfer processes occurring in the solid phase. The potential of the Ni substrate was swept to promote the formation of surface oxides and OER while the tip monitored the consequent transient pH variation near the substrate's surface.

Using this nonconventional SG-TC mode, the researchers could study the electrochemical oxidation of the Ni surface and determine the overpotential of the OER at the formed Ni oxidehydroxide electrocatalyst surface. The OER overpotential is used as a benchmarking parameter to compare the performance of different electrocatalysts and, therefore, its accurate determination is of paramount importance. Snook et al.[447] reported the use of the SG-TC mode to accurately indicate the OER overpotential for different Ni/$Ni(OH)_2$-based electrode materials. The capability of the SECM was demonstrated compared to macroscale cyclic voltammetry, which failed to discriminate between the Ni oxidation potential and the OER overpotential. SECM in the SG-TC mode was also employed to measure the overpotential of perovskites as OER catalysts such as $La_{0.6}Sr_{0.4}Fe_{0.6}Co_{0.4}O_3$, $La_{0.6}Sr_{0.4}FeO_3$, $La_{0.74}Sr_{0.2}Fe_{0.8}Co_{0.2}O_3$, and $La_{0.6}Sr_{0.4}FeO_3$.[448] A Pt UME was employed as SECM tip to monitor the evolved O_2 at the electrocatalysts surface and the high sensitivity and accuracy of the SG-TC-SECM mode was demonstrated by comparison with RuO_2 as internal standard. Figure 4a summarizes the principles of this strategy.[444] The accuracy in the determination of the OER overpotential was further improved.[448] On the one hand, microcavity electrodes (MCE) filled with the interrogated catalyst ($La_{0.6}Sr_{0.4}FeO_3$, $La_{0.74}Sr_{0.2}Fe_{0.8}Co_{0.2}O_3$, or $La_{0.6}Sr_{0.4}FeO$) to avoid the use of binders or other additives that may influence the overpotential. Also, a Pt nanotip was accurately and reproducibly positioned close to the catalyst surface using the shearforce-based constant distance mode of SECM (SF/CD-SECM). Double-barrel MCEs were developed, which allowed for the simultaneous study of the OER with the material of interest and a benchmark material like RuO_2, used as an internal standard. This approach ensures a fair comparison between the materials as the measurements are conducted under the same experimental conditions. Figure 4b shows the overlapping of the substrate and the tip signals versus the potential applied to the substrate, which accurately reveals the OER overpotential.

The investigation of different OER catalysts in the same experiment is of great interest to achieve a valid comparison and consistent benchmarking. SECM enables high-throughput investigations by rapidly screening electrocatalysts libraries with varying compositions or structures, all prepared on the same support. Nevertheless, some precautions need to be considered when using the SG-TC mode in high-throughput experiments with an array of samples since the overlap of the diffusion profiles between neighboring spots have to be avoided. In the specific case, the tip current would be a consequence of the O_2 produced by surrounding spots under investigation, thus misrepresenting the local activity and compromising the resolution. Bard and colleagues reported some strategies to mitigate this issue.[453] In 2008, Minguzzi et al. introduced a tip shield consisting of a gold layer deposited on the external wall of the SECM tip.[453] The tip Au shield was polarized along with the tip Au-UME to consume the oxygen coming from the neighboring spots and guaranteed the correct measurement of the OER activity of the underlying sample area. Experimental and simulation studies allowed for a successful screening of the OER activity of different combinations of mixed Sn–Ir oxides. Nevertheless, the fabrication of the shielded tip was tedious and time-consuming. For this reason, the same research group reported in 2015 a simpler strategy for the rapid screening of an array with similar mixed Sn–Ir oxides.[95] The new method was based on the application of a series of double-potential steps (up to 10) to the substrate, switching between potentials of OER activity and inactivity. The dual potential step is applied shortly to minimize the O_2 diffusion layer and thus the influence of the

https://doi.org/10.1021/acs.chemrev.2c00766
Chem. Rev. 2023, 123, 4972–5019

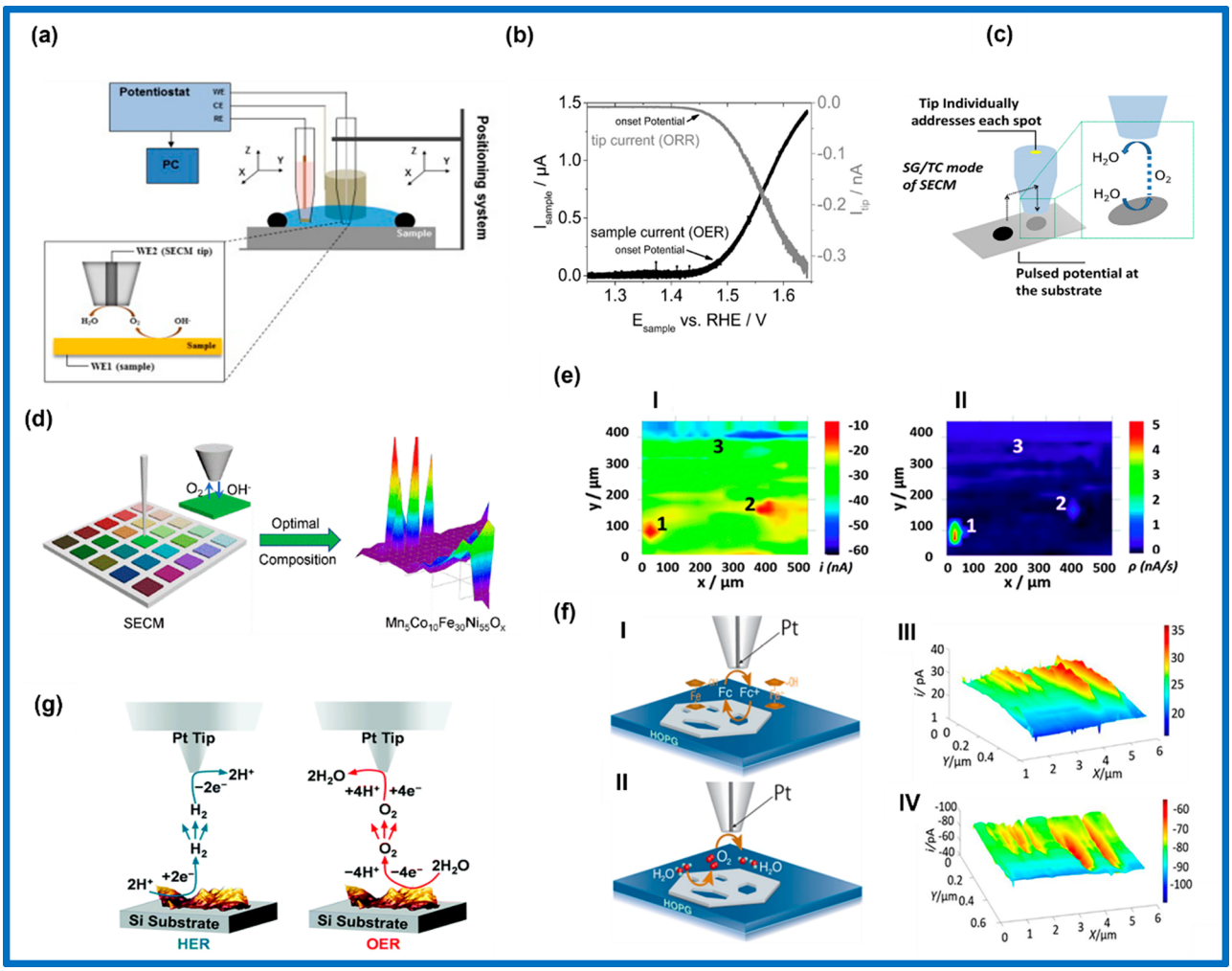

Figure 4. (a) Schematic representation of the SECM setup to study OER in operando conditions in the SG-TC mode. Reproduced with permission from ref 444. Copyright 2014 Elsevier. (b) Current−potential curves for microcavity electrodes filled with RuO_2. The sample current (black) and SECM tip current (gray) are plotted versus the applied potential (SECM tip: Pt disk electrode with 50 μm diameter, 0.1 M NaOH; ν = 1 mV/s). Reproduced with permission from ref 448. Copyright 2015 Elsevier. (c) Pictorial representation of the operando SG-TC-SECM methodology used (from black to gray, indicating different chemical compositions), based on a double pulse potential profile applied to the substrate. Reproduced from ref 95. Copyright 2015 American Chemical Society. (d) High-throughput investigation of an array of MnCoFeNi oxide samples with different compositions using SG-TC-SECM. Reproduced with permission from ref 449. Copyright 2022 Elsevier. (e) Characterization of an industrial DSA anode under OER conditions (E_{sub} = 0.700 V, E_{tip} = 0.400 V) with the noise mode of SG-TC-SECM: SG-TC mode image (I) and corresponding amplitude-by-frequency parameter image of the same electrode area (II). Reproduced with permission from ref 450. Copyright 2012 Royal Society of Chemistry. (f) Schematic representation of the experiments: (i) positive feedback produced by oxidation/reduction of ferrocenemethanol and (ii) SG-TC for oxygen detection at a NiO nanosheet. SECM imaging of NiO nanosheets with defect holes: (iii) feedback mode (III) and SG-TC mode SECM images of the same area of the NiO nanosheet (IV). The substrate was either at (III) open-circuit potential or (IV) biased at E_{Sub} = 0.9 V. Reproduced with permission from ref 451. Copyright 2019 PNAS. (g) Scheme of the SG-TC-SECM study of a nickel foam toward both HER and OER. Reproduced with permission from ref 452. Copyright 2020 Royal Society of Chemistry.

response from surrounding spots. A regular disk-shaped Au UME was employed as SECM tip, and the response is coaligned to the underlying electrocatalyst spot (Figure 4c). In a recent paper, Zhang et al.[449] conducted exhaustive high-throughput experiments by means of the SG-TC for rapid screening of a library of OER catalysts based on a Mn−Co−Fe−Ni multicomponent metal oxide system prepared by the inkjet printing in O_2-free 1 M KOH solution (Figure 4d). A potential program was used to accurately measure the OER activity using square wave voltammetry up to 0.7 V vs Ag/AgCl (OER activity) and alternating potentiostatic steps at 0.3 V vs Ag/AgCl (no OER activity), while the SECM Pt tip (10 μm) was polarized to detect the evolved O_2. Using this method, $Mn_5Co_{10}Fe_{30}Ni_{55}O_x$ was found to be the most active OER catalyst. It can be concluded that the SG-TC mode of SECM is a powerful tool allowing for high-throughput investigations of the OER properties of catalyst libraries under operando conditions. The formation of O_2 bubbles remains an intrinsic challenge in operando OER investigation as continuous bubbles formed on the surface electrically insulate the active sites. The blockage of the surface results in variations in activity, increased overpotentials, change in apparent solution resistance and leads to a localized convection effect.[454] Due to this issue, the SG-TC mode of SECM is generally limited to the investigation of the local electrocatalytic OER activity at low current densities to avoid the blockage of the surfaces (tip and sample). Chen et al.[455] reported an interesting example of an SECM study using the

https://doi.org/10.1021/acs.chemrev.2c00766
Chem. Rev. 2023, 123, 4972−5019

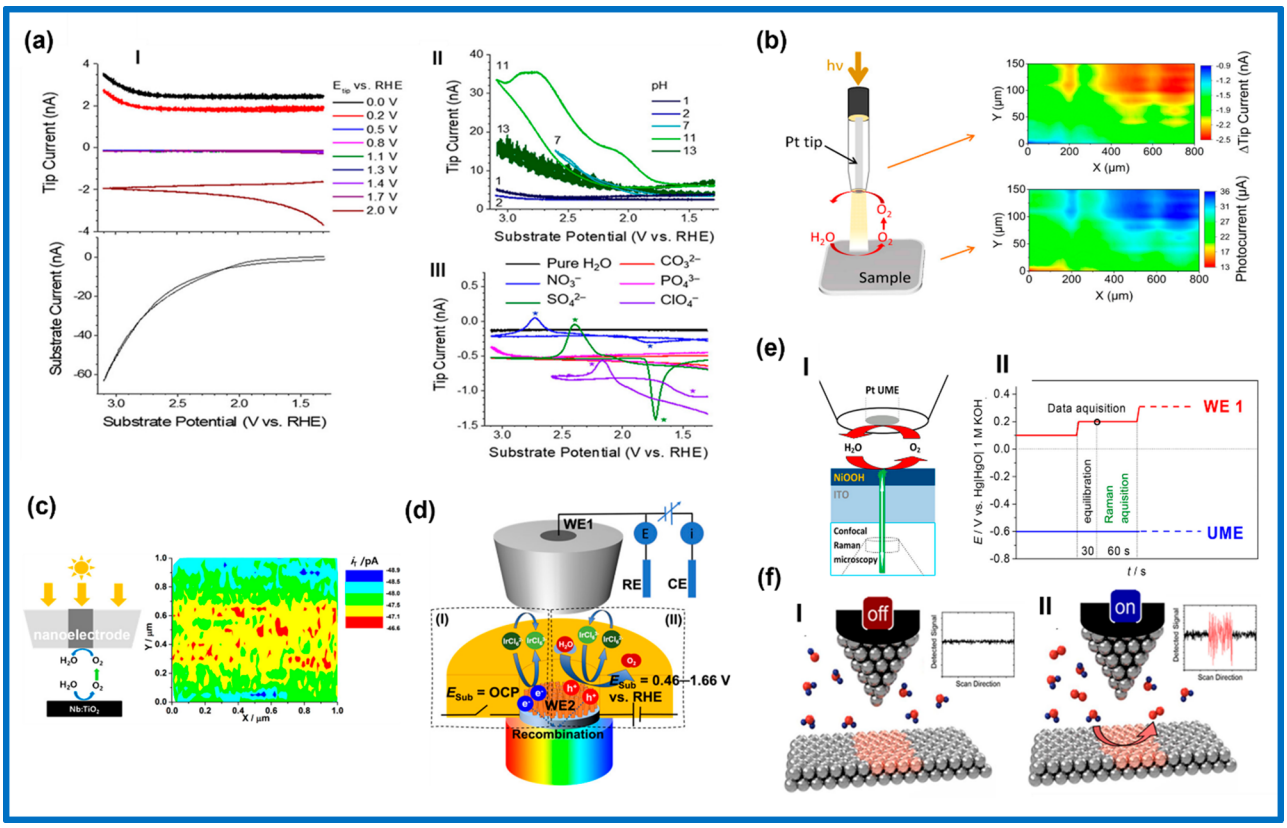

Figure 5. (a) SG-TC-SECM experiments with a BDD electrode during water oxidation: tip current responses at different tip potentials (top) corresponding to evolved products during voltammetric sweeps of the BDD substrate (bottom) (I). The electrolyte was 0.1 M sulfate, pH 2; the scan rate was 50 mV/s. Comparison of tip currents in 0.1 M sulfate electrolyte at various pH values with the tip biased to reduce oxygen at 0.0 V vs RHE (II). Comparison of collection currents in pure water and 0.1 M electrolyte, buffered at pH 11 for various electrolytes containing different anions. The tip was biased to collect ROS to 1.4 V vs RHE. Asterisks denote features on cathodic and anodic substrate scans (III). Reproduced with permission from ref 460. Copyright 2019 John Wiley and Sons. (b) Scheme of the through-tip illumination approach to perform SPECM experiments with high resolution. Reproduced from ref 196. Copyright 2017 American Chemical Society (c) Scheme of SG-TC-SECM to study the photoelectrochemical water oxidation at Nb-doped TiO_2 under through tip illumination (left), SECM OER reactivity map of a specific area of the 0.5% doped Nb:TiO_2 crystal in a 0.1 M phosphate buffer (pH 7). E_{Tip} = −0.9 V; E_S = 0 V vs $Hg/HgSO_4$ (right). Reproduced from ref 199. Copyright 2019 American Chemical Society (d) Schematic of the investigation of potential-dependent interfacial charge-transfer kinetics of PEC water oxidation at TiO_2 nanorods using SECM: reduction of $IrCl_6^{2-}$ by photogenerated electrons at OCP (I); simultaneous oxidation of water and $IrCl_6^{3-}$ by photogenerated holes when E_{Sub} = 0.46−1.66 V (vs RHE) (II). Reproduced from ref 461. Copyright 2021 American Chemical Society. (e) Scheme of the SG-TC-SECM combined with Raman data acquisition (left) and potential profile where the UME is held at a constant potential (−0.6 V) while the sample electrode (WE_1) is modulated with discrete potential steps in the positive direction. Reproduced from ref 462. Copyright 2017 American Chemical Society. (f) Scheme depicting the principle of n-EC-STM. (I) Without a reaction occurring ("off") the EC-STM signal is stable. (II) An ongoing reaction ("on") will increase the noise level of the STM signal. The noise is most distinct when the tip is placed over an active site compared to an inactive site. Reproduced with permission from ref 463. Copyright 2021 Elsevier.

operando SG-TC mode to interrogate the evolution of gas bubbles on the surface of OER catalysts, once the impact of bubbles formation and growth is a relevant feature. The authors studied the OER on RuO_2 and some industrial O_2-forming catalysts and used a Pt UME to measure the evolved O_2. The authors employed the so-called "'noise mode"' of SECM to investigate how O_2 bubbles were formed and departed from the surface. The noise of the tip current is used to deconvolute the contribution of the local formation of bubbles, correlated to the rate of oxygen evolution reaction.[450] Figure 4e presents an example of SG-TC-SECM images of OER activity (left) and the tip current noise (right) for the same area of an OER catalyst. The local formation of bubbles across the surface of the catalyst and their departure could be monitored, which is an influencing aspect of OER electrodes that should not be overlooked.

SECM in operando SG-TC mode has also been demonstrated to study the surface of OER catalysts. For example, Konkena et al.[456] used the SECM in the SG-TC mode to study OER electrocatalysis of $NiPS_3$@NiOOH core−shell heterostructures in an O_2-saturated 0.1 M KOH solution. By combining the SECM results with Raman spectroscopy, SEM, and XPS measurements, the high OER activity of the $NiPS_3$ nanosheets is attributed to a high density of accessible active metallic edges and defect sites due to a structural disorder. Sun et al.[451] demonstrated the capability of the spatial resolution of operando SG-TC-SECM to assess the local electrocatalytic OER activity of semi-2D NiO nanosheets. A spatial resolution of 15 nm was achieved by using a Pt nanotip. The FB mode with a ferrocene redox mediator was used to obtain topographic information (Figure 4f(I,III)) and SG-TC-SECM mapped the local OER activity to ascertain the higher activity of the edges (up to 200 times higher) as compared to the fully coordinated surfaces (Figure 4f(II,IV)). Note that the FB mode was employed to determine the topographic

https://doi.org/10.1021/acs.chemrev.2c00766
Chem. Rev. 2023, 123, 4972−5019

contribution and it is not related to the analysis of the OER electroactivity.

Additionally, the operando SG-TC mode of SECM has demonstrated its versatility for studying of different reactions in the case of bifunctional electrocatalysts. For example, Gao et al.[452] employed the SG-TC mode to investigate a Ni foam-based monolithic electrode with high performance for both HER and OER in neutral media. Figure 4g shows a scheme in which SG-TC-SECM was explored to correlatively study both the OER and HER. Other recent examples studying bifunctional electrocatalysts for the OER and ORR have been presented by Chakrabarty et al. and Lu et al., who used the SG-TC mode to investigate the local OER in alkaline media on flower-like $ZnCo_2O_4$ grafted onto reduced graphene oxide[457] and a Co−B,N,S−graphene composite at different temperatures,[458] respectively. Moreover, the SECM tip is not limited to the detection of evolved O_2 during the OER. Iffelsberger et al.[459] employed a Pt UME (25 μm) to monitor reactive oxygen species (ROS) evolved during water oxidation at Pt and boron-doped diamond (BDD) macroelectrodes in acid media (0.2 M $HClO_4$). Forced convection was enabled by high precision stirring to form a stable diffusion layer of electrochemically produced species and different ROS species. Counihan et al.[460] also employed this strategy to study water oxidation at a BDD surface in different electrolytes (Figure 5a). Besides O_2, the Au-UME tip was used to detect other evolved products like ROS. The OER products (O_2, H_2O_2, and ROS) can be selectively collected at the tip by carefully selecting the applied potential. The study indicated that the condition to evolve more reactive species is at pH 11 in sulfate, nitrate, and perchlorate electrolytes. Moreover, the results correlated the OER products with the chemical heterogeneity of the BDD surface. To characterize the surface, the surface interrogation mode of SECM (SI-SECM) was employed as a correlative measurement. The SI-SECM mode was able to quantify the surface coverage and the chemical characteristics of surface intermediates (mainly adsorbed OH).

SI-SECM provides relevant mechanistic and kinetic information, which is not easily accessible by other spectroscopic and voltammetric techniques.[137] The SI-SECM mode is widely employed for the study of OER electrocatalyst surfaces, because it enables the identification of different active sites within the same OER catalyst,[464] the quantification of short-lived reaction intermediates,[134,465] the detection of different surface metal oxidation states[466] and the calculation of kinetic rate constants of the active sites.[467] Nevertheless, the use of SI-SECM to interrogate the surface toward the OER, is not considered operando as the electrochemical modulation of the substrate surface and the signals registered from the tip are taken at separate times.

In parallel to the study of OER at TMOs, SECM has also been extensively employed in the study of photoelectrochemical systems. Local activity studies are generally performed by the operando SG-TC mode, whereby the generation of O_2 at photoanodes is monitored by ORR at the tip (Figure 5b), while the interrogated surface is illuminated.[196] In 2008, the Bard group introduced an operando SG-TC mode of SECM for rapid screening of photocatalysts arrays.[468] An optical fiber modified with a Pt-plated Au ring that locally illuminated the spots and the tip detected the evolved O_2 by performing ORR. The spots consisted of $BiVO_4$ and Zn-doped $BiVO_4$ with various ratios of Bi:V:Zn. Later the same strategy was used to study arrays of photoelectrocatalysts for water oxidation[469] in different $BiVO_4$-based systems containing various third element compositions, showing that the doping rate with 5−10% of tungsten noticeably enhanced the properties of $BiVO_4$ as photoanode. A similar approach was used to show the enhancement of the OER activity by depositing Pt and Co_3O_4 on a semiconductor film based on 5% W-doped $BiVO_4$ (BiVW-O).[470] However, the Au-coated optical fiber provided low lateral resolution in the photo-SECM analysis. The resolution was improved later by a simple and promising approach introduced by Conzuelo et al.,[196] where a light fiber was coupled to the backside of a 25 μm diameter Pt-disk UME. The SECM tip acted simultaneously as an electrochemical probe and a light guide, which minimized interferences from light screening, reflections, and scattering. The feasibility of this strategy was demonstrated by the investigation of n-type semiconductor-based photoanodes for water splitting such as $BiVO_4$, Mo-doped $BiVO_4$, and CoO_x on Mo-doped $BiVO_4$, all deposited on FTO, as well as sharp-edged TiO_2. Later, the group of Mirkin reported nanoscale resolution using the through-tip illumination approach.[199,408] Water oxidation at a 0.5% Nb-doped:TiO_2 rutile (110) single crystal photoelectrocatalyst (Figure 5c). In the work by Sarkar et al.,[471] the same method was employed to study the photoelectrochemical water oxidation of TiO_2 nanorods. Interestingly, they used a TEM finder grid as conductive support, which allowed complementing the local photo-SG-TC-SECM findings with the atomic-scale structural and bonding information obtained by transmission electron microscopy (TEM), to address the limitations in the SPECM resolution. Despite the nanoscale resolution achieved, one limiting issue was still the mechanical interaction of the rigid optical fiber during the tip motion. In a recently published paper, Askarova and colleagues[472] have reported an improved experimental setup in which the tip is mechanically decoupled from the fiber and the light is delivered to the back of the tip capillary using a complex lens system, with no significant losses in intensity.

Li and Pan[461] published a study using the SECM with three modes of SPECM (FB, RC, and SG-TC) in operando conditions to study the properties of TiO_2 nanorods coated on FTO as photoanode toward photoelectrochemical water oxidation. The FB mode and RC modes were used to study the interfacial charge-transfer kinetics using the redox mediator $IrCl_6^{2-}/IrCl_6^{3-}$. The SG-TC mode was employed to study the OER activity of the substrate by detecting O_2 with the Pt UME tip. Figure 5d provides a graphical summary of the investigation conducted, with a scheme for each one of those different processes. A paper recently published by Iffelsberger, Ng, and Pumera utilizing the SG-TC-photo-SECM is worth noting.[473] Photoelectrocatalysis of TiO_2 toward different reactions of interest like OER, HER, and the chlorine evolution reaction (CER) were studied. Cyclic voltammograms were registered at the TiO_2-modified substrate to select the potential windows where the different reactions take place. Simultaneously a Pt UME (25 μm diameter) was polarized to specific potentials to convert the corresponding species: H_2, O_2, Cl_2, or ROS. In addition to the local analysis, activity maps were registered, with and without illumination, for the different reactions by selectively applying potentials at the substrate and monitoring the corresponding product at the polarized tip. This SG-TC study concluded important findings, such as a heterogeneity of the activity and selectivity of the TiO_2 surface despite the apparently uniform composition according to the morphological characterization. Illumination dramatically

https://doi.org/10.1021/acs.chemrev.2c00766
Chem. Rev. 2023, 123, 4972−5019

Table 3. Summary of Experimental Conditions Made in OER Studies with SEPMs

SEPM	mode	substrate for OER	tip	tip reaction	ref
SECM	SG-TC	polycrystalline Ti	Pt disk UME (Ø, 10 μm)	ORR	445
SECM	SG-TC	Ni	Pt disk UME (Ø, 100 μm)	pH sensor: $Pt + OH^- \rightarrow PtOH + e^-$ $PtOH + OH^- \rightarrow PtO + H_2O + e^-$	446
SECM	SG-TC	Ni-based materials and $Ni(OH)_2$ graphite, glassy carbon, ITO	Pt disk UME (Ø, 10 μm)	ORR	447
SECM	SG-TC	$La_{0.6}Sr_{0.4}Fe_{0.6}Co_{0.4}O_3$ and RuO_2	Pt disk UME (Ø, 25 μm)	ORR	444
SECM	SG-TC	different perovskites $La_{0.6}Sr_{0.4}FeO_3$, $La_{0.6}Sr_{0.4}FeO_3$, $La_{0.74}Sr_{0.2}Fe_{0.8}Co_{0.2}O_3$, and RuO_2 in double-barrel microcavity electrodes (Ø = 100 μm)	Pt disk UME (Ø, 50 μm)	ORR	448
SECM	SG-TC	array of $Sn_{1-x}Ir_xO_2$ mixed oxides (x = from 0 to 1)	Au disk UME (Ø, 100 μm) shielded with an outer Au layer	ORR	453
SECM	SG-TC	array of $Sn_{1-x}Ir_xO_2$ mixed oxides	Au disk UME (Ø, 100 μm)	ORR	95
SECM	SG-TC	Mn−Co−Fe−Ni multicomponent metal oxides in an array of FTO as substrate $Mn_5Co_{10}Fe_{30}Ni_{55}O_x$ as the best OER performing material	Pt disk UME (Ø, 10 μm)	ORR	449[a]
SECM	SG-TC (noise mode)	RuO_2 O_2-evolving industrial catalyst	Pt disk UME (Ø, 25 μm)	ORR-current noise measurement at the tip due to gas bubble departure	455
SECM	SG-TC	$NiPS_3$@NiOOH core−shell heterostructure	Pt disk-nanoelectrode	ORR	456
SECM	SG-TC	NiO nanosheets on HOPG	Pt disk-nanoelectrode (Ø, 80 nm)	ORR	451*a*
SECM	SG-TC	Ni foam-based monolithic electrode	Pt disk UME	ORR/HOR	452[a]
SECM	SG-TC (OER)	Co−B,N,S−graphene composite	Pt disk UME (Ø, 25 μm)	ORR	458[a]
SECM	SG-TC	flower-like $ZnCo_2O_4$ grafted onto the reduced graphene oxide	Pt disk UME (Ø, 25 μm)	ORR/(H_2O_2 oxidation)	457[a]
SECM	SG-TC	Pt BDD	Pt disk UME (Ø, 25 μm)	ORR (E_{tip} = 0.3 V vs Ag/AgCl) ROS reduction (E_{tip} = 1 V vs Ag/AgCl)	459[a]
SECM	SG-TC SI (no operando)	polycrystalline BDD	Au disk UME (Ø, 25 μm) Pt disk UME (Ø, 25 μm)	ORR (0.0 V vs RHE) $H_2O_2 \rightarrow O_2$ (>1.0 V vs RHE) ROS reduction (0.4−1.4 V vs RHE)	460[a]
SPECM	SG-TC	$BiVO_4$ Zn-doped $BiVO_4$ (different ratios Bi:V:Zn)	Pt-plated Au ring optical fiber ring diameter = 275 μm	ORR redox couple: $[Fe(CN)_6]^{3-} + e^- \rightarrow [Fe(CN)_6]^{4-}$ E° = 0.45 V vs Ag/AgCl	468
SPECM	SG-TC	$BiVO_4$-based photocatalysts containing various third element compositions	Pt-plated Au ring optical fiber ring diameter = 275 μm	ORR	469
SPECM	SG-TC	Pt and Co_3O_4 supported on 5% W-doped bismuth vanadate film	Pt-plated Au ring optical fiber ring diameter = 275 μm	ORR	470
SPECM	SG-TC	$BiVO_4$ Mo-doped $BiVO_4$ CoO_x on Mo-doped $BiVO_4$ sharp-edged TiO_2	Pt disk UME (Ø, 25 μm) through-tip illumination	ORR	196
SPECM	SG-TC	0.5% doped Nb:TiO_2 (110) rutile single crystals	Pt (Ø, 580 nm) through-tip illumination	ORR redox couple: $FeMe(OH)^+ + e^- \rightarrow FeMe(OH)$ $E^{\circ\prime}$ = −0.2 V vs $Hg/HgSO_4$	199[a]
SPECM	SG-TC	TiO_2 nanorods supported on a conductive (Au) TEM grid	Pt (Ø, 115 nm) through-tip illumination	ORR	471[a]

https://doi.org/10.1021/acs.chemrev.2c00766
Chem. Rev. 2023, 123, 4972−5019

Table 3. continued

SEPM	mode	substrate for OER	tip	tip reaction	ref
				redox couple: $FeMe(OH)^+ + e^- \rightarrow FeMe(OH)$ $E^{\circ\prime} = -0.2$ V vs $Hg/HgSO_4$	
SPECM	SG-TC	$BiVO_4$ 0.5% doped Nb:TiO_2 (110) rutile single crystals	Pt (Ø, 110 nm) through-tip illumination decoupled from scanning by a system with lenses	ORR redox couple: $FeMe(OH)^+ + e^- \rightarrow FeMe(OH)$ $E^{\circ\prime} = -0.2$ V vs $Hg/HgSO_4$	472[a]
SPECM	SG-TC FB RC	TiO_2 nanorods-coated FTO UMEs (Ø = 25 μm)	Pt disk UME (Ø, 25 μm)	ORR redox couple: $IrCl_6^{2-} + e^- \rightarrow IrCl_6^{3-}$ $E^{\circ} = 0.68$ V vs Ag/AgCl	461[a]
SPECM	SG-TC	TiO_2	Pt disk UME (Ø, 25 μm)	ORR	473[a]
Raman/SECM	SG-TC	Ni and Ni/Fe thin films	Pt	ORR	462
AFM/SECM	SG-TC	polypyrrol intercalated in NiFe-LDH deposited on Au-on-Si	Pt-coated nanoelectrode tip (Ø, ∼25 nm)	ORR	474[a]
SECCM/optical probe	SECCM/UV source	TiO_2 nanotube	SECCM capillary (Ø, 20−100 nm)	photocurrent due to OER occurring at the sample surface.	364[a]
EC-STM	noise mode	highly oriented pyrolytic graphite (HOPG)	ripped Pt/Ir alloy wire (Pt_{80}/Ir_{20}); insulated with Apiezon wax	tunneling current	53[a]
EC-STM	constant tip potential	cobalt oxide on Au(111)	W STM tip insulated with Apiezon wax	tunneling current	475[a]
EC-STM	noise mode	Ir oxide layer after anodically annealed Ir(111) single crystal	ripped Pt/Ir alloy wire (Pt_{80}/Ir_{20}); insulated with Apiezon wax	tunneling current	463[a]

[a]Works published in the last 5 years.

https://doi.org/10.1021/acs.chemrev.2c00766
Chem. Rev. 2023, 123, 4972−5019

changes the selectivity of the competing oxygen and chlorine evolution reaction. The capabilities of the SG-TC mode of SECM as well as the correlative SG-TC and FB modes in SPECM measurements were demonstrated to interrogate materials with respect to the OER in a high-throughput mode. Additionally, the SG-TC-SECM mode has also been combined with other techniques to study the OER, providing spectroscopic or morphological information during the reaction or, in other words, in operando conditions. Steimecke et al.[462] reported a Raman/SECM methodology to investigate OER at Ni and Ni/Fe thin-film electrodes deposited on ITO in 0.1 M KOH solution. During the OER, a UME was placed closely above the substrate to detect the evolved O_2, while a Raman microscope probed the same spot from below (Figure 5e).[462] The authors were able to obtain information about the OER activity and the structural changes tof the materials during the reaction. In 2021, Ju and collaborators[474] used the SG-TC-SECM mode coupled with AFM to study the effect on the OER electrocatalysis caused by intercalating polypyrrole (ppy) in a NiFe-layered double hydroxide (NiFe-LDH). A Pt-nanoelectrode tip detected O_2 while OER was conducted at the substrate. At the same time, the topography was visualized by AFM, which permitted to decouple the topographic and electrochemical information. The combination of both techniques allowed to demonstrate that the as-prepared NiFe-LDH-ppy exhibited a twice as high catalytic current density than the bare NiFe-LDH.

Most SEPM techniques used to study the OER under operando conditions are based on SECM, particularly on the SG-TC mode. Recently, SECCM was coupled to a UV radiation source to probe the photoelectrochemical reactivity of TiO_2 nanotubes toward the OER. The operando SECCM measurements were performed under dark and light conditions to reveal photoelectroactive sites of the photoanode material. The high-resolution SECCM maps did not show a clear difference between the reactivity on the top and wall regions TiO_2 nanotubes. However, this work demonstrated the capability of coupling a method for modulating the surface activity while simultaneously using SECCM to monitor the differences in the OER activity.[364] To the best of our knowledge, SICM has not been used for the investigation of the OER in operando conditions. We understand that the reason is due to the intrinsic limitation of SICM of not being operando by default. Several works have been published in recent years based on the operando EC-STM technique. Stumm et al.[475] investigated the structural properties of layered cobalt oxides on Au(111) in a potential window from OCP to the OER region by EC-STM. EC-STM is proved capable of providing structural information with high resolution directly under potential control. Hence, such measurements are considered operando studies since the EC-STM images are registered while a potential is applied to the substrate. Combining the results of EC-STM with cyclic voltammetry and EC online inductively coupled plasma mass spectrometry; the structure, mobility, and stability of a material can be analyzed. Kluge et al. reported for the first time the suitability of the noise mode of EC-STM under reaction conditions ("noise" or n-EC-STM) to study electrochemical reactions.[53,428] For example, n-EC-STM was employed to study the OER activity of an amorphous iridium oxide surface, which is formed during the electrochemical cycling of an Ir(111) single crystal.[463] With this mode, active areas can be detected when the noise level of the STM signal increases, in contrast to the case of inactive sites (Figure 5f). An electrochemical reaction in the gap between the tip and the surface can locally and continuously rearrange the electrolyte structure and change its composition, which influences the tunneling barrier. By doing so, the authors could monitor local OER activity in operando conditions while analyzing simultaneously the surface morphology.

3.3. Investigation of HER Activity at the Substrate Surface

The hydrogen evolution reaction (HER) is a fundamental process in electrocatalysis that plays an important role in water electrolyzers, the chlor-alkali industry, and chlorate cells.[476] Furthermore, H_2 occupies a very important niche as an indispensable raw material in petroleum refining (hydrocracking and desulfurization), production of steel, aluminum, and ammonia (Haber Bosch process) as well as in the transformation of CO_2 into valuable chemical feedstocks. Besides the highest gravimetric energy density of H_2, HER has attracted great attention because the process yields highly pure H_2 (>99.999%) at fast production rates under mild reaction conditions, and it has a low pollution margin; thus HER is pegged as a potential alternative to fossil fuels.[477−480]

The HER is a classic example of a two-electron-transfer process where protons and water are reduced to H_2 in acidic and alkaline media, respectively. Mechanistically, HER involves three basic steps; the Volmer reaction, which results in the adsorption of a proton on the electrode surface, followed either by the Heyrovsky and/or the Tafel reaction to produce H_2.[477,478]

Although generally regarded as a fast reaction compared to the OER, the very slow kinetics of HER in alkaline media has revived a renewed interest to understand the fundamental parameters governing the reaction. In alkaline media, HER undergoes more complex steps of adsorption and dissociation of water in an environment full of hydroxyl (OH^-) disturbances. Furthermore, it is known that the HER kinetics strongly depends on the electronic properties of the electrode material and the nature of electrolyte used.[477] To this end, operando SEPMs come in handy as they provide a direct way to disclose the HER kinetics at active sites with high mass transport conditions, hard to achieve with others techniques.[477] Scheme 5 summarizes the strategy for HER studies with operando SEPM. Most works explored the strategy to perform HER on the catalyst surface while HOR is carried out by the SEPM tip.

The work by Selzer et al. is perhaps the earliest study to use SECM operated in the FB mode for the study of electron-transfer processes during proton reduction by methyl viologen radical cations at a Pt electrode, although not under operando conditions.[481] The same approach was used later to study HER kinetics at Au NPs,[482] Pd nanoparticles capped with 4-dimethylaminopyridine (Pd-DMAP),[483] and 2D assemblies of Pd on an inert support.[484] Although not conducted under operando conditions, these studies have contributed to the established framework presently used for HER investigations using SECM.[485] Initially, operando SECM use was applied to fundamentals studies of HER at platinum substrates. SECM was essential to achieve high mass-transport conditions to quantify kinetic parameters of the HER on microelectrodes, while the substrate was polarized to HOR. Zhou and co-workers[486] used the operando SECM to calculate the H_2 oxidation rate on Pt in the presence of adsorbed halide anions. Zoski[487] employed the same approach to calculate HOR

https://doi.org/10.1021/acs.chemrev.2c00766
Chem. Rev. 2023, 123, 4972−5019

Scheme 5. Schematic Drawing Representing the Main Operando SEPM Configurations for HER Interrogation[a]

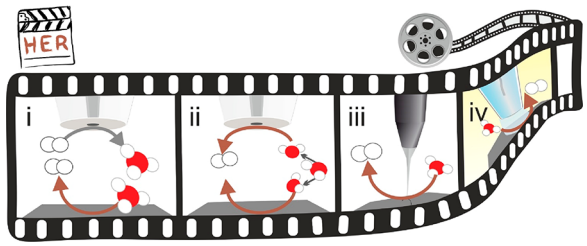

[a]The SEPM tip is employed as spectator while the catalyst is modulated to perform HER (brown arrow): (i) SG-TC-SECM case, where the tip oxidizes the H_2 (HOR, gray arrow); (ii) HER is also performed at the SECM tip; (iii) EC-STM mapping of a polarized surface; (iv) evaluating the electroactivity of semiconductors towards HER in dark and light conditions by SECCM.

kinetic parameters at Pt and Ir. Later, Fernandez and co-workers[488] detailed the use of SECM to reveal the potential-dependence transition between Volmer–Tafel and Volmer–Heyrovsky steps and mechanistic routes on Pt and Au SECM tips. Leveraging this framework, Li and colleagues reported the kinetics of HER at newly identified active sites that consist of S vacancies on the basal plane of MoS_2, by utilizing two approaches of SG-TC mode in tandem with finite difference method (FDM) modeling. In the first experiment, the MoS_2 substrate potential was swept from 0 V to −0.7 V vs Ag/AgCl to generate hydrogen continuously, and the hydrogen was then oxidized at a Pt SECM tip. In the second study, the substrate potential was switched between the open circuit potential (OCP) and the negative potentials for the HER by dual-potential pulses. Figure 6a,b shows schemes of the adopted strategy using the SG-TC setup and the complementary simulation for the spatial distribution of the hydrogen concentration.[485] The reliability of the SECM measurement were confirmed by making four replicates of the experiment on the same substrate, and complementary measurements using a three-electrode electrochemical compression cell. Results were found to be consistent despite variations in electrolytes and sample dimensions.[485] The same SG-TC strategy with a Pt SECM tip to oxidize the evolved hydrogen was used to study the HER activity at a MoS_x catalyst in a flow cell under flow and stationary conditions,[489] individual Au NPs (on HOPG/polyphenylene),[490] in situ growth of NiCoP grains on $Ti_3C_2T_x$ MXenes (NiCoP@MXene) supported on HOPG,[491] and active-metal frameworks ($Al_2(OH)_2$-TCPP and Cu-based MOF HKUST-1).[492]

Kund and co-workers fabricated a Pd-modified dealloyed Au–Ni microelectrode tip, which they used for the detection of H_2 under operando conditions at a Pt UME substrate during HER.[493] In this study, the tip potential was kept constant (2 V vs Ag/AgCl quasi-RE) to oxidize H_2 (HOR) while cycling the substrate potential (0.1 V to −1.2 V vs Ag/AgCl quasi-RE). Figure 6c,d is a schematic of a Pd-modified microelectrode positioned above the spot where H_2 is evolved and over an insulating surface as control measurement. The capability of the proposed probe for the quantification of H_2 at heterogenized Co-based HER catalysts under illumination was demonstrated.[493] Visibile et al. proposed the use of a cavity microelectrode modified with the studied materials in the TG-SC mode as a simple and fast method for screening different semiconductor materials (core–shell CuI/CuO_2 to estimate their efficiencies toward H_2 (or O_2) production under photocorrosion conditions.[494] When a photocathodic material was used, the potential of the Pt substrate was held constant at the value for hydrogen oxidation, while when a photoanodic powder was under study at the value for oxygen reduction. The tip potential was scanned by recording a LSV under pulsed illumination in the potential window specific to the material. The cavity, filled with the photomaterial of interest, produced either hydrogen or oxygen which was then detected by the underlying Pt substrate.[494] Jamali et al. successfully investigated the catalytic activity of photoreduced Pt particles on an immobilized multilayer assembly of unmodified photosystem I (PSI) from spinach toward the HER with the SG-TC mode.[495] During the imaging process, the tip and substrate were polarized at 0.0 V and −1.0 V vs Ag/AgCl, respectively. For the first time the potency of operando SECM to image the catalytic activity of photoreduced Pt particles on the surface of a photoactive protein film was demonstrated.[495] Asserghine and colleagues combined three detection modes to investigate the effect of cathodic polarization on the surface reactivity of a thin TiO_2 film toward the HER for biomaterial application. The FB, RC, and SG-TC modes as depicted in Figure 6e were used to acquire information on the interfacial electrochemical behavior at the substrate. The FB mode was used to monitor proton reduction and H intercalation into the TiO_2 film, and the SG-TC mode was used to monitor H_2 by its oxidation.[111] In another study the amperometric and potentiometric modes of SECM were combined to obtain correlative information about the corrosion of nitinol in saline solution before and after anodic polarization. The potentiometric mode was used to map the pH distribution in the electrolyte volume adjacent to the nitinol surface corresponding to the Ni^{2+} discharge.[29]

Very recently, Iffelsberger and colleagues used SPECM in the SG-TC mode to study HER and OER on 3D-printed Cu electrodes doped with Al_2O_3 (Al_2O_3/3DCu). Figure 6f is a schematic illustration of the setup used in the study. The SPECM HER images were recorded under illumination with a 365 nm light source to invoke HER or without illumination, and a Pt UME SECM tip biased at 1.06 V vs RHE was used to oxidize the substrate-generated H_2. Figure 6g,h shows the optical and SPECM images of the cross-section of the substrate during HER. The authors showed that the activity of the substrate is localized at the interface between the sintered Cu and the Al_2O_3 microcrystals.[496] Hill and co-workers[342,497] employed the operando optical source/SECCM (see Scheme 5iv) to correlate photocatalytic activity with the structure of p-type WSe_2. The high-resolution photocurrent maps revealed a high rate for HER in regions with short steps on the nanosheet. In another work, the SECCM tip was used to locally invoke micrometer-sized corrosion spots on a WSe_2 nanosheet. Afterward, operando SECCM photocurrent maps under intermittent illumination showed a high HER activity on the defect edges.

Operando EC-STM has also been used to shed light on the complex HER mechanism. Mitterreiter et al.[288] demonstrated that the edges of single MoX_2 flakes showed high catalytic activity for HER, whereas their terraces were inactive. The authors accomplished this by using EC-STM to visualize the activity of mechanically exfoliated, few-layer MoS_2 and $MoSe_2$ using a Pt/Ir alloy wire insulated with Apiezon wax as the EC-STM tip. Operated in the constant-current mode, EC-STM images were taken at different potentials from −0.60 to −0.90 V and −500 to −800 V vs Pt for MoS_2 and $MoSe_2$ layers,

https://doi.org/10.1021/acs.chemrev.2c00766
Chem. Rev. 2023, 123, 4972–5019

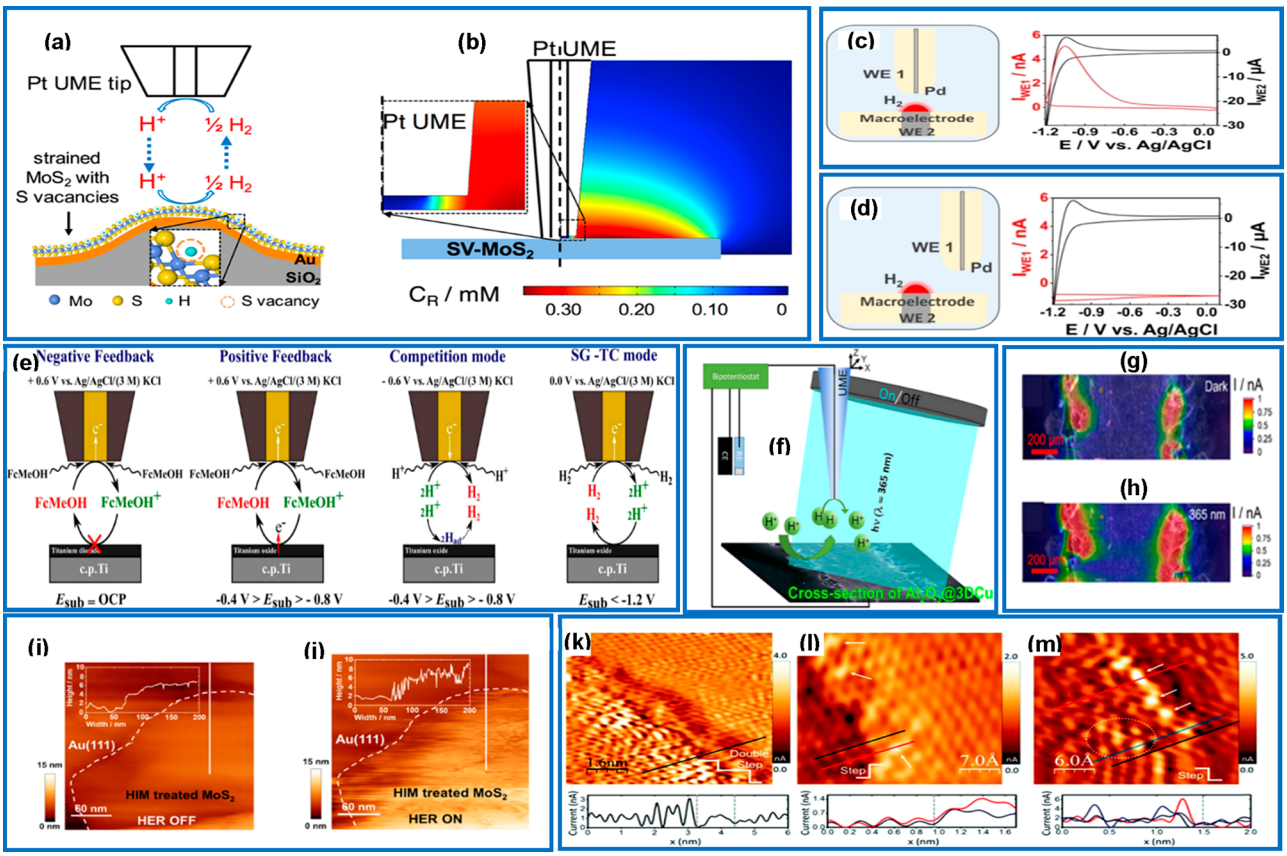

Figure 6. (a) Schematic of the SECM measurement setup for operation in the SG-TC mode. The top trapezoid represents a Pt UME tip, and the bottom a strained MoS_2 monolayer with S vacancies functions as the working electrode. H_2 is generated at the MoS_2 substrate through HER and subsequently collected and oxidized at the Pt UME tip through HOR, Schematic of the complementary COMSOL simulation for the spatial distribution of hydrogen concentration (CR/mM). The left side shows the tip and substrate 2D configuration used in the simulation. (b) Right side shows a representative calculated CR distribution (condition: SV-MoS_2 potential at −0.6 V and Pt UME tip potential at 0 V in 0.1 M $HClO_4$). Left inset: zoomed-in view of CR near the tip−substrate gap. Bottom inset: color bar of CR. Reproduced from ref 485. Copyright 2016 American Chemical Society. (c) Schematic of a Pd-modified microelectrode positioned at a second Pt macroelectrode; $i-t$ curve of H_2 absorption at the Pd microelectrode (red) was recorded for the duration of the cyclic voltammogram recorded at the Pt macroelectrode (gray); for clarity, the time axis is not plotted. (d) Schematic of a Pd-modified microelectrode positioned over the insulating sheath, $i-t$ curve H_2 absorption at the Pd-modified microelectrode (red) and cyclic voltammogram recorded at the Pt macroelectrode (gray). Reproduced with permission from ref 493. Copyright 2022 John Wiley & Sons, Ltd. (e) Schematic illustration of the FB, RC, and SG-TC detection modes. Reproduced with permission from ref 111. Copyright 2020 Elsevier. (f) Schematic illustration of the SPECM examination of the (photo)electrochemical HER at the cross section of a 3D Cu photoelectrode doped with Al_2O_3 as a refractory; composed optical and scanning (photo)electrochemical images of the cross section of an Al_2O_3/3DCu photoelectrode for the HER, (g) composed optical and SG/TC image of the HER without light and (h) with illumination. Reproduced with permission from ref 496. Copyright 2022 American Chemical Society. (i) EC-STM images of He ion-treated MoS_2 for the condition when HER is hindered (−600 mV, "HER off") and (j) when HER is provoked (−800 mV, "HER on"); high-resolution n-EC-STM measurements on HOPG for HER "on" conditions. Reproduced with permission from ref 288. Copyright 2019 Springer Nature. The positions of the line scans below the images are marked in the main image as lines of the corresponding color (black, red, or blue). (k) Active sites which show the highest tunneling currents (white color) are located in the vicinity of a step edge. In addition, the line scan confirms that the sites of the highest tunneling current are indeed located near the step edge (marked by a gray line). (l) Active sites are detected with even higher resolution, confirming their location near step edges. The line scans below indicate the second honeycomb away from the step edge being active, active sites are detected near the defective area, i.e., a deviation from the perfectly ordered carbon lattice (marked by a white circle). (m) Line scan below compares an inactive (black) to an active (red) step edge. Besides, the noise level increase at the defect sites is shown in blue. Reproduced with permission from ref 499. Copyright 2021 Royal Society of Chemistry..

respectively. The setup allowed for a direct comparison of the HER activity at the edge sites and the basal planes. The authors also introduced lattice defects to the basal planes by bombarding large areas of the MoS_2 samples with accelerated He ions (30 keV), and Figure 6i,j compares the EC-STM data for different electrode potentials corresponding to the "HER off" (−0.60 V vs Pt) and "HER on" (−0.80 V vs Pt) conditions, respectively.[288] Kosmala and colleagues developed a method to extract quantitative information from the noise in the tunneling current which they successfully correlated to the faradaic occurrences at single atomic sites.[498] The substrates were made of a graphene monolayer covering either a (111)-oriented Pt single crystal (Gr/Pt(111)), or a few-monolayer Fe film on Pt(111) (Gr/Fe(n ML)/Pt(111)). Under operando conditions and using a tungsten wire as an STM tip, the authors monitored the nanoscale HER events occurring at the substrate in real-time with atomic resolution. They demonstrated that the macroscopic electrocatalytic activity as observed in standard LSV experiments did not only originate from the presence of the Gr/Fe interface, but also stemmed

https://doi.org/10.1021/acs.chemrev.2c00766
Chem. Rev. 2023, 123, 4972−5019

Table 4. Summary of Experimental Conditions Made in HER Studies with SEPMs

SEPM	mode	substrate for HER	tip	tip reaction	ref
SECM	SG-TC	MoS_2 catalyst	Pt disk UME (Ø, 25 μm)	H_2 oxidation	485
SECM	SG-TC	MoS_x catalysts	Pt disk UME (Ø, 25 μm)	H_2 oxidation	489[a]
SECM	SG-TC	Au NPs	Pt disk UME (Ø, 66 μm)	H_2 oxidation	490
SECM	SG-TC	NiCoP@Mxene on HOPG	Pt disk UME (Ø, 80 μm)	H_2 oxidation	491[a]
SECM	SG-TC and RC	$Al_2(OH)_2$-TCPP and Cu-based MOF HKUST-1	Pt disk UME (Ø, 10 μm)	H_2 oxidation	492[a]
SECM	SG-TC	Pt, Co-based HER catalysts	Pd-modified dealloyed Au−Ni microelectrodes	H_2 detection	493[a]
SPECM	TG-SC	core−shell CuI/CuO, CuI and TiO_2 in cavity (modified tip)	cavid-filled Au (Ø, 25 μm)	H_2 or O_2 evolution	494[a]
SECM	SG-TC (not mentioned in paper)	photoreduced platinum particles (on PSI)	Pt disk UME (Ø, 2 μm)	H_2 detection (oxidation)	495
SPECM	SG-TC	Al_2O_3/3DCu	Pt disk UME (Ø, 25 μm)	H_2 oxidation	496[a]
SECM	SG-TC	AuNPs (on HOPG/polyphenylene)	Pt disk nanoelectrode (Ø, 120 nm)	H_2 oxidation	80
SECM	FB, RC, and SG-TC	thin TiO_2 film	Pt disk UME (Ø, 25 μm)	H_2 oxidation	111[a]
SECM	SG-TC	nitinol	Pt disk UME (Ø, 30 μm)	H_2 oxidation	29[a]
SECCM/ optical probe	SECCM/light source	WSe_2 nanosheet	SECCM capillary (Ø, 200−300 nm)	photocurrent due to HER on the sample surface	497[a]
SECCM/ optical probe	SECCM/light source	WSe_2 nanosheet	SECCM capillary (Ø, 500 nm)	photocurrent due to HER on the sample surface	342[a]
EC-STM	constant-current mode	MoS_2 and $MoSe_2$ Flakes	ripped Pt/Ir alloy wire (Pt80/Ir20)	tunneling current	288[a]
EC-STM	constant-current mode	Gr/Fe (0.6 ML)/Pt(111)	W wire	tunneling current	498[a]
n-EC-STM	constant-current mode	HOPG	ripped Pt/Ir alloy wire	tunneling current	499[a]

[a]Works published in the last 5 years.

from defects like carbon vacancies filled by iron atoms, and bent Gr layers covering metal step edges.[498] Kluge et al.[499] employed the n-EC-STM technique[427] to study undoped HOPG under HER conditions and showed that HER activity was due to step edges and defects rather than defect-free terraces. The authors augmented their experimental results with DFT calculations to determine the energetics of hydrogen adsorption at these sites. Figure 6k−m shows the high-resolution n-EC-STM measurements on HOPG for HER "on" conditions.[499]

3.4. Investigation of CO_2RR Activity at the Sample Surface

The electrochemical reduction of CO_2 (CO_2RR) into value-added chemicals using renewable electricity is considered a promising approach to decrease CO_2 emissions, an eco-friendly alternative to fossil fuels as the feedstock of chemicals, and also solve the intermittency challenge of renewable electricity generation.[500−502] As an added advantage, the electrochemical CO_2 reduction process can be controlled by adjusting the applied potential and proceeds under ambient temperature and pressure.[503] These factors make scale-up applications of this technology accessible.

The CO_2RR is a multielectron cathodic reaction comprising coupled multielectron/multiproton transfer pathways and generally follows three key steps:[503−505] the first is the chemisorption of CO_2 at the surface of the electrocatalyst, followed by the activation of the molecule by migration of electron and/or proton with subsequent cleavage of the C−O bond and/or formation of C−H bonds (or intermediates). The final step involves the rearrangement or coupling of the intermediates to form products and their subsequent desorption from the surface of the electrocatalyst. Although great research attention is given to CO_2RR, unravelling the pathways of the process remains a task to be achieved.[503] Among the main reactions discussed in this review (ORR, OER, and HER), the CO_2RR is the most complicated reaction. Whereas the CO_2RR reaction pathway to C_1 products (CO, CH_4, $HCOO^-$, and CH_3OH) is simple and well established, that of multicarbon or C_{2+} products (C_2H_4, C_2H_5OH, CH_3COOH, n-C_3H_7OH, etc.), which are known to possess higher volumetric energy densities and are key organic synthons for the synthesis of long-chain hydrocarbon fuels and oxygenates, is complex and remains ambiguous.[503] The probable factors for the high difficulty in the selectively of CO_2 to C_{2+} products are the high energy barrier of the $CO_2^{\bullet-}$ intermediate formation which is believed to be the key intermediate of the first step; competition between the C−C bond, and C−H and C−O bond formations; multiple coupling steps of electrons and protons; deactivation of catalysts by intermediates, byproducts, and impurities from the electrolyte; and the competitive HER. Furthermore, the much lower energy efficiency and partial reduction of the current density observed for C_{2+} products are stalling the practical application of CO_2 conversion to C_{2+} products technology in commercial electrolyzers[506] For a detailed discourse on the CO_2RR mechanism, the reader is hereby directed to some good reviews.[500,503,506]

Considering the bottlenecks, the goal of research has been to prepare electrocatalysts that can facilitate the CO_2RR at low overpotentials, and selectively generate desirable products at high current densities over sustained periods, while avoiding the formation of unwanted byproducts.[507] So far, Cu-based materials remain the only known electrocatalysts which are close to fitting the criterion concerning the formation of C_{2+} products with acceptable efficiency, although an overpotential of almost 1 V is required and a quite broad mixture of major and minor products are formed during the CO_2RR.[507,508] Recent efforts to optimize CO_2RR electrocatalysts have generally involved exploring a variety of material compositions and morphologies as well as experimental conditions. For example, the effects of transition metal catalysts,[509] alloying,[510]

https://doi.org/10.1021/acs.chemrev.2c00766
Chem. Rev. 2023, 123, 4972−5019

meso- and nanostructuring,[511,512] and electrolyte engineering[513] on the activity and selectivity of the CO_2RR process have been reported. Furthermore, theoretical approaches have been utilized to provide atomistic insights into the reaction mechanism and the nature of active sites (mainly on Cu), and in situ spectroscopic methods have been used to detect reaction intermediates during CO_2RR studies.[514,515] Despite these advances, the CO_2RR mechanism remains a difficult nut to crack, thus necessitating the urgency for advanced high-throughput electrochemical and electroanalytical techniques, that can probe the CO_2 reduction process as well as screen electrocatalysts, especially under reaction or operando conditions. As SEPMs have become powerful tools employed to demystify interfacial phenomena on electrocatalysts at reaction conditions and have afforded better insights into the surface structure, composition, and oxidation state, as well as adsorbed intermediates. Compared to the traditional RRDE and other conventional electrochemical approaches, SEPMs are the go-to techniques for high-throughput and high-precision measurement and have been used in CO_2RR investigations.[516] Generally, CO_2RR studies with operando SEPMs, involves polarizing a substrate (catalyst) to invoke the CO_2RR while a concurrently biased tip monitors the CO_2RR-induced changes at the interface, such as products or local pH changes. Scheme 6 summarizes the main operando SEPM approaches for investigating CO_2RR. The following paragraphs present state-of-the-art utilization of operando SEPMs as qualitative and/or quantitative electrochemical tools employed to probe interfacial dynamics during CO_2RR electrocatalysis. It is worth mentioning that the SECM is possibly the most explored technique for operando investigations in CO_2RR electrocatalysis.

Scheme 6. Schematic Drawing Representing the Main Operando SEPM Configurations for CO_2RR Interrogation[a]

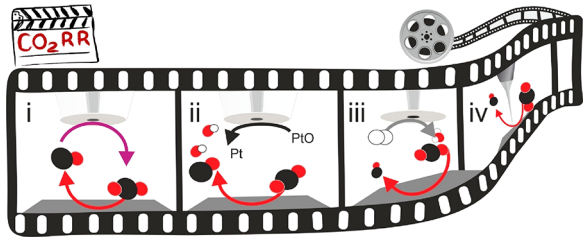

[a]The catalyst is polarized to perform CO_2RR (red arrows), while the SEPM tip is positioned as a spectator, where the tip response depends on the actuator method. (i) SG-TC-SECM with the tip polarized to oxidize CO (CO_2RR product). (ii) SECM tip monitors the local OH^- activity variation using the Pt/PtO potential. (iii) SG-TC-SECM tip registers H_2 oxidation (gray arrow). (iv) EC-STM mapping of a polarized surface performing CO_2RR.

The work by Sreekanth and Phani,[516] in 2014 is perhaps the foremost operando SECM study that was conducted to unravel the interfacial processes on CO_2RR electrocatalyst. The authors used the SG-TC-SECM mode to monitor the selective CO_2 conversion to formate in CO_2-saturated $KHCO_3$ solution at metal electrodes (Au, Pd, Ag, and thin films of Hg and Bi deposited on GC) using a Pt UME as the SECM tip. During the study, the substrate was biased at potentials to reduce HCO_3^- and CO_2, while the Pt tip potential was cycled (−0.6 to 0.9 V vs Ag/AgCl/sat. KCl) to oxidize the substrate-generated products ($HCOO^-$ and CO). Figure 7a–d shows the scheme of the SECM setup, approach curves and the corresponding tip voltammograms registered during the polarization of a Au substrate. The local SECM interrogation showed that the reduction of bicarbonate resulted mainly in formate formation in CO_2-saturated $KHCO_3$ solution whereas at lower pH values (e.g., pH 6.8 and 6.5) and higher potential, CO_2RR produced only CO at the Au substrate.[516] The same SG-TC strategy was replicated in later studies to monitor the electrocatalytic activity of metal-free B-doped graphene,[517] to investigate the role of surface roughness and interfacial pH on product selectivity at Au substrates,[518] monitor the activities of Au, Cu, and Ag electrodes toward CO_2RR in nonmetal cation containing electrolytes,[519] to study the influence of electrolytes containing metal cations on the performance of a Au electrode,[520] and the performance of electrochemically reduced In_2O_3 to $In_0-In_2O_3$ composite[521] toward the CO_2RR.

Mayer et al. investigated the potential of SECM for electrocatalytic screening of Sn/SnO_x-based catalysts for the reduction of CO_2 to formate.[522] The authors employed SG-TC-SECM scans on an array composed of three Sn/SnO_x catalysts, with the substrate biased at a constant potential (−1.5 V vs Ag/AgCl) while recording the tip CVs (1.2 to −1.0 V vs Ag/AgCl). Figure 7e,f shows CV-SECM scans for a catalyst array at a substrate potential of −1.5 V vs Ag/AgCl. The authors recommended the combination of CV-SECM scans with local surface analysis techniques like XPS, to map local hotspots and compositional inhomogeneities on catalyst surfaces.[522] Kim et al. fabricated a Pt- and Sn-modified Pt SECM tip to selectively monitor the production of CO during the CO_2RR on highly dispersed Au NPs on carbon black (Au NPs/CB) substrate using the operando SG-TC-SECM mode. The substrate was polarized at cathodic potentials to induce the reduction of CO_2 while the tip was biased at +0.5 V vs SCE to oxidize the CO generated at the Au NPs/CB substrate. The authors noted that the SG-TC mode coupled with the electrochemical CO microsensor tip was an effective method for the detection of CO during CO_2RR at low overpotentials potential.[523] Monteiro and co-workers also employed a Pt UME tip and a functionalized gold SECM tip to probe CO and H_2 electrooxidation.[524] In this work, the pH evolution in the substrate diffusion layer was monitored during CO_2RR at a Au surface. Figure 7g,h is a scheme of the SG-TC mode employed to detect CO and H_2 and the functionalized Au UME used to measure the pH. The two peaks often observed during CO oxidation were due to diffusion limitation by CO and OH^-.[524]

All of the above-cited CO_2RR studies have been carried out in an aqueous phase. Aqueous-phase reactors, however, have some practical limitations that reduce conversion rates and energy efficiencies of the CO_2RR process.[525] The use of reactors that operate using CO_2 delivered to the cathode in the vapor/gas phase, such as those using gas diffusion electrodes (GDEs), have been successfully used to counterbalance the limitations of aqueous-phase reactors, where CO_2 is dissolved in the electrolyte.[525] GDEs are known to exhibit interconnected pore channels, which enable the formation of the triple-phase boundary between gaseous CO_2, liquid electrolyte, and solid catalyst, making the intraporous electrolyte modulations close to the CO_2RR sites very tantalizing.[525,526] In 2021, the first experimental report was published describing monitoring of the local OH^- and H_2O activities using a Pt nanoelectrode as SECM tip, which was positioned close to a Ag-based GDE during the CO_2RR (Figure 7i).[526] The authors achieved this by potentiodynamically cycling the positioned tip in a potential

https://doi.org/10.1021/acs.chemrev.2c00766
Chem. Rev. 2023, 123, 4972−5019

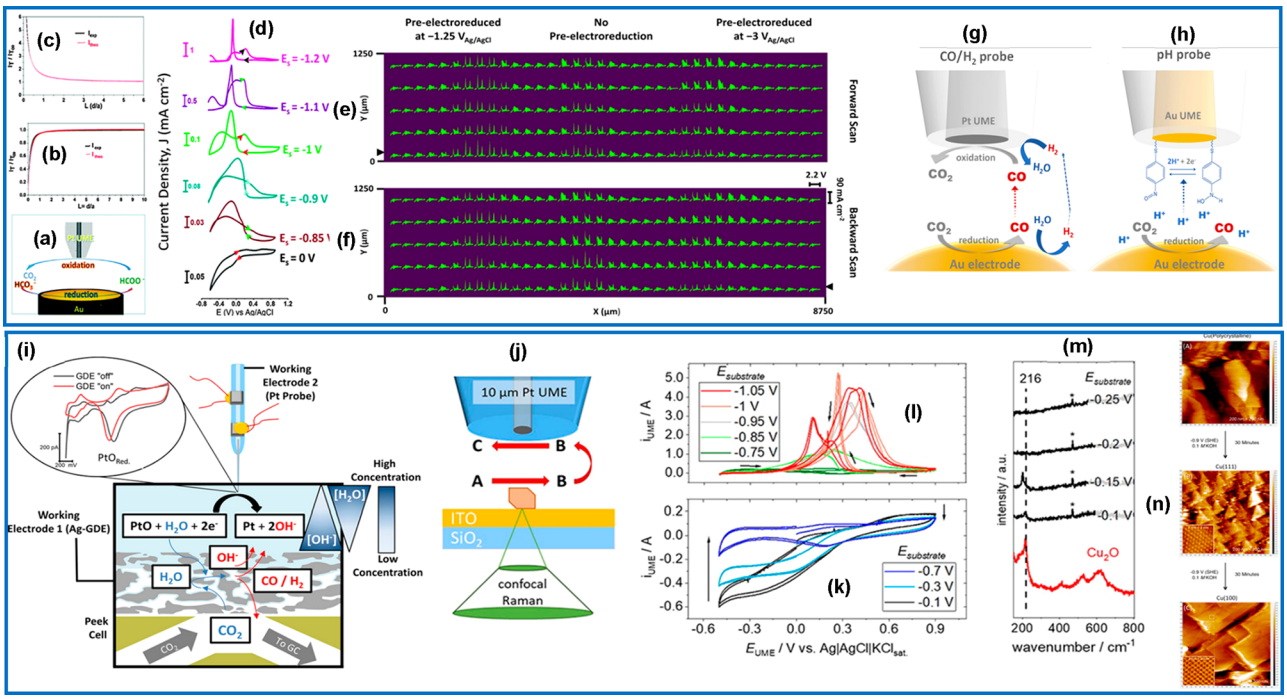

Figure 7. (a) Schematic of the SG-TC mode for CO_2/bicarbonate reduction−formate oxidation, (b) negative feedback, (c) positive feedback approach curves, (d) cyclic voltammetric responses of the Pt UME (10 μm)-tip to $HCOO^-$ generated at the Au substrate in 0.1 M $KHCO_3$. Reproduced with permission from ref 516. Copyright 2014 Royal Society of Chemistry. CV-SECM scans (tip scan rate: 0.05 V s^{-1}) for a catalyst array at a substrate potential of −1.5 V vs Ag/AgCl: (e) forward scan, (f) backward scan. The black arrow indicates the starting scan position of the tip. CV: scan rate 1 V s^{-1}, potential range: 1.2 to −1.0 V vs Ag/AgCl. Tip−substrate distance: 100 μm, tip scan rate 100 μm s^{-1}. Electrolyte: 0.1 M $KHCO_3$ saturated with CO_2 at atmospheric pressure, 293 K. Reproduced with permission from ref 522. Copyright 2020 Springer Nature. Schematic representation of the SG-TC mode (g) where a Pt-UME probes CO and H_2 while CO_2RR occurs on a Au substrate, (h) functionalized Au-UME used for monitoring pH changes. Reproduced from ref 524. Copyright 2020 American Chemical Society. (i) Local H_2O and OH^- activities modulated by the competing HER and CO_2RR are monitored using a precisely positioned Pt nanoelectrode. The PtO reduction peak potential changes with the different ion activities established inside the three-phase boundary of the GDE at varying reaction rates. Reproduced with permission from ref 526. Copyright 2021 John Wiley and Sons. (j) Setup of the Raman-coupled scanning electrochemical microscope, (k,l) selected cyclic voltammograms of the Pt UME in 10 μm tip-to-sample distance to the Cu_2O microcrystal at various substrate potentials ($E_{substrate}$ from −0.1 to −1.05 V); the arrows in (k) indicate the decrease of currents with decreasing substrate potential, whereas in (l), the curve progression is indicated for −1 V, (m) selected corresponding in situ Raman spectra, the asterisk indicates a peak from the quartz substrate. Reproduced with permission from ref 186. Copyright 2022 John Wiley and Sons. (n) Low-resolution (200 nm × 200 nm) and zoomed-in (2 nm × 2 nm) operando EC-STM images at −0.9 V in 0.1 M KOH. Experimental parameters: bias voltage = −300 mV. Tunneling current for low-resolution images = 2 nA; for high-resolution images = 5 nA. Reproduced from ref 530. Copyright 2014 American Chemical Society..

range between Pt oxide formation and Pt oxide reduction (0.60 to −1.1 V vs Ag/AgCl/3 M KCl), while the Ag-based GDE was kept at cathodic potentials to induce the CO_2RR. High turnover HER/CO_2RR at a GDE leads to modulations of the alkalinity at the local electrolyte/electrode interface.[526] The same shear-force-based tip positioning technique was used to simultaneously monitor pH changes and the topography with high resolution.[527] The SG-TC mode was used to study the effect of catalyst loading and CO_2 pressure on the activity of a Au GDEs toward CO_2 reduction to CO. During the experiment, the diffusion-limited CO oxidation current was constantly recorded at the positioned Au-nanoelectrode close to the GDE while the tip was scanned across the loading gradient. At the same time, the potential applied to the substrate and the CO_2 back-pressure was varied. This allowed for a detailed evaluation of the interplay between catalyst loading and CO_2 back-pressure with respect to the optimum performance of the studied GDEs. An optimum local catalyst loading was necessary to achieve high activities and the optimum loading also depended directly on the CO_2 back-pressure.[527] The same approach[527] was employed to study the activity and selectivity of Ag core/porous Cu shell NPs in a H-cell and a GDE cell configuration,[528] and to monitor the local OH^- ion activity of PTFE-modified GDEs of a series of metal−organic framework (MOF) derived $Cu_xO_yC_z$ catalysts.[529]

Recently, Steimecke et al.[186] combined SECM with Raman microscopy to investigate the activity of a single cuprous oxide microcrystal electrochemically deposited on a transparent ITO substrate (Cu_2O/ITO) toward CO_2RR. Figure 7j is a scheme of the Raman-coupled SECM setup that allowed Raman measurements from the backside of the ITO electrode while the SG-TC-SECM mode was run simultaneously. This setup allowed to simultaneously obtain electrochemical and spectroscopic information with high spatial resolution and as complementary data sets from the very same location of the electrode (Figure 7k−m). The Cu_2O/ITO substrate was continuously polarized from −0.1 to −1.05 V vs Ag/AgCl/KCl_{sat} (50 mV $step^{-1}$) to induce the CO_2RR while recording CVs at a Pt SECM tip which was biased potentiodynamically (20 mV s^{-1}) between −0.5 to 0.9 V vs Ag/AgCl/KCl_{sat} to detect the substrate-generated products. Raman spectra revealed that the reduction of Cu_2O crystal to Cu occurred when the substrate was polarized at −0.2 V vs Ag/AgCl/KCl_{sat}.

https://doi.org/10.1021/acs.chemrev.2c00766
Chem. Rev. 2023, 123, 4972−5019

Table 5. Summary of Experimental Conditions Made in CO_2RR Studies with SEPMs

SEPM	mode	substrate	tip	tip reaction(s)	ref
SECM	SG-TC	Au, Pd, Ag, and thin films of Hg and Bi on GC	Pt disk UME (Ø, 10 μm)	CO and HCO_2^- oxidation	516
SECM	SG-TC	B-doped graphene	Pt disk UME (Ø, 10 μm)	HCO_2^- oxidation	517
SECM	SG-TC	Au (varying roughness)	Pt disk UME (Ø, 10 μm)	CO oxidation	518[a]
SECM	SG-TC	Au, Cu, and Ag	Pt disk UME (Ø, 10 μm)	CO oxidation	519[a]
SECM	SG-TC	Au electrode	Pt disk UME (Ø, 50 μm)	CO oxidation	520[a]
SECM	SG-TC	$In_0-In_2O_3$ composites	Pt disk UME (Ø, 200 μm)	CO oxidation	521
SECM	SG-TC	Sn/SnO_x-based catalysts	Pt disk UME (Ø, 10 μm)	detection of $HCOO^-$, CO, and H_2	522[a]
SECM	SG-TC	Au NPs/CB	Pt- and Sn-modified Pt SECM tip (Ø, 76 μm)	CO oxidation	523[a]
SECM	SG-TC	Au UME	Pt- and Au-modified pH sensor	CO oxidation and pH monitoring	524[a]
SECM	SG-TC	Ag-based GDE	Pt nanoelectrode	CO oxidation and pH monitoring	526[a]
SECM	SG-TC (SF-SECM)	Au-based GDEs	Au disk UME (Ø, 2 μm)	CO oxidation	527[a]
SECM	SG-TC (SF-SECM)	Ag core/porous Cu shell NPs	Pt disk UME	reduction of PtO	528[a]
SECM	SG-TC (SF-SECM)	MOF-derived $Cu_xO_yC_z$	Pt disk UME (Ø, 1 μm)	reduction of PtO	529[a]
Raman-SECM	SG-TC	Cu_2O/ITO	Pt disk UME (Ø, 10 μm)	HCO_2^- and H_2O_2 oxidation	186[a]
EC-STM	constant current	Cu(pc)	W (Ø, 25 μm)	tunneling current	530
EC-STM	constant current	p-Cu and g-Cu	ripped Pt/Ir wire	tunneling current	532[a]

[a]Works published in the last 5 years.

The ITO electrode had no relevant contribution to the CO_2RR and as such can be a useful substrate material although its application as a transparent electrode material for optical probing was limited to potential values above −1 V vs Ag/$AgCl/KCl_{sat}$.[186]

SECM in the SG-TC mode has been the most employed SEPM methodology for the operando investigation of CO_2RR. Nevertheless, EC-STM was also used to study the interfacial dynamics of electrocatalysts. Kim et al. used operando EC-STM to investigate the Cu(100)-like behavior of polycrystalline Cu (Cu(pc)) during CO_2RR.[530] Previous investigations suggested that Cu(pc) exhibited Cu(100)-like behavior in that it generated ethylene as a major product.[531] The authors explain the unexpected product selectivity observed for Cu(pc) by operando EC-STM images (Figure 7n), demonstrating that during CO_2RR (at −0.9 V vs SHE, 0.1 M KOH) Cu(pc) facets undergo reconstruction to a pure single-crystal with a Cu(100) surface.[530] This study epitomizes the potency of operando studies to reveal the structure-composition-activity correlation sought after during electrocatalysis. Phan and colleagues also employed operando EC-STM to reveal the dynamics of the morphological evolution of polycrystalline Cu (p-Cu) and graphene-covered polycrystalline Cu(g-Cu) during the CO_2RR. The study unveiled a drastic reconstruction of p-Cu to nanocuboids at negative potentials and even in halide-free electrolytes. They also demonstrated the protective character of a single graphene layer on Cu against the massive reconstruction at operando conditions. Their results showed that Cu exhibited a similar intrinsic activity when normalized by the electrochemically active area which opens a new prospect to reinterpret the mechanism of nanostructured Cu-based materials without the presence of oxidized species or halides.[532]

3.5. SEPM Tip in the Investigation of Other Reactions for Electrolyzers and Bioelectrocatalysis Interests

In this section, we demonstrate the versatility and potency of operando SECM for the investigation of other important reactions. The electrochemical chlorine evolution reaction (CER) is a significant anodic reaction in chlor-alkali electrolysis.[533] Cl_2 gas is an important precursor for many crucial industrial processes including pharmaceuticals, polymer synthesis, pulp and paper, disinfectant production, and wastewater treatment.[533,534] Zeradjanin et al. employed operando SECM in the SG-TC and RC modes as an analytical tool to detect and visualize the local electrocatalytic activity of dimensionally stable anodes (DSA) toward the chlorine evolution from brine.[535] The same techniques were used later to monitor the local activity of CER on Ti−Ru−Ir mixed metal oxide DSA surfaces.[536]

Reactive intermediates play an important role in many electrochemical processes and SECM is well adapted to monitor their formation during electrocatalysis.[537] Chang and Bard reported the detection of the short-lived Sn(III) intermediate and the mechanism of Sn(IV)/Sn(II) electroreduction in bromide media by cyclic voltammetry and operando SECM.[538]

The Bard group employed the TG-SC mode to capture the unstable intermediate $CO_2^{\bullet-}$ to study the mechanism of CO_2RR. This demonstrates the capacity of the SECM to detect and characterize short-lived species which can dimerize, undergo disproportionation, and react with proton donors and even mild oxidants.[539] This work highlighted the advantage of SECM over fast-scan cyclic voltammetry for the study of fast reaction intermediates in that it helps to overcome the limitations of double-layer charging and adsorbed species observed in fast-scan CV. SECM allows for measurements at steady-state while transient currents from adsorbed species do not perturb the measurements. The biochemical and enzymatic

https://doi.org/10.1021/acs.chemrev.2c00766
Chem. Rev. 2023, 123, 4972−5019

activities of substrates have also been monitored by the SECM. Wijayawardhana et al. examined the biochemical activity of beads that were modified with antimouse antibodies using the SG-TC mode by oxidizing 4-aminophenol formed in the alkaline phosphatase-catalyzed hydrolysis of 4-aminophenyl phosphate at the surface of the beads, using a Pt microdisk electrode (10 μm diameter) as a SECM tip.[540]

Maciejewska and co-workers employed the SG-TC-SECM mode to monitor the localized enzymatic activity of enzyme/polymer spots made of resydrol and glucose oxidase on glass surfaces.[541] During the study, they evaluated the complex interplay between glucose and ascorbic acid in a glucose oxidase-based amperometric biosensor.[541] In a closely related study, the SG-TC mode was used to monitor the localized sensor response of glucose oxidase immobilized within a polymer matrix in a spot of about 300−400 μm diameter.[542] Karnicka et al. monitored the spatial distribution of the biocatalytic activity of bilirubin oxidase/Os-complex modified redox polymer toward ORR with RC-SECM.[107] Fernández et al. used the TG-SC-SECM to perform a high-throughput study on the ORR activity of arrays of "wired" bilirubin oxidase and laccase enzymes.[543] The arrays contained spots with different ternary mixtures of enzyme, cross-linker, and redox polymers, and the goal was to find the optimal composition. During the study, a 25 μm diameter Pt tip was polarized to produce locally O_2 by OER while the substrate was held at 0.3 and 0.4 V vs Ag/AgCl (3 M KCl) to trigger the enzymatic ORR activity of the different composites.

Operando SECM operating in the SG-TC mode was used to analyze the reaction mechanism of the electrooxidation of glycerol at copper surfaces in NaOH solutions. A potential sweep from 0 to 0.8 V vs Ag/AgCl was applied to the substrate for glycerol electrooxidation while the tip was kept constant at 0.2 V vs Ag/AgCl to monitor the formation of electroactive species, e.g., reduction of Cu(III) species.[544]

Chronoamperometry and micropipette delivery/substrate collection (MD/SC) mode of SECM was used to investigate the electrocatalytic activity of 5 different metallic nanoparticles (Pt_{100}, $Pt_{75}Pd_{25}$, $Pt_{50}Pd_{50}$, $Pt_{25}Pd_{75}$, and Pd_{100}) toward formic acid oxidation in the presence of simultaneous ORR.[545] The Au UME SECM tip was kept at a potential negative enough to perform ORR under steady-state conditions, and SECM images were collected at 3 different potential values, (0.3 V, 0.5 and 0.7 V vs RHE). The authors demonstrated SECM as a fast and powerful technique for studying the O_2 crossover effect in different electrocatalysts and for identifying highly selective electrocatalyst candidates for mixed-reactant fuel cells.[545]

Operando SECM operated in the SG-TC mode was employed to investigate substrate-generated H_2O_2 by using a highly stable and selective ultramicrosensor (made of Prussian Blue modified with films of iron and nickel hexacyanoferrates) as a tip. A Au surface was biased to generate H_2O_2 while the selective tip was employed for imaging the distribution of H_2O_2.[546] The RC and SG-TC modes were also applied to investigate the electrochemical activities of various AuPd compositions deposited onto ITO toward H_2O_2 and $FcMeOH^+$ reduction reactions.[547] Tomlinson et al. reported the first use of electrochemical imaging to identify the defect and defect-free areas in single crystal boron-doped diamond (BDD) electrodes. Intermittent contact SG-TC-SECM was successfully used to detect defects in single crystal BDD electrodes by measuring variations in the tip current in correlation with changes in the boron dopant levels in the materials.[548] Leonard and Bard reported a new TG-SC mode approach that allowed them to acquire information by the separation of partial currents at multireactional electrochemical interfaces, which they employed to study HER at a Mn tip.[101] During the measurement, the Mn tip potential was scanned from −1.5 to 0 V vs Ag/AgCl to invoke HER, while the substrate potential was held at +0.1 V vs Ag/AgCl to capture solely the tip-generated H_2 (HOR). By this approach, the authors investigated HER on the Mn surface, a reaction that has not been directly studied owing to the highly corrosive nature of Mn. The approach curve showed positive feedback for H_2 production at the tip and H_2 oxidation at the Pt substrate, and at very close distances, ∼100% collection efficiency was obtained, highlighting the powerful sensitivity of SECM measurements.[101] HOR electrocatalysts for fuel-cell applications have also been studied with SECM. Kim et al. studied the HOR activity of Pt NPs electrodeposited on highly oriented pyrolytic graphite (HOPG). They used the operando TG-SC mode to generate H_2 at the Pt-nanoelectrode tip (134 nm of diameter), while HOR was performed at the polarized substrate (Pt NPs on HOPG) with large effective rate constant (higher than 2 cm/s) caused by the effective mass transfer rate.[549]

The mechanism for the electrosynthesis of nanoparticles has also been probed using operando SECM. Miranda Vieira and co-workers employed operando SECM for the local electrosynthesis of Ag_2O nanocubes. The TG-SC mode was used to electro-generate Ag^+ at an anodic potential (+0.3 V) using a Ag sacrificial electrode as SECM tip while the substrate (Au electrode) was biased at a cathodic potential (−0.4 V) to induce ORR producing the OH^- needed for Ag_2O nanocubes formation. The nanocubes were also detected at the Au-UME substrate by nanoimpact coulometry using the electroreduction of Ag_2O to Ag.[550] This approach showed how electrochemical impact in SECM can be applied to reveal NP formation and growth mechanism.

Another interesting study that exemplifies the capability of operando SECM to study electrocatalytic processes was reported by He and co-workers, who studied the electrochemical reductions of NO_3^- to NO_2^- and NO_2^- to NH_3 on a $Cu-Co(OH)_2$ catalyst using various in situ characterization techniques including operando SECM. During the operando SECM measurements, the $Cu-Co(OH)_2$ catalyst substrate was polarized at −0.12 V (vs RHE) to trigger the NO_3RR while CV scans were carried out at the Pt-UME (SECM tip, diameter of ∼1 μm) between −0.12 and 1.58 V (vs RHE) to identify NO_2^- (at 0.06 V vs RHE) and NH_3 (at 0.76 V vs RHE).[551] The authors showed that the NO_2^- was selectively formed on the Cu layer and then diffuses to the near by $Co(OH)_2$ layer, where the NO_2^- is further reduced to NH_3.

The potential of FB mode SECM for investigating surface charge transfer properties of semiconductors used as photoelectrodes was introduced by Horrocks, Mirkin, and Bard already in 1994.[121,552] The substrate (biased or not) is illuminated to generate reactive charge carriers. A redox mediator in the electrolyte is converted at the polarized tip and the so-transformed species further interact with the photogenerated charge carriers of the substrate, giving a negative or positive feedback current as the tip response. The FB mode of SECM in these cases is interpreted as an operando tool since simultaneously reactive species generated at the substrate surface under illumination are indirectly monitored at the

https://doi.org/10.1021/acs.chemrev.2c00766
Chem. Rev. 2023, 123, 4972−5019

SECM tip. Such a strategy generates information about the surface processes that are directly correlated to photoelectrocatalysis, which occurs in a short time regime, highlighting the spatial and temporal capability of operando SECM investigation. Zhang and co-workers[553] used the FB mode to investigate the charge-transfer kinetics at the photoelectrode/electrolyte interface of the photocatalysts $BiVO_4$ and Mo-doped $BiVO_4$ using the redox couple $[Fe(CN)_6]^{3-}/[Fe(CN)_6]^{4-}$ as a mediator. The researchers concluded that the introduction of the Mo^{6+} ion into $BiVO_4$ can facilitate light-induced OER and suppress the interfacial back reaction at the photoanode/electrolyte interface. A similar approach was employed to study charge-transfer dynamics on the surface of $BiVO_4$ and $BiVO_4$/NiFe-LDH.[554] This work showed that the back transfer of electrons is suppressed when adding the NiFe-LDH cocatalyst onto the $BiVO_4$ semiconductor surface, explaining the enhanced water oxidation properties of the combined material.

4. SUMMARY AND FUTURE PROSPECTIVE

A comprehensive review of state-of-the-art advances made with SEPM to understand interfacial processes aims on demonstrating the versatility of SEPMs to probe the catalytic activity of various substrates, understand structure dynamics, establish structure/composition−activity−selectivity relations, and disclose reaction mechanisms. The potential of SEPM is shown through the various local studies conducted with SECM, SICM, EC-STM, and SECCM. The working principle of each SEPM technique, their scope of applicability, advantages, and limitations are discussed. In addition, the concept of operando SEPM is delineated, i.e., the use of the SEPM tip to probe local surface property changes while tailoring the surface reactivity independently with another method.

Furthermore, the use of operando SEPM to investigate electrocatalytic reactions (ORR, OER, HER, and CO_2RR) is presented systematically to demonstrate the extensive and exciting trajectory of operando SEPMs studies. In the application section, the uniqueness and utility of operando SEPMs have been portrayed in the many research studies that were reviewed. Beyond the general advantages of micro/nanoelectrochemistry, the use of operando SEPMs makes it possible to identify active sites, disclose reaction pathways, quantify reaction intermediates, and study the effects of the reaction environment on electrocatalytic processes. Moreover, the use of hybrid SEPM techniques for the extraction of additional information during the electrochemical reaction has been shown. Evidently, most operando SEPM studies were done using SECM and EC-STM, which are intrinsically operando SEPM techniques.

Although SECCM and SICM were not yet intensively explored for operando studies, the techniques have been shown as a powerful tool for local investigations in single-entity and sub-entity studies because of its high-resolution (some nm) and high-throughput features. However, the flexibility of the pipette-SEPM techniques still need improvement to allow easy and simultaneous coupling with other methods to enable operando investigations. We encourage the community on exploring operando SICM for charge mapping of electrodes surface, as well as the coupled SECCM-hybrid methods to investigate simultaneously single entity catalysts.

Finally, we advocate the incorporation of simulations and machine learning into general SEPM studies. This will pave the way for systematic benchmarking and design of electrocatalysts.

AUTHOR INFORMATION

Corresponding Authors

Corina Andronescu − *Technical Chemistry III, Center for Nanointegration Duisburg-Essen (CENIDE), University of Duisburg-Essen, 47057 Duisburg, Germany;* orcid.org/0000-0002-1227-1209; Email: corina.andronescu@uni-due.de

Wolfgang Schuhmann − *Analytical Chemistry − Center for Electrochemical Sciences (CES), Faculty of Chemistry and Biochemistry, Ruhr University Bochum, D-44780 Bochum, Germany;* orcid.org/0000-0003-2916-5223; Email: wolfgang.schuhmann@rub.de

Authors

Carla Santana Santos − *Analytical Chemistry − Center for Electrochemical Sciences (CES), Faculty of Chemistry and Biochemistry, Ruhr University Bochum, D-44780 Bochum, Germany*

Bright Nsolebna Jaato − *Technical Chemistry III, Center for Nanointegration Duisburg-Essen (CENIDE), University of Duisburg-Essen, 47057 Duisburg, Germany;* orcid.org/0000-0002-1118-6723

Ignacio Sanjuán − *Technical Chemistry III, Center for Nanointegration Duisburg-Essen (CENIDE), University of Duisburg-Essen, 47057 Duisburg, Germany*

Complete contact information is available at: https://pubs.acs.org/10.1021/acs.chemrev.2c00766

Author Contributions

#C.S.S., B.N.J., and I.S. contributed equally. The manuscript was written through contributions of all authors. All authors have given approval to the final version of the manuscript. CRediT: **Carla Santana Santos** writing-original draft, writing-review & editing; **Bright Nsolebna Jaato** writing-original draft, writing -review & editing; **Ignacio Sanjuán** writing-original draft, writing-review & editing; **Wolfgang Schuhmann** conceptualization, funding acquisition, project administration, writing-review & editing; **Corina Andronescu** conceptualization, funding acquisition, supervision, writing-review & editing.

Funding

C.A., I.S.M., and B.N.J. acknowledge funding by the BMBF in the framework of the NanoMatFutur project "MatGasDif" (03XP0263). C.S.S. and W.S. acknowledge funding from the European Union's Horizon 2020 research and innovation program under the Grant Agreement No. 861962 (NanoBat), from the European Research Council (ERC) under the Grant Agreement No. 833498 (CasCat), and by the European Innovation Council (EIC) under the Grant Agreement No. 101046742 (MeBattery). C.A. and W.S. acknowledge funding by the Deutsche Forschungsgemeinschaft (DFG, German Research Foundation) in the framework of the CRC247-388390466.

Notes

The authors declare no competing financial interest.

Biographies

Carla S. Santos received her Ph.D. (2019) degree from the University of Sao Paulo (Brazil) under the supervision of Prof. Mauro Bertotti.

https://doi.org/10.1021/acs.chemrev.2c00766
Chem. Rev. 2023, 123, 4972−5019

During her Ph.D., she worked on applying micro- and nanoelectrochemistry to study metabolism processes of cells and organisms. Since 2020, she has been a research fellow in the Schuhmann group at Ruhr-Universität Bochum. Her current research interests are focused on studying interfacial processes of materials for batteries employing scanning electrochemical probe microscopies.

Bright N. Jaato holds a B.Sc. and an M.Phil. in chemistry from the University of Ghana. In 2018, he was a Commonwealth Split-Site Scholar at the University of Cambridge, UK, where he studied and carried out research in "Applied Photochemistry and Nanotechnology for use in Water Purification" under the supervision of Prof. R. Vasant Kumar. Bright is currently a doctoral researcher in the Andronescu group at the University of Duisburg-Essen. His research focuses on the optimization of reactor designs for CO_2 electroreduction.

Ignacio Sanjuán Moltó completed his Ph.D. in electrochemistry (2020) at the University of Alicante under the supervision of Vicente Montiel Leguey and Eduardo Expósito Rodríguez. During this time, he studied different electrochemical techniques to treat the reject water of an electrodialysis plant in collaboration with the company Global Omnium. Currently, he is a postdoctoral researcher in the group of Corina Andronescu at the University of Duisburg-Essen. His research focuses on the electrochemical CO_2 reduction, specifically on preparation of electrocatalysts and fabrication of gas diffusion electrodes.

Wolfgang Schuhmann studied chemistry at the University of Karlsruhe and completed his Ph.D. degree in 1986 at the Technical University of Munich. After finishing his habilitation at Technical University of Munich in 1993, he was appointed Professor for Analytical Chemistry at the Ruhr University Bochum in 1996. His research interests cover a broad spectrum of different fields of electrochemistry, including biosensors, biofuel cells, batteries, photoelectrochemistry, electrocatalysts for energy conversion including high-entropy materials, scanning electrochemical microscopy, scanning electrochemical cell microscopy, in situ electrochemistry-spectroscopy techniques, micro- and nanoelectrochemistry, among others.

Corina Andronescu received her B.Sc. and M.Sc. from the University Politehnica of Bucharest in 2009 and 2011, respectively, where she also obtained her Ph.D. in 2014 in chemical engineering. In 2016 she joined the group of Prof. W. Schuhmann (Ruhr University Bochum), first as a postdoctoral researcher and later as a group leader. In December 2018, she was appointed Junior Professor at the University of Duisburg-Essen, where she leads the Electrochemical Catalysis group within the Faculty of Chemistry. The research interests include fundamental and applied topics, focusing on understanding electrocatalysts and electrode design for CO_2 electroreduction and alcohol electrooxidation, paired electrolysis, ranging to high-throughput materials discovery and single entity electrochemistry.

ABBREVIATIONS

AC	alternating current
AFM	atomic force microscopy
BDD	boron-doped diamond
C_1	single carbon-containing CO_2RR products
C_{2+}	multiple carbon-containing CO_2RR products
CB	carbon black
CD	constant distance
CE	counter electrode
CER	chlorine evolution reaction
CNT	carbon nanotubes
CO_2RR	CO_2 reduction reaction
CoTPP	5,10,15,20-tetraphenyl-21*H*,23*H*-porphine cobalt-(II)
CV	cyclic voltamogramm
DC	direct current
DEMS	differential electrochemical mass spectrometry
DFT	density functional theory
DSA	dimensionally stable anode
EC-STM	electrochemical scanning tunneling microscopy
EQCM	quartz crystal microbalance
FB	feedback
FTIR	Fourier transform infrared spectroscopy
FTO	fluorine-doped tin oxide
GC	glassy carbon
GDE	gas diffusion electrode
Gr	graphene
HER	hydrogen evolution reaction
HOPG	highly oriented pyrolytic graphite
HOR	hydrogen oxidation reaction
ICR	ion current rectification
ITO	indium tin oxide
LDH	layered double hydroxide
LEIS	local electrochemical impedance spectroscopy
LSV	linear sweep voltammogram
MCE	microcavity electrodes
ML	monolayer
MOF	metal−organic framework
MWCNTs	multiwalled carbon nanotubes
NC	nitrogen-doped carbon
n-EC-STM	noise electrochemical scanning tunneling microscopy
NHE	normal hydrogen electrode
NO_3RR	nitrate reduction
NP	nanoparticle
OCP	open circuit potential
OER	oxygen evolution reaction
ORR	oxygen reduction reaction
pc	polycrystalline
PSI	photosystem I
QRCE	quasi-reference counter electrode
RC	redox competition
RDE	rotating disk electrode
RE	reference electrode
rGO	reduced graphene oxide composite
RHE	reversible hydrogen electrode
ROS	reactive oxygen species
RRDE	rotating ring-disk electrode
SAM	self-assembled monolayer
SCE	saturated calomel electrode
SC-TG	substrate collection−tip generation
SECCM	scanning electrochemical cell microscopy
SECM	scanning electrochemical microscopy
SEI	solid-electrolyte interphase
SEM	scanning electron microscope
SEPM	scanning electrochemical probe microscopy
SF	shear force
SHE	standard hydrogen electrode
SI	surface interrogation
SICM	scanning ion conductance microscopy
SMCM	scanning micropipette contact method
SNEI	single nanoparticle electrochemical impact
SPECM	scanning photoelectrochemical microscopy
SPR	surface plasmon resonance
STM	scanning tunneling microscopy

https://doi.org/10.1021/acs.chemrev.2c00766
Chem. Rev. 2023, 123, 4972−5019

STS	scanning tunneling spectroscopy
SVET	scanning vibrating electrode technique
TC-SG	tip collection−substrate generation
TEM	transmission electron microscopy
TMO	transition metal oxide
TOF	turnover frequency
UME	ultra-microelectrode
WE	working electrode
XPS	X-ray photoelectron spectroscopy

REFERENCES

(1) Masa, J.; Andronescu, C.; Schuhmann, W. Electrocatalysis as the Nexus for Sustainable Renewable Energy: The Gordian Knot of Activity, Stability, and Selectivity. *Angew. Chem., Int. Ed.* **2020**, *59*, 15298−15312.

(2) Long, C.; Han, J.; Guo, J.; Yang, C.; Liu, S.; Tang, Z. Operando Toolbox for Heterogeneous Interface in Electrocatalysis. *Chem. Catalysis* **2021**, *1*, 509−522.

(3) Zhang, H.; Zhu, M.; Schmidt, O. G.; Chen, S.; Zhang, K. Covalent Organic Frameworks for Efficient Energy Electrocatalysis: Rational Design and Progress. *Adv. Energy Sustainability Res.* **2021**, *2*, 2000090.

(4) Kumar, A.; Vashistha, V. K.; Das, D. K.; Ibraheem, S.; Yasin, G.; Iqbal, R.; Nguyen, T. A.; Gupta, R. K.; Rasidul Islam, M. M-N-C-Based Single-Atom Catalysts for H_2, O_2 & CO_2 Electrocatalysis: Activity Descriptors, Active Sites Identification, Challenges and Prospects. *Fuel* **2021**, *304*, 121420.

(5) Campos-Roldán, C. A.; Jones, D. J.; Rozière, J.; Cavaliere, S. Platinum-Rare Earth Alloy Electrocatalysts for the Oxygen Reduction Reaction: A Brief Overview. *ChemCatChem.* **2022**, *14*, No. e202200334.

(6) Yang, Y.; Peltier, C. R.; Zeng, R.; Schimmenti, R.; Li, Q.; Huang, X.; Yan, Z.; Potsi, G.; Selhorst, R.; Lu, X.; et al. Electrocatalysis in Alkaline Media and Alkaline Membrane-Based Energy Technologies. *Chem. Rev.* **2022**, *122*, 6117−6321.

(7) Masa, J.; Schuhmann, W. Electrocatalysis and Bioelectrocatalysis − Distinction Without a Difference. *Nano Energy* **2016**, *29*, 466−475.

(8) Liu, F.; Shi, C.; Guo, X.; He, Z.; Pan, L.; Huang, Z.-F.; Zhang, X.; Zou, J.-J. Rational Design of Better Hydrogen Evolution Electrocatalysts for Water Splitting: A Review. *Adv. Sci.* **2022**, *9*, No. 2200307.

(9) Gewirth, A. A.; Niece, B. K. Electrochemical Applications of in Situ Scanning Probe Microscopy. *Chem. Rev.* **1997**, *97*, 1129−1162.

(10) Chen, S.; Kucernak, A. Electrocatalysis under Conditions of High Mass Transport Rate: Oxygen Reduction on Single Submicrometer-Sized Pt Particles Supported on Carbon. *J. Phys. Chem. B* **2004**, *108*, 3262−3276.

(11) Rao, S. R. *Physical Chemistry of Interfaces:Surface Chemistry of Froth Flotation*; Springer: Boston, MA, 2004.

(12) Brett, C. M.; Brett, A. M. O. *Electrochemistry:Principles, Methods and Applications*; Oxford University Press: New York, 1994.

(13) Yang, Y.; Xiong, Y.; Zeng, R.; Lu, X.; Krumov, M.; Huang, X.; Xu, W.; Wang, H.; DiSalvo, F. J.; Brock, J. D.; et al. Operando Methods in Electrocatalysis. *ACS Catal.* **2021**, *11*, 1136−1178.

(14) Chee, S. W.; Lunkenbein, T.; Schlogl, R.; Cuenya, B. R. In Situ and Operando Electron Microscopy in Heterogeneous Catalysis-Insights into Multi-scale Chemical Dynamics. *J. Condens. Matter Phys.* **2021**, *33*, 153001.

(15) Zuo, S.; Wu, Z.-P.; Zhang, H.; Lou, X. W. Operando Monitoring and Deciphering the Structural Evolution in Oxygen Evolution Electrocatalysis. *Adv. Energy Mater.* **2022**, *12*, 2103383.

(16) Zhu, Y.; Wang, J.; Chu, H.; Chu, Y.-C.; Chen, H. M. In Situ/Operando Studies for Designing Next-Generation Electrocatalysts. *ACS Energy Lett.* **2020**, *5*, 1281−1291.

(17) Li, J.; Gong, J. Operando Characterization Techniques for Electrocatalysis. *Energy Environ. Sci.* **2020**, *13*, 3748−3779.

(18) Timoshenko, J.; Roldan Cuenya, B. In Situ/Operando Electrocatalyst Characterization by X-ray Absorption Spectroscopy. *Chem. Rev.* **2021**, *121*, 882−961.

(19) Park, J.; Zhao, H.; Kang, S. D.; Lim, K.; Chen, C.-C.; Yu, Y.-S.; Braatz, R. D.; Shapiro, D. A.; Hong, J.; Toney, M. F.; et al. Fictitious Phase Separation in Li Layered Oxides Driven by Electro-Autocatalysis. *Nat. Mater.* **2021**, *20*, 991−999.

(20) Rüscher, M.; Herzog, A.; Timoshenko, J.; Jeon, H. S.; Frandsen, W.; Kühl, S.; Roldan Cuenya, B. Tracking Heterogeneous Structural Motifs and the Redox Behaviour of Copper-Zinc Nanocatalysts for the Electrocatalytic CO_2 Reduction using Operando Time Resolved Spectroscopy and Machine Learning. *Catal. Sci. Technol.* **2022**, *12*, 3028−3043.

(21) Oja, S. M.; Wood, M.; Zhang, B. Nanoscale Electrochemistry. *Anal. Chem.* **2013**, *85*, 473−486.

(22) Li, Y.; Ning, X.; Ma, Q.; Qin, D.; Lu, X. Recent Advances in Electrochemistry by Scanning Electrochemical Microscopy. *TrAC - Trends Anal. Chem.* **2016**, *80*, 242−254.

(23) Wittstock, G.; Burchardt, M.; Pust, S. E.; Shen, Y.; Zhao, C. Scanning Electrochemical Microscopy for Direct Imaging of Reaction Rates. *Angew. Chem., Int. Ed.* **2007**, *46*, 1584−1617.

(24) Bentley, C. L.; Edmondson, J.; Meloni, G. N.; Perry, D.; Shkirskiy, V.; Unwin, P. R. Nanoscale Electrochemical Mapping. *Anal. Chem.* **2019**, *91*, 84−108.

(25) Zoski, C. G. Nanoscale Scanning Electrochemical Microscopy:Emerging Advances in Applications and Theory. *Curr. Opin. Electrochem.* **2017**, *1*, 46−52.

(26) Polcari, D.; Dauphin-Ducharme, P.; Mauzeroll, J. Scanning Electrochemical Microscopy: A Comprehensive Review of Experimental Parameters from 1989 to 2015. *Chem. Rev.* **2016**, *116*, 13234−13278.

(27) Barton, Z. J.; Rodríguez-López, J. Emerging Scanning Probe Approaches to the Measurement of Ionic Reactivity at Energy Storage Materials. *Anal. Bioanal. Chem.* **2016**, *408*, 2707−2715.

(28) Daviddi, E.; Shkirskiy, V.; Kirkman, P. M.; Robin, M. P.; Bentley, C. L.; Unwin, P. R. Nanoscale Electrochemistry in a copper/aqueous/oil Three-Phase System: Surface Structure-Activity-Corrosion Potential Relationships. *Chem. Sci.* **2021**, *12*, 3055−3069.

(29) Asserghine, A.; Medvidović-Kosanović, M.; Stanković, A.; Nagy, L.; Souto, R. M.; Nagy, G. A Scanning Electrochemical Microscopy Characterization of the Localized Corrosion Reactions Occurring on Nitinol in Saline Solution after Anodic Polarization. *Sens. Actuators B Chem.* **2020**, *321*, 128610.

(30) Kunze, J.; Maurice, V.; Klein, L. H.; Strehblow, H.-H.; Marcus, P. In situ STM Study of the Duplex Passive Films formed on Cu(111) and Cu(001) in 0.1 M NaOH. *Corros. Sci.* **2004**, *46*, 245−264.

(31) Eckhard, K.; Erichsen, T.; Stratmann, M.; Schuhmann, W. Frequency-Dependent Alternating-Current Scanning Electrochemical Microscopy (4D AC-SECM) for Local Visualisation of Corrosion Sites. *Chem.—Eur. J.* **2008**, *14*, 3968−3976.

(32) Chen, R.; Alanis, K.; Welle, T. M.; Shen, M. Nanoelectrochemistry in the Study of Single-Cell Signaling. *Anal. Bioanal. Chem.* **2020**, *412*, 6121−6132.

(33) Bergner, S.; Wegener, J.; Matysik, F.-M. Simultaneous Imaging and Chemical Attack of a Single Living Cell Within a Confluent Cell Monolayer by means of Scanning Electrochemical Microscopy. *Anal. Chem.* **2011**, *83*, 169−174.

(34) Beaulieu, I.; Kuss, S.; Mauzeroll, J.; Geissler, M. Biological Scanning Electrochemical Microscopy and its Application to Live Cell Studies. *Anal. Chem.* **2011**, *83*, 1485−1492.

(35) Nagy, L.; Nagy, G. Application of Scanning Electrochemical Microscopy in Bioanalytical Chemistry. *Bioanal. Rev.* **2016**, *6*, 281−339.

(36) Nebel, M.; Grützke, S.; Diab, N.; Schulte, A.; Schuhmann, W. Microelectrochemical Oisualization of Oxygen Consumption of Single Living Cells. *Faraday Discuss.* **2013**, *164*, 19−32.

(37) Santos, C. S.; Macedo, F.; Kowaltowski, A. J.; Bertotti, M.; Unwin, P. R.; Marques da Cunha, F.; Meloni, G. N. Unveiling the Contribution of the Reproductive System of Individual Caenorhabdi-

https://doi.org/10.1021/acs.chemrev.2c00766
Chem. Rev. 2023, 123, 4972−5019

tis elegans on Oxygen Consumption by Single-Point Scanning Electrochemical Microscopy Measurements. *Anal. Chim. Acta* **2021**, *1146*, 88−97.
(38) Santos, C. S.; Kowaltowski, A. J.; Bertotti, M. Single Cell Oxygen Mapping (SCOM) by Scanning Electrochemical Microscopy Uncovers Heterogeneous Intracellular Oxygen Consumption. *Sci. Rep.* **2017**, *7*, 11428.
(39) Shi, M.; Wang, L.; Xie, Z.; Zhao, L.; Zhang, X.; Zhang, M. High-Content Label-Free Single-Cell Analysis with a Microfluidic Device Using Programmable Scanning Electrochemical Microscopy. *Anal. Chem.* **2021**, *93*, 12417−12425.
(40) Actis, P.; Tokar, S.; Clausmeyer, J.; Babakinejad, B.; Mikhaleva, S.; Cornut, R.; Takahashi, Y.; López Córdoba, A.; Novak, P.; Shevchuck, A. I.; et al. Electrochemical Nanoprobes for Single-Cell Analysis. *ACS Nano* **2014**, *8*, 875−884.
(41) Wittstock, G.; Schuhmann, W. Formation and Imaging of Microscopic Enzymatically Active Spots on an Alkanethiolate-Covered Gold Electrode by Scanning Electrochemical Microscopy. *Anal. Chem.* **1997**, *69*, 5059−5066.
(42) Liu, D.; Shadike, Z.; Lin, R.; Qian, K.; Li, H.; Li, K.; Wang, S.; Yu, Q.; Liu, M.; Ganapathy, S.; et al. Review of Recent Development of In Situ/Operando Characterization Techniques for Lithium Battery Research. *Adv. Mater.* **2019**, *31*, 1806620.
(43) Daboss, S.; Rahmanian, F.; Stein, H. S.; Kranz, C. The Potential of Scanning Electrochemical Probe Microscopy and Scanning Droplet Cells in Battery Research. *Electrochem. Sci. Adv.* **2022**, *2*, No. e2100122.
(44) Kempaiah, R.; Vasudevamurthy, G.; Subramanian, A. Scanning Probe Microscopy Based Characterization of Battery Materials, Interfaces, and Processes. *Nano Energy* **2019**, *65*, 103925.
(45) Krueger, B.; Balboa, L.; Dohmann, J. F.; Winter, M.; Bieker, P.; Wittstock, G. Solid Electrolyte Interphase Evolution on Lithium Metal Electrodes Followed by Scanning Electrochemical Microscopy Under Realistic Battery Cycling Current Densities. *ChemElectroChem.* **2020**, *7*, 3590−3596.
(46) Ventosa, E. Why Nanoelectrochemistry is Necessary in Battery Research? *Curr. Opin. Electrochem.* **2021**, *25*, 100635.
(47) Kumatani, A.; Matsue, T. Recent Advances in Scanning Electrochemical Microscopic Analysis and Visualization on Lithium-ion Battery Electrodes. *Curr. Opin. Electrochem.* **2020**, *22*, 228−233.
(48) Santos, C. S.; Botz, A.; Bandarenka, A. S.; Ventosa, E.; Schuhmann, W. Correlative Electrochemical Microscopy for the Elucidation of the Local Ionic and Electronic Properties of the Solid Electrolyte Interphase in Li-Ion Batteries. *Angew. Chem., Int. Ed.* **2022**, *61*, No. e202202744.
(49) Conzuelo, F.; Grützke, S.; Stratmann, L.; Pingarrón, J. M.; Schuhmann, W. Interrogation of Immunoassay Platforms by SERS and SECM after Enzyme-Catalyzed Deposition of Silver Nanoparticles. *Microchim. Acta* **2016**, *183*, 281−287.
(50) Fortin, E.; Mailley, P.; Lacroix, L.; Szunerits, S. Imaging of DNA Hybridization on Microscopic Polypyrrole Patterns using Scanning Electrochemical Microscopy (SECM): The HRP Bio-Catalyzed Oxidation of 4-Chloro-1-Naphthol. *Analyst* **2006**, *131*, 186−193.
(51) Lei, R.; Stratmann, L.; Schäfer, D.; Erichsen, T.; Neugebauer, S.; Li, N.; Schuhmann, W. Imaging Biocatalytic Activity of Enzyme−Polymer Spots by Means of Combined Scanning Electrochemical Microscopy/Electrogenerated Chemiluminescence. *Anal. Chem.* **2009**, *81*, 5070−5074.
(52) Kluge, R. M.; Psaltis, E.; Haid, R. W.; Hou, S.; Schmidt, T. O.; Schneider, O.; Garlyyev, B.; Calle-Vallejo, F.; Bandarenka, A. S. Revealing the Nature of Active Sites on Pt-Gd and Pt-Pr Alloys During the Oxygen Reduction Reaction. *ACS Appl. Mater. Interfaces* **2022**, *14*, 19604−19613.
(53) Haid, R. W.; Kluge, R. M.; Schmidt, T. O.; Bandarenka, A. S. In-Situ Detection of Active Sites for Carbon-Based Bifunctional Oxygen Reduction and Evolution Catalysis. *Electrochim. Acta* **2021**, *382*, 138285.
(54) Bard, A. J.; Fan, F. R. F.; Kwak, J.; Lev, O. Scanning Electrochemical Microscopy. *Introduction and Principles. Anal. Chem.* **1989**, *61*, 132−138.
(55) Kalinin, S. V.; Dyck, O.; Balke, N.; Neumayer, S.; Tsai, W.-Y.; Vasudevan, R.; Lingerfelt, D.; Ahmadi, M.; Ziatdinov, M.; McDowell, M. T.; et al. Toward Electrochemical Studies on the Nanometer and Atomic Scales: Progress, Challenges, and Opportunities. *ACS Nano* **2019**, *13*, 9735−9780.
(56) Kalinin, S. V.; Strelcov, E.; Belianinov, A.; Somnath, S.; Vasudevan, R. K.; Lingerfelt, E. J.; Archibald, R. K.; Chen, C.; Proksch, R.; Laanait, N.; et al. Big, Deep, and Smart Data in Scanning Probe Microscopy. *ACS Nano* **2016**, *10*, 9068−9086.
(57) Franklin, M. J.; White, D. C.; Isaacs, H. S. Pitting Corrosion by Bacteria on Carbon Steel, Determined by the Scanning Vibrating Electrode Technique. *Corros. Sci.* **1991**, *32*, 945−952.
(58) Ishikawa, M.; Morita, M.; Matsuda, Y. In Situ Scanning Vibrating Electrode Technique for Lithium Metal Anodes. *J. Power Sources* **1997**, *68*, 501−505.
(59) Montemor, M. F.; Pinto, R.; Ferreira, M. Chemical Composition and Corrosion Protection of Silane Films Modified with CeO_2 Nanoparticles. *Electrochim. Acta* **2009**, *54*, 5179−5189.
(60) Xiao, X.; Bard, A. J. Observing Single Nanoparticle Collisions at an Ultramicroelectrode by Electrocatalytic Amplification. *J. Am. Chem. Soc.* **2007**, *129*, 9610−9612.
(61) Kwon, S. J.; Fan, F.-R. F.; Bard, A. J. Observing Iridium Oxide (IrO_x) Single Nanoparticle Collisions at Ultramicroelectrodes. *J. Am. Chem. Soc.* **2010**, *132*, 13165−13167.
(62) Stuart, E. J. E.; Tschulik, K.; Batchelor-McAuley, C.; Compton, R. G. Electrochemical Observation of Single Collision Events: Fullerene Nanoparticles. *ACS Nano* **2014**, *8*, 7648−7654.
(63) Stevenson, K. J.; Tschulik, K. A Materials Driven Approach for Understanding Single Entity Nano Impact Electrochemistry. *Curr. Opin. Electrochem.* **2017**, *6*, 38−45.
(64) Kazinczi, R.; Szöcs, E.; Kálmán, E.; Nagy, P. Novel Methods for Preparing EC-STM Tips. *Appl. Phys. A: Mater. Sci. Process.* **1998**, *66*, S535−S538.
(65) Salerno, M. Coating of Tips for Electrochemical Scanning Tunneling Microscopy by Means of Silicon, Magnesium, and Tungsten Oxides. *Rev. Sci. Instrum.* **2010**, *81*, 093703.
(66) Dong, C.; Meng, G.; Saji, S. E.; Gao, X.; Zhang, P.; Wu, D.; Pan, Y.; Yin, Z.; Cheng, Y. Simulation-Guided Nanofabrication of High-Quality Practical Tungsten Probes. *RSC Adv.* **2020**, *10*, 24280−24287.
(67) Binnig, G.; Rohrer, H.; Gerber, C.; Weibel, E. Surface Studies by Scanning Tunneling Microscopy. *Phys. Rev. Lett.* **1982**, *49*, 57−61.
(68) Bard, A. J.; Mirkin, M. V.; Unwin, P. R.; Wipf, D. O. Scanning Electrochemical Microscopy. 12. Theory and Experiment of the Feedback Mode with Finite Heterogeneous Electron-Transfer Kinetics and Arbitrary Substrate Size. *J. Phys. Chem.* **1992**, *96*, 1861−1868.
(69) Ishimatsu, R.; Kim, J.; Jing, P.; Striemer, C. C.; Fang, D. Z.; Fauchet, P. M.; McGrath, J. L.; Amemiya, S. Ion-selective Permeability of an Ultrathin Nanoporous Silicon Membrane as Probed by Scanning Electrochemical Microscopy Using Micropipet-supported ITIES Tips. *Anal. Chem.* **2010**, *82*, 7127−7134.
(70) Danis, L.; Snowden, M. E.; Tefashe, U. M.; Heinemann, C. N.; Mauzeroll, J. Development of Nano-Disc electrodes for Application as Shear Force Sensitive Electrochemical Probes. *Electrochim. Acta* **2014**, *136*, 121−129.
(71) Kranz, C. Recent Advancements in Nanoelectrodes and Nanopipettes used in Combined Scanning Electrochemical Microscopy Techniques. *Analyst* **2014**, *139*, 336−352.
(72) Katemann, B. B.; Schuhmann, W. Fabrication and Characterization of Needle-Type Pt-Disk Nanoelectrodes. *Electroanalysis* **2002**, *14*, 22−28.
(73) Hansma, P. K.; Drake, B.; Marti, O.; Gould, S. A.; Prater, C. B. The Scanning Ion-Conductance Microscope. *Science* **1989**, *243*, 641−643.

https://doi.org/10.1021/acs.chemrev.2c00766
Chem. Rev. 2023, 123, 4972−5019

(74) Snowden, M. E.; Güell, A. G.; Lai, S. C. S.; McKelvey, K.; Ebejer, N.; O'Connell, M. A.; Colburn, A. W.; Unwin, P. R. Scanning Electrochemical Cell Microscopy: Theory and Experiment for Quantitative High Resolution Spatially-Resolved Voltammetry and Simultaneous Ion-Conductance Measurements. *Anal. Chem.* **2012**, *84*, 2483−2491.
(75) Morris, C. A.; Chen, C.-C.; Baker, L. A. Transport of Redox Probes through Single Pores Measured by Scanning Electrochemical-Scanning Ion Conductance Microscopy (SECM-SICM). *Analyst* **2012**, *137*, 2933−2938.
(76) Binnig, G.; Rohrer, H. Scanning Tunneling Microscopy. *Surf. Sci.* **1983**, *126*, 236−244.
(77) Binnig, G.; Quate, C. F.; Gerber, C. Atomic Force Microscope. *Phys. Rev. Lett.* **1986**, *56*, 930−933.
(78) Kwak, J.; Bard, A. J. Scanning Electrochemical Microscopy. *Theory of the Feedback Mode. Anal. Chem.* **1989**, *61*, 1221−1227.
(79) Sun, P.; Mirkin, M. V. Kinetics of Electron-Transfer Reactions at Nanoelectrodes. *Anal. Chem.* **2006**, *78*, 6526−6534.
(80) Sun, T.; Yu, Y.; Zacher, B. J.; Mirkin, M. V. Scanning Electrochemical Microscopy of Individual Catalytic Nanoparticles. *Angew. Chem., Int. Ed.* **2014**, *53*, 14120−14123.
(81) Sonnenfeld, R.; Hansma, P. K. Atomic-Resolution Microscopy in Water. *Science* **1986**, *232*, 211−213.
(82) Lai, S. C. S.; Dudin, P. V.; Macpherson, J. V.; Unwin, P. R. Visualizing Zeptomole (Electro)Catalysis at Single Nanoparticles within an Ensemble. *J. Am. Chem. Soc.* **2011**, *133*, 10744−10747.
(83) Izquierdo, J.; Knittel, P.; Kranz, C. Scanning Electrochemical Microscopy: An Analytical Perspective. *Anal. Bioanal. Chem.* **2018**, *410*, 307−324.
(84) Mirkin, M. V.; Sun, T.; Yu, Y.; Zhou, M. Electrochemistry at One Nanoparticle. *Acc. Chem. Res.* **2016**, *49*, 2328−2335.
(85) Lazenby, R.; White, R. Advances and Perspectives in Chemical Imaging in Cellular Environments using Electrochemical Methods. *Chemosensors* **2018**, *6*, 24.
(86) Caniglia, G.; Kranz, C. Scanning Electrochemical Microscopy and its Potential for Studying Biofilms and Antimicrobial Coatings. *Anal. Bioanal. Chem.* **2020**, *412*, 6133−6148.
(87) Zhou, F.; Unwin, P. R.; Bard, A. J. Scanning Electrochemical Microscopy. 16. Study of Second-Order Homogeneous Chemical Reactions via the Feedback and Generation/Collection Modes. *J. Phys. Chem.* **1992**, *96*, 4917−4924.
(88) Lefrou, C.; Cornut, R. Analytical Expressions for Quantitative Scanning Electrochemical Microscopy (SECM). *ChemPhysChem* **2010**, *11*, 547−556.
(89) Wipf, D. O.; Bard, A. J. Scanning Electrochemical Microscopy VII. Effect of Heterogeneous Electron-Transfer Rate at the Substrate on the Tip Feedback Current. *J. Electrochem. Soc.* **1991**, *138*, 469−474.
(90) Cornut, R.; Lefrou, C. New Analytical Approximations for Negative Feedback Currents with a Microdisk SECM Tip. *J. Electroanal. Chem.* **2007**, *604*, 91−100.
(91) Zampardi, G.; Ventosa, E.; La Mantia, F.; Schuhmann, W. In Situ Visualization of Li-ion Intercalation and Formation of the Solid Electrolyte Interphase on TiO_2 Based Paste Electrodes using Scanning Electrochemical Microscopy. *Chem. Commun.* **2013**, *49*, 9347−9349.
(92) Lee, C.; Kwak, J.; Anson, F. C. Application of Scanning Electrochemical Microscopy to Generation/Collection Experiments with High Collection Efficiency. *Anal. Chem.* **1991**, *63*, 1501−1504.
(93) Martin, R. D.; Unwin, P. R. Scanning Electrochemical Microscopy Kinetics of Chemical Reactions Following Electron-Transfer Measured with the Substrate-Generation−Tip-Collection Mode. *J. Chem. Soc., Faraday Trans.* **1998**, *94*, 753−759.
(94) Tefashe, U. M.; Loewenstein, T.; Miura, H.; Schlettwein, D.; Wittstock, G. Scanning Electrochemical Microscope Studies of Dye Regeneration in Indoline (D149)-Sensitized ZnO Photoelectrochemical Cells. *J. Electroanal. Chem.* **2010**, *650*, 24−30.
(95) Minguzzi, A.; Battistel, D.; Rodríguez-López, J.; Vertova, A.; Rondinini, S.; Bard, A. J.; Daniele, S. Rapid Characterization of Oxygen-Evolving Electrocatalyst Spot Arrays by the Substrate Generation/Tip Collection Mode of Scanning Electrochemical Microscopy with Decreased O_2 Diffusion Layer Overlap. *J. Phys. Chem. C* **2015**, *119*, 2941−2947.
(96) Park, H. S.; Kweon, K. E.; Ye, H.; Paek, E.; Hwang, G. S.; Bard, A. J. Factors in the Metal Doping of $BiVO_4$ for Improved Photoelectrocatalytic Activity as Studied by Scanning Electrochemical Microscopy and First-Principles Density-Functional Calculation. *J. Phys. Chem. C* **2011**, *115*, 17870−17879.
(97) Rastgar, S.; Wittstock, G. Characterization of Photoactivity of Nanostructured $BiVO_4$ at Polarized Liquid−Liquid Interfaces by Scanning Electrochemical Microscopy. *J. Phys. Chem. C* **2017**, *121*, 25941−25948.
(98) Fernández, J. L.; Bard, A. J. Scanning Electrochemical Microscopy 50. Kinetic Study of Electrode Reactions by the Tip Generation-Substrate Collection Mode. *Anal. Chem.* **2004**, *76*, 2281−2289.
(99) Fernández, J. L.; Bard, A. J. Scanning Electrochemical Microscopy. 47. Imaging Electrocatalytic Activity for Oxygen Reduction in an Acidic Medium by the Tip Generation-Substrate Collection Mode. *Anal. Chem.* **2003**, *75*, 2967−2974.
(100) Johnson, L.; Walsh, D. A. Tip Generation−Substrate Collection−Tip Collection Mode Scanning Electrochemical Microscopy of Oxygen Reduction Electrocatalysts. *J. Electroanal. Chem.* **2012**, *682*, 45−52.
(101) Leonard, K. C.; Bard, A. J. The Study of Multireactional Electrochemical Interfaces via a Tip Generation/Substrate Collection Mode of Scanning Electrochemical Microscopy: The Hydrogen Evolution Reaction for Mn in Acidic Solution. *J. Am. Chem. Soc.* **2013**, *135*, 15890−15896.
(102) Zhang, Q.; Ye, Z.; Zhu, Z.; Liu, X.; Zhang, J.; Cao, F. Separation and Kinetic Study of Iron Corrosion in Acidic Solution via a Modified Tip Generation/Substrate Collection Mode by SECM. *Corros. Sci.* **2018**, *139*, 403−409.
(103) Conzuelo, F.; Stratmann, L.; Grützke, S.; Pingarrón, J. M.; Schuhmann, W. Detection and Quantification of Sulfonamide Antibiotic Residues in Milk using Scanning Electrochemical Microscopy. *Electroanalysis* **2014**, *26*, 481−487.
(104) Pitta Bauermann, L.; Schuhmann, W.; Schulte, A. An Advanced Biological Scanning Electrochemical Microscope (Bio-SECM) for Studying Individual Living Cells. *Phys. Chem. Chem. Phys.* **2004**, *6*, 4003−4008.
(105) Sklyar, O.; Wittstock, G. Numerical Simulations of Complex Nonsymmetrical 3D Systems for Scanning Electrochemical Microscopy using the Boundary Element Method. *J. Phys. Chem. B* **2002**, *106*, 7499−7508.
(106) Eckhard, K.; Chen, X. X.; Turcu, F.; Schuhmann, W. Redox Competition Mode of Scanning Electrochemical Microscopy (RC-SECM) for Visualisation of Local Catalytic Activity. *Phys. Chem. Chem. Phys.* **2006**, *8*, 5359−5365.
(107) Karnicka, K.; Eckhard, K.; Guschin, D. A.; Stoica, L.; Kulesza, P. J.; Schuhmann, W. Visualisation of the Local Bio-Electrocatalytic Activity in Biofuel Cell Cathodes by Means of Redox Competition Scanning Electrochemical Microscopy (RC-SECM). *Electrochem. Commun.* **2007**, *9*, 1998−2002.
(108) Okunola, A. O.; Nagaiah, T. C.; Chen, X.; Eckhard, K.; Schuhmann, W.; Bron, M. Visualization of Local Electrocatalytic Activity of Metalloporphyrins Towards Oxygen Reduction by Means of Redox Competition Scanning electrochemical microscopy (RC-SECM). *Electrochim. Acta* **2009**, *54*, 4971−4978.
(109) Ivanauskas, F.; Morkvenaite-Vilkonciene, I.; Astrauskas, R.; Ramanavicius, A. Modelling of Scanning Electrochemical Microscopy at Redox Competition Mode using Diffusion and Reaction Equations. *Electrochim. Acta* **2016**, *222*, 347−354.
(110) González-García, Y.; García, S. J.; Hughes, A. E.; Mol, J. A Combined Redox-Competition and Negative-Feedback SECM Study of Self-Healing Anticorrosive Coatings. *Electrochem. Commun.* **2011**, *13*, 1094−1097.
(111) Asserghine, A.; Medvidović-Kosanović, M.; Nagy, L.; Souto, R. M.; Nagy, G. A Study of the Electrochemical Reactivity of

https://doi.org/10.1021/acs.chemrev.2c00766
Chem. Rev. 2023, 123, 4972−5019

Titanium under Cathodic Polarization by Means of Combined Feedback and Redox Competition Modes of Scanning Electrochemical Microscopy. *Sens. Actuators B Chem.* **2020**, *320*, 128339.
(112) Morkvenaite-Vilkonciene, I.; Ramanaviciene, A.; Ramanavicius, A. Redox Competition and Generation-Collection Modes Based Scanning Electrochemical Microscopy for the Evaluation of Immobilised Glucose Oxidase-Catalysed Reactions. *RSC Adv.* **2014**, *4*, 50064−50069.
(113) Morkvenaite-Vilkonciene, I.; Ramanaviciene, A.; Genys, P.; Ramanavicius, A. Evaluation of Enzymatic Kinetics of GO_x-based Electrodes by Scanning Electrochemical Microscopy at Redox Competition Mode. *Electroanalysis* **2017**, *29*, 1532−1542.
(114) Zinovicius, A.; Morkvenaite-Vilkonciene, I.; Ramanaviciene, A.; Rozene, J.; Popov, A.; Ramanavicius, A. Scanning Electrochemical Impedance Microscopy in Redox-Competition Mode for the Investigation of Antibodies Labelled with Horseradish Peroxidase. *Materials* **2021**, *14*, 4301.
(115) Eckhard, K.; Schuhmann, W. Localised Visualisation of O_2 Consumption and H_2O_2 Formation by Means of SECM for the Characterisation of Fuel Cell Catalyst Activity. *Electrochim. Acta* **2007**, *53*, 1164−1169.
(116) Nebel, M.; Erichsen, T.; Schuhmann, W. Constant-Distance Mode SECM as a Tool to Visualize Local Electrocatalytic Activity of Oxygen Reduction Catalysts. *Beilstein J. Nanotechnol.* **2014**, *5*, 141−151.
(117) Henrotte, O.; Boudet, A.; Limani, N.; Bergonzo, P.; Zribi, B.; Scorsone, E.; Jousselme, B.; Cornut, R. Steady-State Electrocatalytic Activity Evaluation with the Redox Competition Mode of Scanning Electrochemical Microscopy: A Gold Probe and a Boron-Doped Diamond Substrate. *ChemElectroChem.* **2020**, *7*, 4633−4640.
(118) Nishizawa, M.; Takoh, K.; Matsue, T. Micropatterning of HeLa Cells on Glass Substrates and Evaluation of Respiratory Activity Using Microelectrodes. *Langmuir* **2002**, *18*, 3645−3649.
(119) Shiku, H.; Shiraishi, T.; Ohya, H.; Matsue, T.; Abe, H.; Hoshi, H.; Kobayashi, M. Oxygen Consumption of Single Bovine Embryos Probed by Scanning Electrochemical Microscopy. *Anal. Chem.* **2001**, *73*, 3751−3758.
(120) Yasukawa, T.; Kaya, T.; Matsue, T. Characterization and Imaging of Single Cells with Scanning Electrochemical Microscopy. *Electroanalysis* **2000**, *12*, 653−659.
(121) Horrocks, B. R.; Mirkin, M. V.; Pierce, D. T.; Bard, A. J.; Nagy, G.; Toth, K. Scanning Electrochemical Microscopy. 19. Ion-Selective Potentiometric Microscopy. *Anal. Chem.* **1993**, *65*, 1213−1224.
(122) Baranski, A. S.; Szulborska, A. High Frequency Impedance Measurements at Ultramicroelectrodes. *Electrochim. Acta* **1996**, *41*, 985−991.
(123) Eckhard, K.; Schuhmann, W. Alternating Current Techniques in Scanning Electrochemical Microscopy (AC-SECM). *Analyst* **2008**, *133*, 1486−1497.
(124) Bandarenka, A. S.; Eckhard, K.; Maljusch, A.; Schuhmann, W. Localized Electrochemical Impedance Spectroscopy: Visualization of Spatial Distributions of the Key Parameters Describing Solid/Liquid Interfaces. *Anal. Chem.* **2013**, *85*, 2443−2448.
(125) Zou, F.; Thierry, D.; Isaacs, H. S. A High-Resolution Probe for Localized Electrochemical Impedance Spectroscopy Measurements. *J. Electrochem. Soc.* **1997**, *144*, 1957−1965.
(126) Estrada-Vargas, A.; Bandarenka, A.; Kuznetsov, V.; Schuhmann, W. In Situ Characterization of Ultrathin Films by Scanning Electrochemical Impedance Microscopy. *Anal. Chem.* **2016**, *88*, 3354−3362.
(127) Rodríguez-López, J.; Alpuche-Avilés, M. A.; Bard, A. J. Interrogation of Surfaces for the Quantification of Adsorbed Species on Electrodes: Oxygen on Gold and Platinum in Neutral Media. *J. Am. Chem. Soc.* **2008**, *130*, 16985−16995.
(128) Rodríguez-López, J.; Bard, A. J. Scanning Electrochemical Microscopy: Surface Interrogation of Adsorbed Hydrogen and the Open Circuit Catalytic Decomposition of Formic Acid at Platinum. *J. Am. Chem. Soc.* **2010**, *132*, 5121−5129.
(129) Papaderakis, A.; Tsiplakides, D.; Balomenou, S.; Sotiropoulos, S. Probing the Hydrogen Adsorption Affinity of Pt and Ir by Surface Interrogation Scanning Electrochemical Microscopy (SI-SECM). *Electrochem. Commun.* **2017**, *83*, 77−80.
(130) Liang, Z.; Ahn, H. S.; Bard, A. J. A Study of the Mechanism of the Hydrogen Evolution Reaction on Nickel by Surface Interrogation Scanning Electrochemical Microscopy. *J. Am. Chem. Soc.* **2017**, *139*, 4854−4858.
(131) Simpson, B. H.; Rodríguez-López, J. Redox Titrations via Surface Interrogation Scanning Electrochemical Microscopy at an Extended Semiconducting Surface for the Quantification of Photogenerated Adsorbed Intermediates. *Electrochim. Acta* **2015**, *179*, 74−83.
(132) Huang, C. C.; Wang, Q.; Xiang, D. B.; Shao, H. B. Surface Interrogation Mode of Scanning Electrochemical Microscopy for Oxidation Study of Adsorbed CO Generated from Serine on Platinum. *Chin. Chem. Lett.* **2011**, *22*, 1481−1484.
(133) Wang, Q.; Rodríguez-López, J.; Bard, A. J. Reaction of Br_2 with Adsorbed CO on Pt, Studied by the Surface Interrogation Mode of Scanning Electrochemical Microscopy. *J. Am. Chem. Soc.* **2009**, *131*, 17046−17047.
(134) Park, H. S.; Leonard, K. C.; Bard, A. J. Surface Interrogation Scanning Electrochemical Microscopy (SI-SECM) of Photoelectrochemistry at a W/Mo-$BiVO_4$ Semiconductor Electrode: Quantification of Hydroxyl Radicals During Water Oxidation. *J. Phys. Chem. C* **2013**, *117*, 12093−12102.
(135) Zigah, D.; Rodríguez-López, J.; Bard, A. J. Quantification of Photoelectrogenerated Hydroxyl Radical on TiO_2 by Surface Interrogation Scanning Electrochemical Microscopy. *Phys. Chem. Chem. Phys.* **2012**, *14*, 12764−12772.
(136) Ma, Y.; Shinde, P. S.; Li, X.; Pan, S. High-Throughput Screening and Surface Interrogation Studies of Au-Modified Hematite Photoanodes by Scanning Electrochemical Microscopy for Solar Water Splitting. *ACS Omega* **2019**, *4*, 17257−17268.
(137) Lorenz, J.; Yu, M.; Tüysüz, H.; Harms, C.; Dyck, A.; Wittstock, G. Coulometric Titration of Active Sites at Mesostructured Cobalt Oxide Spinel by Surface Interrogation Mode of Scanning Electrochemical Microscopy. *J. Phys. Chem. C* **2020**, *124*, 7737−7748.
(138) Kim, J. Y.; Ahn, H. S.; Bard, A. J. Surface Interrogation Scanning Electrochemical Microscopy for a Photoelectrochemical Reaction: Water Oxidation on a Hematite Surface. *Anal. Chem.* **2018**, *90*, 3045−3049.
(139) Sugimura, H.; Uchida, T.; Kitamura, N.; Shimo, N.; Masuhara, H. Direct-Mode Scanning Electrochemical Microscopy with Three electrodes: Application to Fluorescent Micropattern Formation. *J. Electroanal. Chem.* **1993**, *361*, 57−63.
(140) Schwamborn, S.; Stoica, L.; Neugebauer, S.; Reda, T.; Schmidt, H.-L.; Schuhmann, W. Local Modulation of the Redox State of p-Nitrothiophenol Self-Assembled Monolayers Using the Direct Mode of Scanning Electrochemical Microscopy. *ChemPhysChem* **2009**, *10*, 1066−1070.
(141) Danieli, T.; Mandler, D. Local Surface Patterning by Chitosan-Stabilized Gold Nanoparticles using the Direct Mode of Scanning Electrochemical Microscopy (SECM). *J. Solid State Electrochem.* **2013**, *17*, 2989−2997.
(142) Stratmann, L.; Clausmeyer, J.; Schuhmann, W. Non-destructive Patterning of Carbon Electrodes by using the Direct Mode of Scanning Electrochemical Microscopy. *ChemPhysChem* **2015**, *16*, 3477−3482.
(143) Han, L.; Hu, Z.; Sartin, M. M.; Wang, X.; Zhao, X.; Cao, Y.; Yan, Y.; Zhan, D.; Tian, Z.-Q. Direct Nanomachining on Semiconductor Wafer By Scanning Electrochemical Microscopy. *Angew. Chem., Int. Ed.* **2020**, *59*, 21129−21134.
(144) Evans, S. A.; Brakha, K.; Billon, M.; Mailley, P.; Denuault, G. Scanning Electrochemical Microscopy (SECM): Localized Glucose Oxidase Immobilization via the Direct Electrochemical Microspotting of Polypyrrole−Biotin Films. *Electrochem. Commun.* **2005**, *7*, 135−140.

https://doi.org/10.1021/acs.chemrev.2c00766
Chem. Rev. 2023, 123, 4972−5019

(145) Matrab, T.; Combellas, C.; Kanoufi, F. Scanning Electrochemical Microscopy for the Direct Patterning of a Gold Surface with Organic Moities Derived from Iodonium Salt. *Electrochem. Commun.* **2008**, *10*, 1230−1234.
(146) Eifert, A.; Mizaikoff, B.; Kranz, C. Advanced Fabrication Process for Combined Atomic Force-Scanning Electrochemical Microscopy (AFM-SECM) Probes. *Micron (Oxford, England: 1993)* **2015**, *68*, 27−35.
(147) O'Connell, M. A.; Wain, A. J. Mapping Electroactivity at Individual Catalytic Nanostructures using High-Resolution Scanning Electrochemical-Scanning Ion Conductance Microcopy. *Anal. Chem.* **2014**, *86*, 12100−12107.
(148) Etienne, M.; Anderson, E. C.; Evans, S. R.; Schuhmann, W.; Fritsch, I. Feedback-Independent Pt Nanoelectrodes for Shear Force-Based Constant-Distance Mode Scanning Electrochemical Microscopy. *Anal. Chem.* **2006**, *78*, 7317−7324.
(149) Adam, C.; Kanoufi, F.; Sojic, N.; Etienne, M. Shearforce Positioning of Nanoprobe Electrode Arrays for Scanning Electrochemical Microscopy Experiments. *Electrochim. Acta* **2015**, *179*, 45−56.
(150) Ballesteros Katemann, B.; Schulte, A.; Schuhmann, W. Constant-Distance Mode Scanning Electrochemical Microscopy (SECM) - Part I: Adaptation of a Non-Optical Shear-Force-Based Positioning Mode for SECM Tips. *Chemistry* **2003**, *9*, 2025−2033.
(151) Hussien, E. M.; Schuhmann, W.; Schulte, A. Shearforce-Based Constant-Distance Scanning Electrochemical Microscopy as Fabrication Tool for Needle-Type Carbon-Fiber Nanoelectrodes. *Anal. Chem.* **2010**, *82*, 5900−5905.
(152) Nebel, M.; Eckhard, K.; Erichsen, T.; Schulte, A.; Schuhmann, W. 4D Shearforce-Based Constant-Distance Mode Scanning Electrochemical Microscopy. *Anal. Chem.* **2010**, *82*, 7842−7848.
(153) Izquierdo, J.; Fernández-Pérez, B. M.; Eifert, A.; Souto, R. M.; Kranz, C. Simultaneous Atomic Force - Scanning Electrochemical Microscopy (AFM-SECM) Imaging of Copper Dissolution. *Electrochim. Acta* **2016**, *201*, 320−332.
(154) Kranz, C.; Friedbacher, G.; Mizaikoff, B.; Lugstein, A.; Smoliner, J.; Bertagnolli, E. Integrating an Ultramicroelectrode in an AFM Cantilever: Combined Technology for Enhanced Information. *Anal. Chem.* **2001**, *73*, 2491−2500.
(155) Kueng, A.; Kranz, C.; Lugstein, A.; Bertagnolli, E.; Mizaikoff, B. Integrated AFM-SECM in Tapping Mode: Simultaneous Topographical and Electrochemical Imaging of Enzyme Activity. *Angew. Chem., Int. Ed.* **2003**, *42*, 3238−3240.
(156) Zampardi, G.; Klink, S.; Kuznetsov, V.; Erichsen, T.; Maljusch, A.; La Mantia, F.; Schuhmann, W.; Ventosa, E. Combined AFM/SECM Investigation of the Solid Electrolyte Interphase in Li-Ion Batteries. *ChemElectroChem.* **2015**, *2*, 1607−1611.
(157) Takahashi, Y.; Shevchuk, A. I.; Novak, P.; Murakami, Y.; Shiku, H.; Korchev, Y. E.; Matsue, T. Simultaneous Noncontact Topography and Electrochemical Imaging by SECM/SICM Featuring Ion Current Feedback Regulation. *J. Am. Chem. Soc.* **2010**, *132*, 10118−10126.
(158) Etienne, M.; Schulte, A.; Mann, S.; Jordan, G.; Dietzel, I. D.; Schuhmann, W. Constant-Distance Mode Scanning Potentiometry. 1. Visualization of Calcium Carbonate Dissolution in Aqueous Solution. *Anal. Chem.* **2004**, *76*, 3682−3688.
(159) Etienne, M.; Dierkes, P.; Erichsen, T.; Schuhmann, W.; Fritsch, I. Constant-Distance Mode Scanning Potentiometry. High Resolution pH Measurements in Three-Dimensions. *Electroanalysis* **2007**, *19*, 318−323.
(160) Wain, A. J.; Pollard, A. J.; Richter, C. High-resolution electrochemical and topographical imaging using batch-fabricated cantilever probes. *Anal. Chem.* **2014**, *86*, 5143−5149.
(161) Eckhard, K.; Shin, H.; Mizaikoff, B.; Schuhmann, W.; Kranz, C. Alternating Current (AC) Impedance Imaging with Combined Atomic Force Scanning Electrochemical Microscopy (AFM-SECM). *Electrochem. Commun.* **2007**, *9*, 1311−1315.
(162) Etienne, M.; Lhenry, S.; Cornut, R.; Lefrou, C. Optimization of the Shearforce Signal for Scanning Electrochemical Microscopy and Application for Kinetic Analysis. *Electrochim. Acta* **2013**, *88*, 877−884.
(163) Etienne, M.; Moulin, J.-P.; Gourhand, S. Accurate Control of the Electrode Shape for High Resolution Shearforce Regulated SECM. *Electrochim. Acta* **2013**, *110*, 16−21.
(164) Tefashe, U. M.; Wittstock, G. Quantitative Characterization of Shear Force Regulation for Scanning Electrochemical Microscopy. *C. R. Chim.* **2013**, *16*, 7−14.
(165) Schulte, A.; Nebel, M.; Schuhmann, W. Single Live Cell Topography and Activity Imaging with the Shear-Force-Based Constant-Distance Scanning Electrochemical Microscope. *Methods Enzymol.* **2012**, *504*, 237−254.
(166) Holder, M. N.; Gardner, C. E.; Macpherson, J. V.; Unwin, P. R. Combined Scanning Electrochemical-Atomic Force Microscopy (SECM-AFM): Simulation and Experiment for Flux-Generation at Un-Insulated Metal-Coated Probes. *J. Electroanal. Chem.* **2005**, *585*, 8−18.
(167) Takahashi, Y.; Hirano, Y.; Yasukawa, T.; Shiku, H.; Yamada, H.; Matsue, T. Topographic, Electrochemical, and Optical Images Captured using Standing Approach Mode Scanning Electrochemical/Optical Microscopy. *Langmuir* **2006**, *22*, 10299−10306.
(168) Takahashi, Y.; Shevchuk, A. I.; Novak, P.; Babakinejad, B.; Macpherson, J.; Unwin, P. R.; Shiku, H.; Gorelik, J.; Klenerman, D.; Korchev, Y. E.; et al. Topographical and Electrochemical Nanoscale Imaging of Living Cells using Voltage-Switching Mode Scanning Electrochemical Microscopy. *Proc. Natl. Acad. Sci. U.S.A.* **2012**, *109*, 11540−11545.
(169) Schulte, A.; Nebel, M.; Schuhmann, W. Single Live Cell Topography and Activity Imaging with the Shear-Force-Based Constant-Distance Scanning Electrochemical Microscope. *Methods Enzymol.* **2012**, *504*, 237−254.
(170) Jantz, D. T.; Balla, R. J.; Huang, S.-H.; Kurapati, N.; Amemiya, S.; Leonard, K. C. Simultaneous Intelligent Imaging of Nanoscale Reactivity and Topography by Scanning Electrochemical Microscopy. *Anal. Chem.* **2021**, *93*, 8906−8914.
(171) Mirabal, A.; Calabrese Barton, S. Numerical Correction of In Situ AFM-SECM Measurements. *Anal. Chem.* **2021**, *93*, 12495−12503.
(172) Wei, C.; Bard, A. J.; Kapui, I.; Nagy, G.; Tóth, K. Scanning Electrochemical Microscopy. 32. Gallium Ultramicroelectrodes and their Application in Ion-Selective Probes. *Anal. Chem.* **1996**, *68*, 2651−2655.
(173) Filotás, D.; Fernández-Pérez, B. M.; Kiss, A.; Nagy, L.; Nagy, G.; Souto, R. M. Double Barrel Microelectrode Assembly to Prevent Electrical Field Effects in Potentiometric SECM Imaging of Galvanic Corrosion Processes. *J. Electrochem. Soc.* **2018**, *165*, C270−C277.
(174) Filotás, D.; Fernández-Pérez, B. M.; Izquierdo, J.; Kiss, A.; Nagy, L.; Nagy, G.; Souto, R. M. Improved Potentiometric SECM Imaging of Galvanic Corrosion Reactions. *Corros. Sci.* **2017**, *129*, 136−145.
(175) Filotás, D.; Fernández-Pérez, B. M.; Nagy, L.; Nagy, G.; Souto, R. M. Multi-Barrel Electrodes Containing an Internal Micro-Reference for the Improved Visualization of Galvanic Corrosion Processes in Magnesium-Based Materials using Potentiometric Scanning Electrochemical Microscopy. *Sens. Actuators B Chem.* **2019**, *296*, 126625.
(176) Shin, M.; Jeon, C. Frequency-Distance Responses in SECM-EQCM: A Novel Method for Calibration of the Tip-Sample Distance. *Bull. Korean Chem. Soc.* **1998**, *19*, 1227−1232.
(177) Cliffel, D. E.; Bard, A. J. Scanning Electrochemical Microscopy. 36. A combined Scanning Electrochemical Microscope-Quartz Crystal Microbalance Instrument for Studying Thin Films. *Anal. Chem.* **1998**, *70*, 1993−1998.
(178) Gollas, B.; Bartlett, P. N.; Denuault, G. An Instrument for Simultaneous EQCM Impedance and SECM Measurements. *Anal. Chem.* **2000**, *72*, 349−356.
(179) Hess, C.; Borgwarth, K.; Heinze, J. Integration of an Electrochemical Quartz Crystal Microbalance into a Scanning

https://doi.org/10.1021/acs.chemrev.2c00766
Chem. Rev. 2023, 123, 4972−5019

Electrochemical Microscope for Mechanistic Studies of Surface Patterning Reactions. *Electrochim. Acta* **2000**, *45*, 3725−3736.
(180) Blanc, C.; Pébère, N.; Tribollet, B.; Vivier, V. Galvanic Coupling Between Copper and Aluminium in a Thin-Layer Cell. *Corros. Sci.* **2010**, *52*, 991−995.
(181) Gabrielli, C.; Joiret, S.; Keddam, M.; Perrot, H.; Portail, N.; Rousseau, P.; Vivier, V. Development of a Coupled SECM-EQCM Technique for the Study of Pitting Corrosion on Iron. *J. Electrochem. Soc.* **2006**, *153*, B68.
(182) Gabrielli, C.; Joiret, S.; Keddam, M.; Perrot, H.; Portail, N.; Rousseau, P.; Vivier, V. A SECM Assisted EQCM Study of Iron Pitting. *Electrochim. Acta* **2007**, *52*, 7706−7714.
(183) Clausmeyer, J.; Nebel, M.; Grützke, S.; Kayran, Y. U.; Schuhmann, W. Local Surface Modifications Investigated by Combining Scanning Electrochemical Microscopy and Surface-Enhanced Raman Scattering. *ChemPlusChem.* **2018**, *83*, 414−417.
(184) Gossage, Z. T.; Schorr, N. B.; Hernández-Burgos, K.; Hui, J.; Simpson, B. H.; Montoto, E. C.; Rodríguez-López, J. Interrogating Charge Storage on Redox Active Colloids via Combined Raman Spectroscopy and Scanning Electrochemical Microscopy. *Langmuir* **2017**, *33*, 9455−9463.
(185) Hatfield, K. O.; Gole, M. T.; Schorr, N. B.; Murphy, C. J.; Rodríguez-López, J. Surface-Enhanced Raman Spectroscopy-Scanning Electrochemical Microscopy: Observation of Real-Time Surface pH Perturbations. *Anal. Chem.* **2021**, *93*, 7792−7796.
(186) Steimecke, M.; Araújo-Cordero, A. M.; Dieterich, E.; Bron, M. Probing Individual Cuprous Oxide Microcrystals towards Carbon Dioxide Reduction by using In Situ Raman-coupled Scanning Electrochemical Microscopy. *ChemElectroChem.* **2022**, *9*, No. e202101221.
(187) Szunerits, S.; Knorr, N.; Calemczuk, R.; Livache, T. New Approach to Writing and Simultaneous Reading of Micropatterns: Combining Surface Plasmon Resonance Imaging with Scanning Electrochemical Microscopy (SECM). *Langmuir* **2004**, *20*, 9236−9241.
(188) Xiang, J.; Guo, J.; Zhou, F. Scanning Electrochemical Microscopy Combined with Surface Plasmon Resonance: Studies of Localized Film Thickness Variations and Molecular Conformation Changes. *Anal. Chem.* **2006**, *78*, 1418−1424.
(189) Xin, Y.; Gao, Y.; Guo, J.; Chen, Q.; Xiang, J.; Zhou, F. Real-Time Detection of Cu^{2+} Sequestration and Release by Immobilized Apo-Metallothioneins using SECM Combined with SPR. *Biosens. Bioelectron.* **2008**, *24*, 369−375.
(190) Wang, L.; Kowalik, J.; Mizaikoff, B.; Kranz, C. Combining Scanning Electrochemical Microscopy with Infrared Attenuated Total Reflection Spectroscopy for in situ Studies of Electrochemically Induced Processes. *Anal. Chem.* **2010**, *82*, 3139−3145.
(191) Wang, L.; Kranz, C.; Mizaikoff, B. Monitoring Scanning Electrochemical Microscopy Approach Curves with Mid-Infrared Spectroscopy: Toward a Novel Current-Independent Positioning Mode. *Anal. Chem.* **2010**, *82*, 3132−3138.
(192) Fan, F.-R. F.; Cliffel, D.; Bard, A. J. Scanning Electrochemical Microscopy. 37. Light Emission by Electrogenerated Chemiluminescence at SECM Tips and Their Application to Scanning Optical Microscopy. *Anal. Chem.* **1998**, *70*, 2941−2948.
(193) Kanoufi, F.; Cannes, C.; Zu, Y.; Bard, A. J. Scanning Electrochemical Microscopy. 43. Investigation of Oxalate Oxidation and Electrogenerated Chemiluminescence across the Liquid−Liquid Interface. *J. Phys. Chem. B* **2001**, *105*, 8951−8962.
(194) Miao, W.; Choi, J.-P.; Bard, A. J. Electrogenerated Chemiluminescence 69: The Tris(2,2'-bipyridine)ruthenium(II), (Ru(bpy)3(2+))/tri-n-propylamine (TPrA) System Revisited- A new Route Involving TPrA*+ Cation Radicals. *J. Am. Chem. Soc.* **2002**, *124*, 14478−14485.
(195) Boldt, F.-M.; Heinze, J.; Diez, M.; Petersen, J.; Börsch, M. Real-time pH Microscopy Down to the Molecular Level by Combined Scanning Electrochemical Microscopy/Single-Molecule Fluorescence Spectroscopy. *Anal. Chem.* **2004**, *76*, 3473−3481.
(196) Conzuelo, F.; Sliozberg, K.; Gutkowski, R.; Grützke, S.; Nebel, M.; Schuhmann, W. High-Resolution Analysis of Photoanodes for Water Splitting by Means of Scanning Photoelectrochemical Microscopy. *Anal. Chem.* **2017**, *89*, 1222−1228.
(197) Zhao, F.; Plumeré, N.; Nowaczyk, M. M.; Ruff, A.; Schuhmann, W.; Conzuelo, F. Interrogation of a PS1-Based Photocathode by Means of Scanning Photoelectrochemical Microscopy. *Small* **2017**, *13*, 1604093.
(198) Shinde, P. S.; Peng, X.; Wang, J.; Ma, Y.; McNamara, L. E.; Hammer, N. I.; Gupta, A.; Pan, S. Rapid Screening of Photoanode Materials Using Scanning Photoelectrochemical Microscopy Technique and Formation of Z-Scheme Solar Water Splitting System by Coupling p- and n-type Heterojunction Photoelectrodes. *ACS Appl. Energy Mater.* **2018**, *1*, 2283−2294.
(199) Bae, J. H.; Nepomnyashchii, A. B.; Wang, X.; Potapenko, D. V.; Mirkin, M. V. Photo-Scanning Electrochemical Microscopy on the Nanoscale with Through-Tip Illumination. *Anal. Chem.* **2019**, *91*, 12601−12605.
(200) Zhao, F.; Hartmann, V.; Ruff, A.; Nowaczyk, M. M.; Rögner, M.; Schuhmann, W.; Conzuelo, F. Unravelling Electron Transfer Processes at Photosystem 2 Embedded in an Os-Complex Modified Redox Polymer. *Electrochim. Acta* **2018**, *290*, 451−456.
(201) James, P.; Casillas, N.; Smyrl, W. H. Simultaneous Scanning Electrochemical and Photoelectrochemical Microscopy by Use of a Metallized Optical Fiber. *J. Electrochem. Soc.* **1996**, *143*, 3853−3865.
(202) Chen, C.-C.; Zhou, Y.; Baker, L. A. Scanning Ion Conductance Microscopy. *Annu. Rev. Anal. Chem.* **2012**, *5*, 207−228.
(203) Edwards, M. A.; Williams, C. G.; Whitworth, A. L.; Unwin, P. R. Scanning Ion Conductance Microscopy: A Model for Experimentally Realistic Conditions and Image Interpretation. *Anal. Chem.* **2009**, *81*, 4482−4492.
(204) Rheinlaender, J.; Schäffer, T. E. Image Formation, Resolution, and Height Measurement in Scanning Ion Conductance Microscopy. *J. Appl. Phys.* **2009**, *105*, 094905.
(205) Zhu, C.; Huang, K.; Siepser, N. P.; Baker, L. A. Scanning Ion Conductance Microscopy. *Chem. Rev.* **2021**, *121*, 11726−11768.
(206) Rheinlaender, J.; Geisse, N. A.; Proksch, R.; Schäffer, T. E. Comparison of Scanning Ion Conductance Microscopy with Atomic Force Microscopy for Cell Imaging. *Langmuir* **2011**, *27*, 697−704.
(207) Takahashi, Y.; Murakami, Y.; Nagamine, K.; Shiku, H.; Aoyagi, S.; Yasukawa, T.; Kanzaki, M.; Matsue, T. Topographic Imaging of Convoluted Surface of Live Cells by Scanning Ion Conductance Microscopy in a Standing Approach Mode. *Phys. Chem. Chem. Phys.* **2010**, *12*, 10012−10017.
(208) Happel, P.; Thatenhorst, D.; Dietzel, I. D. Scanning Ion Conductance Microscopy for Studying Biological Samples. *Sensors* **2012**, *12*, 14983−15008.
(209) Korchev, Y. E.; Gorelik, J.; Lab, M. J.; Sviderskaya, E. V.; Johnston, C. L.; Coombes, C. R.; Vodyanoy, I.; Edwards, C. R. Cell Volume Measurement Using Scanning Ion Conductance Microscopy. *Biophys. J.* **2000**, *78*, 451−457.
(210) Gorelik, J.; Zhang, Y.; Shevchuk, A. I.; Frolenkov, G. I.; Sánchez, D.; Lab, M. J.; Vodyanoy, I.; Edwards, C. R. W.; Klenerman, D.; Korchev, Y. E. The Use of Scanning Ion Conductance Microscopy to Image A6 Cells. *Mol. Cell. Endocrinol.* **2004**, *217*, 101−108.
(211) Seifert, J.; Rheinlaender, J.; Novak, P.; Korchev, Y. E.; Schäffer, T. E. Comparison of Atomic Force Microscopy and Scanning Ion Conductance Microscopy for Live Cell Imaging. *Langmuir* **2015**, *31*, 6807−6813.
(212) Böcker, M.; Muschter, S.; Schmitt, E. K.; Steinem, C.; Schäffer, T. E. Imaging and Patterning of Pore-Suspending Membranes with Scanning Ion Conductance Microscopy. *Langmuir* **2009**, *25*, 3022−3028.
(213) McKelvey, K.; Perry, D.; Byers, J. C.; Colburn, A. W.; Unwin, P. R. Bias Modulated Scanning Ion Conductance Microscopy. *Anal. Chem.* **2014**, *86*, 3639−3646.
(214) Pastré, D.; Iwamoto, H.; Liu, J.; Szabo, G.; Shao, Z. Characterization of AC Mode Scanning Ion-Conductance Microscopy. *Ultramicroscopy* **2001**, *90*, 13−19.

https://doi.org/10.1021/acs.chemrev.2c00766
Chem. Rev. 2023, 123, 4972−5019

(215) Chen, C.-C.; Derylo, M. A.; Baker, L. A. Measurement of Ion Currents Through Porous Membranes with Scanning Ion Conductance Microscopy. *Anal. Chem.* **2009**, *81*, 4742−4751.
(216) Shkirskiy, V.; Kang, M.; McPherson, I. J.; Bentley, C. L.; Wahab, O. J.; Daviddi, E.; Colburn, A. W.; Unwin, P. R. Electrochemical Impedance Measurements in Scanning Ion Conductance Microscopy. *Anal. Chem.* **2020**, *92*, 12509−12517.
(217) Happel, P.; Hoffmann, G.; Mann, S. A.; Dietzel, I. D. Monitoring Cell Movements and Volume Changes with Pulse-Mode Scanning Ion Conductance Microscopy. *J. Microsc.* **2003**, *212*, 144−151.
(218) Mann, S. A.; Hoffmann, G.; Hengstenberg, A.; Schuhmann, W.; Dietzel, I. D. Pulse-Mode Scanning Ion Conductance Microscopy - A Method to Investigate Cultured Hippocampal Cells. *J. Neurosci. Meth.* **2002**, *116*, 113−117.
(219) Liu, S.; Dong, Y.; Zhao, W.; Xie, X.; Ji, T.; Yin, X.; Liu, Y.; Liang, Z.; Momotenko, D.; Liang, D.; et al. Studies of Ionic Current Rectification using Polyethyleneimines Coated Glass Nanopipettes. *Anal. Chem.* **2012**, *84*, 5565−5573.
(220) Sa, N.; Lan, W.-J.; Shi, W.; Baker, L. A. Rectification of Ion Current in Nanopipettes by External Substrates. *ACS Nano* **2013**, *7*, 11272−11282.
(221) Lan, W.-J.; Edwards, M. A.; Luo, L.; Perera, R. T.; Wu, X.; Martin, C. R.; White, H. S. Voltage-Rectified Current and Fluid Flow in Conical Nanopores. *Acc. Chem. Res.* **2016**, *49*, 2605−2613.
(222) He, X.; Zhang, K.; Li, T.; Jiang, Y.; Yu, P.; Mao, L. Micrometer-Scale Ion Current Rectification at Polyelectrolyte Brush-Modified Micropipets. *J. Am. Chem. Soc.* **2017**, *139*, 1396−1399.
(223) Bard, A. J., Mirkin, M. V., Eds. *Scanning Electrochemical Microscopy*, 3rd ed.; Taylor and Francis, 2001.
(224) Deng, X. L.; Takami, T.; Son, J. W.; Kang, E. J.; Kawai, T.; Park, B. H. Effect of Concentration Gradient on Ionic Current Rectification in Polyethyleneimine Modified Glass Nano-Pipettes. *Sci. Rep.* **2014**, *4*, 4005.
(225) Liu, G.-C.; Gao, M.-J.; Chen, W.; Hu, X.-Y.; Song, L.-B.; Liu, B.; Zhao, Y.-D. pH-Modulated Ion-Current Rectification in a Cysteine-Functionalized Glass Nanopipette. *Electrochem. Commun.* **2018**, *97*, 6−10.
(226) Macazo, F. C.; White, R. J. Bioinspired Protein Channel-Based Scanning Ion Conductance Microscopy (Bio-SICM) for Simultaneous Conductance and Specific Molecular Imaging. *J. Am. Chem. Soc.* **2016**, *138*, 2793−2801.
(227) Lab, M. J.; Bhargava, A.; Wright, P. T.; Gorelik, J. The Scanning Ion Conductance Microscope for Cellular Physiology. *Am. J. Physiol. Heart Circ.* **2013**, *304*, H1−11.
(228) Zhou, L.; Zeng, Y.; Baker, L. A.; Hou, J. A Proposed Route to Independent Measurements of Tight Junction Conductance at Discrete Cell Junctions. *Tissue Barriers* **2015**, *3*, No. e1105907.
(229) Shevchuk, A.; Tokar, S.; Gopal, S.; Sanchez-Alonso, J. L.; Tarasov, A. I.; Vélez-Ortega, A. C.; Chiappini, C.; Rorsman, P.; Stevens, M. M.; Gorelik, J.; et al. Angular Approach Scanning Ion Conductance Microscopy. *Biophys. J.* **2016**, *110*, 2252−2265.
(230) Gorelik, J.; Gu, Y.; Spohr, H. A.; Shevchuk, A. I.; Lab, M. J.; Harding, S. E.; Edwards, C. R.; Whitaker, M.; Moss, G. W.; Benton, D. C.; et al. Ion Channels in Small Cells and Subcellular Structures Can Be Studied with a Smart Patch-Clamp System. *Biophys. J.* **2002**, *83*, 3296−3303.
(231) Anariba, F.; Anh, J. H.; Jung, G.-E.; Cho, N.-J.; Cho, S.-J. Biophysical Applications of Scanning Ion Conductance Microscopy (SICM). *Mod. Phys. Lett. B* **2012**, *26*, 1130003.
(232) Pan, R.; Hu, K.; Jia, R.; Rotenberg, S. A.; Jiang, D.; Mirkin, M. V. Resistive-Pulse Sensing Inside Single Living Cells. *J. Am. Chem. Soc.* **2020**, *142*, 5778−5784.
(233) McKelvey, K.; Kinnear, S. L.; Perry, D.; Momotenko, D.; Unwin, P. R. Surface Charge Mapping with a Nanopipette. *J. Am. Chem. Soc.* **2014**, *136*, 13735−13744.
(234) Perry, D.; Paulose Nadappuram, B.; Momotenko, D.; Voyias, P. D.; Page, A.; Tripathi, G.; Frenguelli, B. G.; Unwin, P. R. Surface Charge Visualization at Viable Living Cells. *J. Am. Chem. Soc.* **2016**, *138*, 3152−3160.
(235) Page, A.; Perry, D.; Young, P.; Mitchell, D.; Frenguelli, B. G.; Unwin, P. R. Fast Nanoscale Surface Charge Mapping with Pulsed-Potential Scanning Ion Conductance Microscopy. *Anal. Chem.* **2016**, *88*, 10854−10859.
(236) Perry, D.; Page, A.; Chen, B.; Frenguelli, B. G.; Unwin, P. R. Differential-Concentration Scanning Ion Conductance Microscopy. *Anal. Chem.* **2017**, *89*, 12458−12465.
(237) Fuhs, T.; Klausen, L. H.; Sønderskov, S. M.; Han, X.; Dong, M. Direct Measurement of Surface Charge Distribution in Phase Separating Supported Lipid Bilayers. *Nanoscale* **2018**, *10*, 4538−4544.
(238) Cremin, K.; Jones, B. A.; Teahan, J.; Meloni, G. N.; Perry, D.; Zerfass, C.; Asally, M.; Soyer, O. S.; Unwin, P. R. Scanning Ion Conductance Microscopy Reveals Differences in the Ionic Environments of Gram-Positive and Negative Bacteria. *Anal. Chem.* **2020**, *92*, 16024−16032.
(239) Perry, D.; Al Botros, R.; Momotenko, D.; Kinnear, S. L.; Unwin, P. R. Simultaneous Nanoscale Surface Charge and Topographical Mapping. *ACS Nano* **2015**, *9*, 7266−7276.
(240) Zhu, C.; Zhou, L.; Choi, M.; Baker, L. A. Mapping Surface Charge of Individual Microdomains with Scanning Ion Conductance Microscopy. *ChemElectroChem.* **2018**, *5*, 2986−2990.
(241) Wang, Y.; Shan, X.; Wang, S.; Tao, N.; Blanchard, P.-Y.; Hu, K.; Mirkin, M. V. Imaging Local Electric Field Distribution by Plasmonic Impedance Microscopy. *Anal. Chem.* **2016**, *88*, 1547−1552.
(242) Teahan, J.; Perry, D.; Chen, B.; McPherson, I. J.; Meloni, G. N.; Unwin, P. R. Scanning Ion Conductance Microscopy: Surface Charge Effects on Electroosmotic Flow Delivery from a Nanopipette. *Anal. Chem.* **2021**, *93*, 12281−12288.
(243) Tao, L.; Qiao, M.; Jin, R.; Li, Y.; Xiao, Z.; Wang, Y.; Zhang, N.; Xie, C.; He, Q.; Jiang, D.; et al. Bridging the Surface Charge and Catalytic Activity of a Defective Carbon Electrocatalyst. *Angew. Chem., Int. Ed.* **2019**, *58*, 1019−1024.
(244) Comstock, D. J.; Elam, J. W.; Pellin, M. J.; Hersam, M. C. Integrated ultramicroelectrode-Nanopipet Probe for Concurrent Scanning Electrochemical Microscopy and Scanning Ion Conductance Microscopy. *Anal. Chem.* **2010**, *82*, 1270−1276.
(245) Zhou, Y.; Chen, C.-C.; Weber, A. E.; Zhou, L.; Baker, L. A. Potentiometric-Scanning Ion Conductance Microscopy. *Langmuir* **2014**, *30*, 5669−5675.
(246) Chen, C.-C.; Zhou, Y.; Morris, C. A.; Hou, J.; Baker, L. A. Scanning Ion Conductance Microscopy Measurement of Paracellular Channel Conductance in Tight Junctions. *Anal. Chem.* **2013**, *85*, 3621−3628.
(247) Nadappuram, B. P.; McKelvey, K.; Al Botros, R.; Colburn, A. W.; Unwin, P. R. Fabrication and Characterization of Dual Function Nanoscale pH-Scanning Ion Conductance Microscopy (SICM) Probes for High Resolution pH Mapping. *Anal. Chem.* **2013**, *85*, 8070−8074.
(248) Rothery, A. M.; Gorelik, J.; Bruckbauer, A.; Yu, W.; Korchev, Y. E.; Klenerman, D. A Novel Light Source for SICM-SNOM of Living Cells. *J. Microsc.* **2003**, *209*, 94−101.
(249) Clarke, R. W.; White, S. S.; Zhou, D.; Ying, L.; Klenerman, D. Trapping of Proteins Under Physiological Conditions in a Nanopipette. *Angew. Chem., Int. Ed.* **2005**, *44*, 3747−3750.
(250) Lyon, A. R.; MacLeod, K. T.; Zhang, Y.; Garcia, E.; Kanda, G. K.; Lab, M. J.; Korchev, Y. E.; Harding, S. E.; Gorelik, J. Loss of T-tubules and other Changes to Surface Topography in Ventricular Myocytes from Failing Human and Rat Heart. *Proc. Natl. Acad. Sci. U.S.A.* **2009**, *106*, 6854−6859.
(251) Bergner, S.; Vatsyayan, P.; Matysik, F.-M. Recent Advances in High Resolution Scanning Electrochemical Microscopy of Living Cells - A Review. *Anal. Chim. Acta* **2013**, *775*, 1−13.
(252) Zhou, Y.; Saito, M.; Miyamoto, T.; Novak, P.; Shevchuk, A. I.; Korchev, Y. E.; Fukuma, T.; Takahashi, Y. Nanoscale Imaging of Primary Cilia with Scanning Ion Conductance Microscopy. *Anal. Chem.* **2018**, *90*, 2891−2895.

https://doi.org/10.1021/acs.chemrev.2c00766
Chem. Rev. 2023, 123, 4972−5019

(253) Bednarska, J.; Novak, P.; Korchev, Y.; Rorsman, P.; Tarasov, A. I.; Shevchuk, A. Release of Insulin Granules by Simultaneous, High-Speed Correlative SICM-FCM. *J. Microsc.* **2021**, *282*, 21−29.
(254) Zhou, L.; Zhou, Y.; Baker, L. A. Measuring Ions with Scanning Ion Conductance Microscopy. *Electrochem. Soc. Interface* **2014**, *23*, 47−52.
(255) Bednarska, J.; Pelchen-Matthews, A.; Novak, P.; Burden, J. J.; Summers, P. A.; Kuimova, M. K.; Korchev, Y.; Marsh, M.; Shevchuk, A. Rapid Formation of Human Immunodeficiency Virus-Like Particles. *Proc. Natl. Acad. Sci. U.S.A.* **2020**, *117*, 21637−21646.
(256) Halbritter, J.; Repphun, G.; Vinzelberg, S.; Staikov, G.; Lorenz, W. J. Tunneling Mechanisms in Electrochemical STM - Distance and Voltage Tunneling Spectroscopy. *Electrochim. Acta* **1995**, *40*, 1385−1394.
(257) Kuznetsov, A. M.; Ulstrup, J. Mechanisms of in Situ Scanning Tunnelling Microscopy of Organized Redox Molecular Assemblies. *J. Phys. Chem. A* **2000**, *104*, 11531−11540.
(258) Matsushima, H.; Lin, S.-W.; Morin, S.; Magnussen, O. M. In situ video-STM Studies of the Mechanisms and Dynamics of Electrochemical Bismuth Nanostructure Formation on Au. *Faraday Discuss.* **2016**, *193*, 171−185.
(259) Gewirth, A. A.; Bard, A. J. In Situ Scanning Tunneling Microscopy of the Anodic Oxidation of Highly Oriented Pyrolytic Graphite Surfaces. *J. Phys. Chem.* **1988**, *92*, 5563−5566.
(260) Itaya, K.; Tomita, E. Scanning Tunneling Microscope for Electrochemistry - A New Concept for the in situ Scanning Tunneling Microscope in Electrolyte Solutions. *Surf. Sci.* **1988**, *201*, L507−L512.
(261) Lustenberger, P.; Rohrer, H.; Christoph, R.; Siegenthaler, H. Scanning Tunneling Microscopy at Potential Controlled Electrode Surfaces in Electrolytic Environment. *J. Electroanal. Chem.* **1988**, *243*, 225−235.
(262) Lev, O.; Fan, F.-R.; Bard, A. J. The Application of Scanning Tunneling Microscopy to In Situ Studies of Nickel Electrodes under Potential Control. *J. Electrochem. Soc.* **1988**, *135*, 783−784.
(263) Hachiya, T.; Honbo, H.; Itaya, K. Detailed Underpotential Deposition of Copper on Gold(III) in Aqueous Solutions. *J. Electroanal. Chem.* **1991**, *315*, 275−291.
(264) Nagahara, L. A.; Thundat, T.; Lindsay, S. M. Preparation and Characterization of STM Tips for Electrochemical Studies. *Rev. Sci. Instrum.* **1989**, *60*, 3128−3130.
(265) Hudson, J. E.; Abruña, H. D. STM and ECSTM Study of the Formation and Structure of Self-Assembling Osmium Complexes on Pt(111). *J. Phys. Chem.* **1996**, *100*, 1036−1042.
(266) Güell, A. G.; Díez-Pérez, I.; Gorostiza, P.; Sanz, F. Preparation of Reliable Probes for Electrochemical Tunneling Spectroscopy. *Anal. Chem.* **2004**, *76*, 5218−5222.
(267) Pobelov, I. V.; Li, Z.; Wandlowski, T. Electrolyte Gating in Redox-Active Tunneling Junctions - An Electrochemical STM Approach. *J. Am. Chem. Soc.* **2008**, *130*, 16045−16054.
(268) Li, Z.; Liu, Y.; Mertens, S. F. L.; Pobelov, I. V.; Wandlowski, T. From Redox Gating to Quantized Charging. *J. Am. Chem. Soc.* **2010**, *132*, 8187−8193.
(269) Bodappa, N.; Fluch, U.; Fu, Y.; Mayor, M.; Moreno-García, P.; Siegenthaler, H.; Wandlowski, T. Controlled Assembly and Single Electron Charging of Monolayer Protected Au_{144} Clusters: An Electrochemistry and Scanning Tunneling Spectroscopy Study. *Nanoscale* **2014**, *6*, 15117−15126.
(270) Rudnev, A. V.; Pobelov, I. V.; Wandlowski, T. Structural Aspects of Redox-Mediated Electron Tunneling. *J. Electroanal. Chem.* **2011**, *660*, 302−308.
(271) Herrera, S.; Adam, C.; Ricci, A.; Calvo, E. J. Electrochemical Gating of Single Osmium Molecules Tethered to Au Surfaces. *J. Solid State Electrochem.* **2016**, *20*, 957−967.
(272) Wolfschmidt, H.; Baier, C.; Gsell, S.; Fischer, M.; Schreck, M.; Stimming, U. STM, SECPM, AFM and Electrochemistry on Single Crystalline Surfaces. *Materials* **2010**, *3*, 4196−4213.
(273) Chi, Q.; Farver, O.; Ulstrup, J. Long-Range Protein Electron Transfer Observed at the Single-Molecule Level: In Situ Mapping of Redox-Gated Tunneling Resonance. *Proc. Natl. Acad. Sci. U.S.A.* **2005**, *102*, 16203−16208.
(274) Auer, A.; Ding, X.; Bandarenka, A. S.; Kunze-Liebhäuser, J. The Potential of Zero Charge and the Electrochemical Interface Structure of Cu(111) in Alkaline Solutions. *J. Phys. Chem. C* **2021**, *125*, 5020−5028.
(275) Alessandrini, A.; Gerunda, M.; Canters, G. W.; Verbeet, M.; Facci, P. Electron Tunnelling Through Azurin is Mediated by the Active Site Cu Ion. *Chem. Phys. Lett.* **2003**, *376*, 625−630.
(276) Ryan, M. P.; Newman, R. C.; Thompson, G. E. An STM Study of the Passive Film Formed on Iron in Borate Buffer Solution. *J. Electrochem. Soc.* **1995**, *142*, L177−L179.
(277) Díez-Pérez, I.; Gorostiza, P.; Sanz, F. Direct Evidence of the Electronic Conduction of the Passive Film on Iron by EC-STM. *J. Electrochem. Soc.* **2003**, *150*, B348.
(278) Díez-Pérez, I.; Sanz, F.; Gorostiza, P. In situ studies of metal passive films. *Curr. Opin. Solid State Mater. Sci.* **2006**, *10*, 144−152.
(279) Zamborini, F. P.; Crooks, R. M. Corrosion Passivation of Gold by n -Alkanethiol Self-Assembled Monolayers: Effect of Chain Length and End Group. *Langmuir* **1998**, *14*, 3279−3286.
(280) Alessandrini, A.; Corni, S.; Facci, P. Unravelling Single Metalloprotein Electron Transfer by Scanning Probe Techniques. *Phys. Chem. Chem. Phys.* **2006**, *8*, 4383−4397.
(281) Wang, M.; Bugarski, S.; Stimming, U. Topological and Electron-Transfer Properties of Glucose Oxidase Adsorbed on Highly Oriented Pyrolytic Graphite Electrodes. *J. Phys. Chem. C* **2008**, *112*, 5165−5173.
(282) Artés, J. M.; Díez-Pérez, I.; Sanz, F.; Gorostiza, P. Direct Measurement of Electron Transfer Distance Decay Constants of Single Redox Proteins by Electrochemical Tunneling Spectroscopy. *ACS Nano* **2011**, *5*, 2060−2066.
(283) Artés, J. M.; López-Martínez, M.; Giraudet, A.; Díez-Pérez, I.; Sanz, F.; Gorostiza, P. Current-Voltage Characteristics and Transition Voltage Spectroscopy of Individual Redox Proteins. *J. Am. Chem. Soc.* **2012**, *134*, 20218−20221.
(284) Yagati, A. K.; Lee, J.-Y.; Nam, E.-S.; Cho, S.; Choi, J. W. Electrochemical Scanning Tunneling Microscopy Analysis on Protein Based Electronic Devices. *Sci. Adv. Mater.* **2017**, *9*, 102−121.
(285) Hahn, C.; Hatsukade, T.; Kim, Y.-G.; Vailionis, A.; Baricuatro, J. H.; Higgins, D. C.; Nitopi, S. A.; Soriaga, M. P.; Jaramillo, T. F. Engineering Cu surfaces for the electrocatalytic conversion of CO_2: Controlling selectivity toward oxygenates and hydrocarbons. *Proc. Natl. Acad. Sci. U.S.A.* **2017**, *114*, 5918−5923.
(286) Liang, Y.; Pfisterer, J. H. K.; McLaughlin, D.; Csoklich, C.; Seidl, L.; Bandarenka, A. S.; Schneider, O. Electrochemical Scanning Probe Microscopies in Electrocatalysis. *Small Methods* **2019**, *3*, 1800387.
(287) Gu, J.-Y.; Cai, Z.-F.; Wang, D.; Wan, L.-J. Single-Molecule Imaging of Iron-Phthalocyanine-Catalyzed Oxygen Reduction Reaction by in Situ Scanning Tunneling Microscopy. *ACS Nano* **2016**, *10*, 8746−8750.
(288) Mitterreiter, E.; Liang, Y.; Golibrzuch, M.; McLaughlin, D.; Csoklich, C.; Bartl, J. D.; Holleitner, A.; Wurstbauer, U.; Bandarenka, A. S. In-Situ Visualization of Hydrogen Evolution Sites on Helium Ion Treated Molybdenum Dichalcogenides Under Reaction Conditions. *npj 2D Mater. Appl.* **2019**, *3*, 25.
(289) Inaba, M.; Siroma, Z.; Funabiki, A.; Ogumi, Z.; Abe, T.; Mizutani, Y.; Asano, M. Electrochemical Scanning Tunneling Microscopy Observation of Highly Oriented Pyrolytic Graphite Surface Reactions in an Ethylene Carbonate-Based Electrolyte Solution. *Langmuir* **1996**, *12*, 1535−1540.
(290) Inaba, M.; Siroma, Z.; Kawatate, Y.; Funabiki, A.; Ogumi, Z. Electrochemical Scanning Tunneling Microscopy Analysis of the Surface Reactions on Graphite Basal Plane in Ethylene Carbonate-Based Solvents and Propylene Carbonate. *J. Power Sources* **1997**, *68*, 221−226.
(291) Wang, X.; Cai, Z.-F.; Wang, D.; Wan, L.-J. Molecular Evidence for the Catalytic Process of Cobalt Porphyrin Catalyzed Oxygen

Evolution Reaction in Alkaline Solution. *J. Am. Chem. Soc.* **2019**, *141*, 7665−7669.
(292) Wang, X.; Cai, Z.-F.; Wang, Y.-Q.; Feng, Y.-C.; Yan, H.-J.; Wang, D.; Wan, L.-J. In Situ Scanning Tunneling Microscopy of Cobalt-Phthalocyanine-Catalyzed CO_2 Reduction Reaction. *Angew. Chem., Int. Ed.* **2020**, *59*, 16098−16103.
(293) Yoshimoto, S.; Honda, Y.; Ito, O.; Itaya, K. Supramolecular Pattern of Fullerene on 2D Bimolecular "Chessboard" Consisting of Bottom-Up Assembly of Porphyrin and Phthalocyanine Molecules. *J. Am. Chem. Soc.* **2008**, *130*, 1085−1092.
(294) Seidl, L.; Martens, S.; Ma, J.; Stimming, U.; Schneider, O. In Situ Scanning Tunneling Microscopy Studies of the SEI Formation on Graphite Electrodes for Li(+)-Ion Batteries. *Nanoscale* **2016**, *8*, 14004−14014.
(295) Treutler, T. H.; Wittstock, G. Combination of an Electrochemical Tunneling Microscope (ECSTM) and a Scanning Electrochemical Microscope (SECM): Application for Tip-Induced Modification of Self-Assembled Monolayers. *Electrochim. Acta* **2003**, *48*, 2923−2932.
(296) Kim, Y.-G.; Javier, A.; Baricuatro, J. H.; Torelli, D.; Cummins, K. D.; Tsang, C. F.; Hemminger, J. C.; Soriaga, M. P. Surface Reconstruction of Pure-Cu Single-Crystal Electrodes Under CO-Reduction Potentials in Alkaline Solutions: A Study by Seriatim ECSTM-DEMS. *J. Electroanal. Chem.* **2016**, *780*, 290−295.
(297) Williams, C. G.; Edwards, M. A.; Colley, A. L.; Macpherson, J. V.; Unwin, P. R. Scanning Micropipet Contact Method for High-Resolution Imaging of Electrode Surface Redox Activity. *Anal. Chem.* **2009**, *81*, 2486−2495.
(298) Ebejer, N.; Schnippering, M.; Colburn, A. W.; Edwards, M. A.; Unwin, P. R. Localized High Resolution Electrochemistry and Multifunctional Imaging: Scanning Electrochemical Cell Microscopy. *Anal. Chem.* **2010**, *82*, 9141−9145.
(299) Ebejer, N.; Güell, A. G.; Lai, S. C. S.; McKelvey, K.; Snowden, M. E.; Unwin, P. R. Scanning Electrochemical Cell Microscopy: A Versatile Technique for Nanoscale Electrochemistry and Functional Imaging. *Annu. Rev. Anal. Chem.* **2013**, *6*, 329−351.
(300) Wahab, O. J.; Kang, M.; Unwin, P. R. Scanning Electrochemical Cell Microscopy: A Natural Technique for Single Entity Electrochemistry. *Curr. Opin. Electrochem.* **2020**, *22*, 120−128.
(301) Martín-Yerga, D.; Costa-García, A.; Unwin, P. R. Correlative Voltammetric Microscopy: Structure-Activity Relationships in the Microscopic Electrochemical Behavior of Screen Printed Carbon Electrodes. *ACS sensors* **2019**, *4*, 2173−2180.
(302) Yamamoto, T.; Ando, T.; Kawabe, Y.; Fukuma, T.; Enomoto, H.; Nishijima, Y.; Matsui, Y.; Kanamura, K.; Takahashi, Y. Characterization of the Depth of Discharge-Dependent Charge Transfer Resistance of a Single LiFePO4 Particle. *Anal. Chem.* **2021**, *93*, 14448−14453.
(303) Gao, R.; Edwards, M. A.; Qiu, Y.; Barman, K.; White, H. S. Visualization of Hydrogen Evolution at Individual Platinum Nanoparticles at a Buried Interface. *J. Am. Chem. Soc.* **2020**, *142*, 8890−8896.
(304) Chen, C.-H.; Ravenhill, E. R.; Momotenko, D.; Kim, Y.-R.; Lai, S. C. S.; Unwin, P. R. Impact of Surface Chemistry on Nanoparticle-Electrode Interactions in the Electrochemical Detection of Nanoparticle Collisions. *Langmuir* **2015**, *31*, 11932−11942.
(305) Ustarroz, J.; Kang, M.; Bullions, E.; Unwin, P. R. Impact and Oxidation of Single Silver Nanoparticles at Electrode Surfaces:One Shot Versus Multiple Events. *Chem. Sci.* **2017**, *8*, 1841−1853.
(306) Saha, P.; Hill, J. W.; Walmsley, J. D.; Hill, C. M. Probing Electrocatalysis at Individual Au Nanorods via Correlated Optical and Electrochemical Measurements. *Anal. Chem.* **2018**, *90*, 12832−12839.
(307) Valavanis, D.; Ciocci, P.; Meloni, G. N.; Morris, P.; Lemineur, J.-F.; McPherson, I. J.; Kanoufi, F.; Unwin, P. R. Hybrid Scanning Electrochemical Cell Microscopy-Interference Reflection Microscopy (SECCM-IRM): Tracking Phase Formation on Surfaces in Small Volumes. *Faraday Discuss.* **2022**, *233*, 122−148.
(308) Cheng, L.; Jin, R.; Jiang, D.; Zhuang, J.; Liao, X.; Zheng, Q. Scanning Electrochemical Cell Microscopy Platform with Local Electrochemical Impedance Spectroscopy. *Anal. Chem.* **2021**, *93*, 16401−16408.
(309) Momotenko, D.; Byers, J. C.; McKelvey, K.; Kang, M.; Unwin, P. R. High-Speed Electrochemical Imaging. *ACS Nano* **2015**, *9*, 8942−8952.
(310) Brunet Cabré, M.; Djekic, D.; Romano, T.; Hanna, N.; Anders, J.; McKelvey, K. Microscale Electrochemical Cell on a Custom CMOS Transimpedance Amplifier for High Temporal Resolution Single Entity Electrochemistry. *ChemElectroChem.* **2020**, *7*, 4724−4729.
(311) Blount, B.; Juarez, G.; Wang, Y.; Ren, H. iR Drop in Scanning Electrochemical Cell Microscopy. *Faraday Discuss.* **2022**, *233*, 149−162.
(312) Li, Y.; Morel, A.; Gallant, D.; Mauzeroll, J. Ag+ Interference from Ag/AgCl Wire Quasi-Reference Counter Electrode Inducing Corrosion Potential Shift in an Oil-Immersed Scanning Micropipette Contact Method Measurement. *Anal. Chem.* **2021**, *93*, 9657−9662.
(313) Hill, J. W.; Hill, C. M. Directly Visualizing Carrier Transport and Recombination at Individual Defects Within 2D Semiconductors. *Chem. Sci.* **2021**, *12*, 5102−5112.
(314) Tolbert, C. L.; Hill, C. M. Electrochemically Probing Exciton Transport in Monolayers of Two-Dimensional Semiconductors. *Faraday Discuss.* **2022**, *233*, 163.
(315) Fu, Z.; Hill, J. W.; Parkinson, B.; Hill, C. M.; Tian, J. Layer and Material-Type Dependent Photoresponse in WSe_2 /WS_2 Vertical Heterostructures. *2D Mater.* **2022**, *9*, 015022.
(316) Güell, A. G.; Ebejer, N.; Snowden, M. E.; McKelvey, K.; Macpherson, J. V.; Unwin, P. R. Quantitative Nanoscale Visualization of Heterogeneous Electron Transfer Rates in 2D Carbon Nanotube Networks. *Proc. Natl. Acad. Sci. U.S.A.* **2012**, *109*, 11487−11492.
(317) Güell, A. G.; Meadows, K. E.; Dudin, P. V.; Ebejer, N.; Byers, J. C.; Macpherson, J. V.; Unwin, P. R. Selection, Characterisation and Mapping of Complex Electrochemical Processes at Individual Single-Walled Carbon Nanotubes: The Case of Serotonin Oxidation. *Faraday Discuss.* **2014**, *172*, 439−455.
(318) Aaronson, B. D. B.; Chen, C.-H.; Li, H.; Koper, M. T. M.; Lai, S. C. S.; Unwin, P. R. Pseudo-Single-Crystal Electrochemistry on Polycrystalline Electrodes:Visualizing Activity at Grains and Grain Boundaries on Platinum for the Fe^{2+}/Fe^{3+} Redox Reaction. *J. Am. Chem. Soc.* **2013**, *135*, 3873−3880.
(319) Wang, Y.; Gordon, E.; Ren, H. Mapping the Nucleation of H_2 Bubbles on Polycrystalline Pt via Scanning Electrochemical Cell Microscopy. *J. Phys. Chem. Lett.* **2019**, *10*, 3887−3892.
(320) Yule, L. C.; Daviddi, E.; West, G.; Bentley, C. L.; Unwin, P. R. Surface Microstructural Controls on Electrochemical Hydrogen Absorption at Polycrystalline Palladium. *J. Electroanal. Chem.* **2020**, *872*, 114047.
(321) Mariano, R. G.; McKelvey, K.; White, H. S.; Kanan, M. W. Selective Increase in CO_2 Electroreduction Activity at Grain-Boundary Surface Terminations. *Science* **2017**, *358*, 1187−1192.
(322) Mariano, R. G.; Kang, M.; Wahab, O. J.; McPherson, I. J.; Rabinowitz, J. A.; Unwin, P. R.; Kanan, M. W. Microstructural Origin of Locally Enhanced CO_2 Electroreduction Activity on Gold. *Nat. Mater.* **2021**, *20*, 1000−1006.
(323) Bentley, C. L.; Unwin, P. R. Nanoscale Electrochemical Movies and Synchronous Topographical Mapping of Electrocatalytic Materials. *Faraday Discuss.* **2018**, *210*, 365−379.
(324) Patten, H. V.; Lai, S. C. S.; Macpherson, J. V.; Unwin, P. R. Active sites for Outer-Sphere, Inner-Sphere, and Complex Multistage Electrochemical Reactions at Polycrystalline Boron-Doped Diamond Electrodes (pBDD) Revealed with Scanning Electrochemical Cell Microscopy (SECCM). *Anal. Chem.* **2012**, *84*, 5427−5432.
(325) Ando, T.; Asai, K.; Macpherson, J.; Einaga, Y.; Fukuma, T.; Takahashi, Y. Nanoscale Reactivity Mapping of a Single-Crystal Boron-Doped Diamond Particle. *Anal. Chem.* **2021**, *93*, 5831−5838.
(326) Liu, D.-Q.; Chen, C.-H.; Perry, D.; West, G.; Cobb, S. J.; Macpherson, J. V.; Unwin, P. R. Facet-Resolved Electrochemistry of Polycrystalline Boron-Doped Diamond Electrodes: Microscopic

https://doi.org/10.1021/acs.chemrev.2c00766
Chem. Rev. 2023, 123, 4972−5019

Factors Determining the Solvent Window in Aqueous Potassium Chloride Solutions. *ChemElectroChem.* **2018**, *5*, 3028−3035.
(327) Maddar, F. M.; Lazenby, R. A.; Patel, A. N.; Unwin, P. R. Electrochemical Oxidation of Dihydronicotinamide Adenine Dinucleotide (NADH): Comparison of Highly Oriented Pyrolytic Graphite (HOPG) and Polycrystalline Boron-Doped Diamond (pBDD) Electrodes. *Phys. Chem. Chem. Phys.* **2016**, *18*, 26404−26411.
(328) Aaronson, B. D. B.; Lai, S. C. S.; Unwin, P. R. Spatially Resolved Electrochemistry in Ionic Liquids: Surface Structure Effects on Triiodide Reduction at Platinum Electrodes. *Langmuir* **2014**, *30*, 1915−1919.
(329) Daviddi, E.; Chen, Z.; Beam Massani, B.; Lee, J.; Bentley, C. L.; Unwin, P. R.; Ratcliff, E. L. Nanoscale Visualization and Multiscale Electrochemical Analysis of Conductive Polymer Electrodes. *ACS Nano* **2019**, *13*, 13271−13284.
(330) Wahab, O. J.; Kang, M.; Meloni, G. N.; Daviddi, E.; Unwin, P. R. Nanoscale Visualization of Electrochemical Activity at Indium Tin Oxide Electrodes. *Anal. Chem.* **2022**, *94*, 4729−4736.
(331) Bentley, C. L.; Agoston, R.; Tao, B.; Walker, M.; Xu, X.; O'Mullane, A. P.; Unwin, P. R. Correlating the Local Electrocatalytic Activity of Amorphous Molybdenum Sulfide Thin Films with Microscopic Composition, Structure, and Porosity. *ACS Appl. Mater. Interfaces* **2020**, *12*, 44307−44316.
(332) Lai, S. C. S.; Patel, A. N.; McKelvey, K.; Unwin, P. R. Definitive Evidence for Fast Electron Transfer at Pristine Basal Plane Graphite from High-Resolution Electrochemical Imaging. *Angew. Chem., Int. Ed.* **2012**, *51*, 5405−5408.
(333) Zhang, G.; Kirkman, P. M.; Patel, A. N.; Cuharuc, A. S.; McKelvey, K.; Unwin, P. R. Molecular Functionalization of Graphite Surfaces: Basal Plane Versus Step Edge Electrochemical Activity. *J. Am. Chem. Soc.* **2014**, *136*, 11444−11451.
(334) E, S. P.; Kim, Y.-R.; Perry, D.; Bentley, C. L.; Unwin, P. R. Nanoscale Electrocatalysis of Hydrazine Electro-Oxidation at Blistered Graphite Electrodes. *ACS Appl. Mater. Interfaces* **2016**, *8*, 30458−30466.
(335) Payne, N. A.; Mauzeroll, J. Identifying Nanoscale Pinhole Defects in Nitroaryl Layers with Scanning Electrochemical Cell Microscopy. *ChemElectroChem.* **2019**, *6*, 5439−5445.
(336) Güell, A. G.; Ebejer, N.; Snowden, M. E.; Macpherson, J. V.; Unwin, P. R. Structural Correlations in Heterogeneous Electron Transfer at Monolayer and Multilayer Graphene Electrodes. *J. Am. Chem. Soc.* **2012**, *134*, 7258−7261.
(337) Yu, Y.; Zhang, K.; Parks, H.; Babar, M.; Carr, S.; Craig, I. M.; van Winkle, M.; Lyssenko, A.; Taniguchi, T.; Watanabe, K.; et al. Tunable Angle-Dependent Electrochemistry at Twisted Bilayer Graphene with Moiré Flat Bands. *Nat. Chem.* **2022**, *14*, 267−273.
(338) Thompson, A. C.; Simpson, B. H.; Lewis, N. S. Macroscale and Nanoscale Photoelectrochemical Behavior of p-Type Si(111) Covered by a Single Layer of Graphene or Hexagonal Boron Nitride. *ACS Appl. Mater. Interfaces* **2020**, *12*, 11551−11561.
(339) Kumatani, A.; Miura, C.; Kuramochi, H.; Ohto, T.; Wakisaka, M.; Nagata, Y.; Ida, H.; Takahashi, Y.; Hu, K.; Jeong, S.; et al. Chemical Dopants on Edge of Holey Graphene Accelerate Electrochemical Hydrogen Evolution Reaction. *Adv. Sci.* **2019**, *6*, 1900119.
(340) Cabré, M. B.; Paiva, A. E.; Velický, M.; Colavita, P. E.; McKelvey, K. Electrochemical Detection of Isolated Nanoscale Defects in 2D Transition Metal Dichalcogenides. *J. Phys. Chem. C* **2022**, *126*, 11636.
(341) Bentley, C. L.; Kang, M.; Maddar, F. M.; Li, F.; Walker, M.; Zhang, J.; Unwin, P. R. Electrochemical Maps and Movies of the Hydrogen Evolution Reaction on Natural Crystals of Molybdenite (MoS_2): Basal vs. Edge Plane Activity. *Chem. Sci.* **2017**, *8*, 6583−6593.
(342) Hill, J. W.; Fu, Z.; Tian, J.; Hill, C. M. Locally Engineering and Interrogating the Photoelectrochemical Behavior of Defects in Transition Metal Dichalcogenides. *J. Phys. Chem. C* **2020**, *124*, 17141−17149.
(343) Bentley, C. L.; Kang, M.; Unwin, P. R. Nanoscale Structure Dynamics within Electrocatalytic Materials. *J. Am. Chem. Soc.* **2017**, *139*, 16813−16821.
(344) Takahashi, Y.; Kobayashi, Y.; Wang, Z.; Ito, Y.; Ota, M.; Ida, H.; Kumatani, A.; Miyazawa, K.; Fujita, T.; Shiku, H.; et al. High-Resolution Electrochemical Mapping of the Hydrogen Evolution Reaction on Transition-Metal Dichalcogenide Nanosheets. *Angew. Chem., Int. Ed.* **2020**, *59*, 3601−3608.
(345) Tao, B.; Unwin, P. R.; Bentley, C. L. Nanoscale Variations in the Electrocatalytic Activity of Layered Transition-Metal Dichalcogenides. *J. Phys. Chem. C* **2020**, *124*, 789−798.
(346) Bentley, C. L.; Andronescu, C.; Smialkowski, M.; Kang, M.; Tarnev, T.; Marler, B.; Unwin, P. R.; Apfel, U.-P.; Schuhmann, W. Local Surface Structure and Composition Control the Hydrogen Evolution Reaction on Iron Nickel Sulfides. *Angew. Chem., Int. Ed.* **2018**, *57*, 4093−4097.
(347) Choi, M.; Siepser, N. P.; Jeong, S.; Wang, Y.; Jagdale, G.; Ye, X.; Baker, L. A. Probing Single-Particle Electrocatalytic Activity at Facet-Controlled Gold Nanocrystals. *Nano Lett.* **2020**, *20*, 1233−1239.
(348) Liu, G.; Hao, L.; Li, H.; Zhang, K.; Yu, X.; Li, D.; Zhu, X.; Hao, D.; Ma, Y.; Ma, L. Topography Mapping with Scanning Electrochemical Cell Microscopy. *Anal. Chem.* **2022**, *94*, 5248−5254.
(349) Georgescu, N. S.; Robinson, D. A.; White, H. S. Effect of Nonuniform Mass Transport on Nanobubble Nucleation at Individual Pt Nanoparticles. *J. Phys. Chem. C* **2021**, *125*, 19724−19732.
(350) Liu, Y.; Jin, C.; Liu, Y.; Ruiz, K. H.; Ren, H.; Fan, Y.; White, H. S.; Chen, Q. Visualization and Quantification of Electrochemical H_2 Bubble Nucleation at Pt, Au, and MoS_2 Substrates. *ACS sensors* **2021**, *6*, 355−363.
(351) Liu, Y.; Lu, X.; Peng, Y.; Chen, Q. Electrochemical Visualization of Gas Bubbles on Superaerophobic Electrodes Using Scanning Electrochemical Cell Microscopy. *Anal. Chem.* **2021**, *93*, 12337−12345.
(352) Wang, Y.; Gordon, E.; Ren, H. Mapping the Potential of Zero Charge and Electrocatalytic Activity of Metal-Electrolyte Interface via a Grain-by-Grain Approach. *Anal. Chem.* **2020**, *92*, 2859−2865.
(353) Wang, Y.; Li, M.; Ren, H. Voltammetric Mapping of Hydrogen Evolution Reaction on Pt Locally via Scanning Electrochemical Cell Microscopy. *ACS Meas. Sci. Au* **2022**, *2*, 304−308.
(354) Ciocci, P.; Lemineur, J.-F.; Noël, J.-M.; Combellas, C.; Kanoufi, F. Differentiating Electrochemically Active Regions of Indium Tin Oxide Electrodes for Hydrogen Evolution and Reductive Decomposition Reactions. An In Situ Optical Microscopy Approach. *Electrochim. Acta* **2021**, *386*, 138498.
(355) Shkirskiy, V.; Yule, L. C.; Daviddi, E.; Bentley, C. L.; Aarons, J.; West, G.; Unwin, P. R. Nanoscale Scanning Electrochemical Cell Microscopy and Correlative Surface Structural Analysis to Map Anodic and Cathodic Reactions on Polycrystalline Zn in Acid Media. *J. Electrochem. Soc.* **2020**, *167*, 041507.
(356) Jin, R.; Cheng, L.; Lu, H.; Zhuang, J.; Jiang, D.; Chen, H.-Y. High Spatial Resolution Electrochemical Microscopic Observation of Enhanced Charging under Bias at Active Sites of N-rGO. *ACS Appl. Energy Mater.* **2021**, *4*, 3502−3507.
(357) Yule, L. C.; Shkirskiy, V.; Aarons, J.; West, G.; Bentley, C. L.; Shollock, B. A.; Unwin, P. R. Nanoscale Active Sites for the Hydrogen Evolution Reaction on Low Carbon Steel. *J. Phys. Chem. C* **2019**, *123*, 24146−24155.
(358) Ustarroz, J.; Ornelas, I. M.; Zhang, G.; Perry, D.; Kang, M.; Bentley, C. L.; Walker, M.; Unwin, P. R. Mobility and Poisoning of Mass-Selected Platinum Nanoclusters during the Oxygen Reduction Reaction. *ACS Catal.* **2018**, *8*, 6775−6790.
(359) Tetteh, E. B.; Banko, L.; Krysiak, O. A.; Löffler, T.; Xiao, B.; Varhade, S.; Schumacher, S.; Savan, A.; Andronescu, C.; Ludwig, A.; et al. Zooming-In − Visualization of Active Site Heterogeneity in High Entropy Alloy Electrocatalysts using Scanning Electrochemical Cell Microscopy. *Electrochem. Sci. Adv.* **2022**, *2*, No. e2100105.
(360) Tetteh, E. B.; Löffler, T.; Tarnev, T.; Quast, T.; Wilde, P.; Aiyappa, H. B.; Schumacher, S.; Andronescu, C.; Tilley, R. D.; Chen,

https://doi.org/10.1021/acs.chemrev.2c00766
Chem. Rev. 2023, 123, 4972−5019

X.; et al. Calibrating SECCM Measurements by Means of a Nanoelectrode Ruler. The Intrinsic Oxygen Reduction Activity of PtNi Catalyst Nanoparticles. *Nano Res.* **2022**, *15*, 1564−1569.
(361) Mariano, R. G.; Wahab, O. J.; Rabinowitz, J. A.; Oppenheim, J.; Chen, T.; Unwin, P. R.; Dincă, M. Thousand-Fold Increase in O_2 Electroreduction Rates with Conductive MOFs. *ACS Cent. Sci.* **2022**, *8*, 975−982.
(362) Lu, X.; Li, M.; Peng, Y.; Xi, X.; Li, M.; Chen, Q.; Dong, A. Direct Probing of the Oxygen Evolution Reaction at Single $NiFe_2O_4$ Nanocrystal Superparticles with Tunable Structures. *J. Am. Chem. Soc.* **2021**, *143*, 16925−16929.
(363) Quast, T.; Varhade, S.; Saddeler, S.; Chen, Y.-T.; Andronescu, C.; Schulz, S.; Schuhmann, W. Single Particle Nanoelectrochemistry Reveals the Catalytic Oxygen Evolution Reaction Activity of Co_3O_4 Nanocubes. *Angew. Chem., Int. Ed.* **2021**, *60*, 23444−23450.
(364) Makarova, M. V.; Amano, F.; Nomura, S.; Tateishi, C.; Fukuma, T.; Takahashi, Y.; Korchev, Y. E. Direct Electrochemical Visualization of the Orthogonal Charge Separation in Anatase Nanotube Photoanodes for Water Splitting. *ACS Catal.* **2022**, *12*, 1201−1208.
(365) Tsujiguchi, T.; Kawabe, Y.; Jeong, S.; Ohto, T.; Kukunuri, S.; Kuramochi, H.; Takahashi, Y.; Nishiuchi, T.; Masuda, H.; Wakisaka, M.; et al. Acceleration of Electrochemical CO_2 Reduction to Formate at the Sn/Reduced Graphene Oxide Interface. *ACS Catal.* **2021**, *11*, 3310−3318.
(366) Jeong, S.; Choi, M.-H.; Jagdale, G. S.; Zhong, Y.; Siepser, N. P.; Wang, Y.; Zhan, X.; Baker, L. A.; Ye, X. Unraveling the Structural Sensitivity of CO_2 Electroreduction at Facet-Defined Nanocrystals via Correlative Single-Entity and Macroelectrode Measurements. *J. Am. Chem. Soc.* **2022**, *144*, 12673.
(367) Kirkman, P. M.; Güell, A. G.; Cuharuc, A. S.; Unwin, P. R. Spatial and Temporal Control of the Diazonium Modification of sp2 Carbon Surfaces. *J. Am. Chem. Soc.* **2014**, *136*, 36−39.
(368) Lai, S. C. S.; Lazenby, R. A.; Kirkman, P. M.; Unwin, P. R. Nucleation, Aggregative Growth and Detachment of Metal Nanoparticles during Electrodeposition at Electrode Surfaces. *Chem. Sci.* **2015**, *6*, 1126−1138.
(369) Parker, A. S.; Al Botros, R.; Kinnear, S. L.; Snowden, M. E.; McKelvey, K.; Ashcroft, A. T.; Carvell, M.; Joiner, A.; Peruffo, M.; Philpotts, C.; et al. Combinatorial Localized Dissolution Analysis: Application to Acid-Induced Dissolution of Dental Enamel and the Effect of Surface Treatments. *J. Colloid Interface Sci.* **2016**, *476*, 94−102.
(370) Parker, A. S.; Patel, A. N.; Al Botros, R.; Snowden, M. E.; McKelvey, K.; Unwin, P. R.; Ashcroft, A. T.; Carvell, M.; Joiner, A.; Peruffo, M. Measurement of the Efficacy of Calcium Silicate for the Protection and Repair of Dental Enamel. *J. Dent.* **2014**, *42*, S21−S29.
(371) Zhan, D.; Yang, D.; Zhu, Y.; Wu, X.; Tian, Z.-Q. Fabrication and Characterization of Nanostructured ZnO Thin Film Microdevices by Scanning Electrochemical Cell Microscopy. *Chem. Commun.* **2012**, *48*, 11449−11451.
(372) Majumdar, P.; Gao, R.; White, H. S. Electroprecipitation of Nanometer-Thick Films of $Ln(OH)_3$ Ln = La, Ce, and Lu at Pt Microelectrodes and Their Effect on Electron-Transfer Reactions. *Langmuir* **2022**, *38*, 8125−8134.
(373) McKelvey, K.; O'Connell, M. A.; Unwin, P. R. Meniscus Confined Fabrication of Multidimensional Conducting Polymer Nanostructures with Scanning Electrochemical Cell Microscopy (SECCM). *Chem. Commun.* **2013**, *49*, 2986−2988.
(374) Aaronson, B. D. B.; Garoz-Ruiz, J.; Byers, J. C.; Colina, A.; Unwin, P. R. Electrodeposition and Screening of Photoelectrochemical Activity in Conjugated Polymers Using Scanning Electrochemical Cell Microscopy. *Langmuir* **2015**, *31*, 12814−12822.
(375) Oseland, E. E.; Ayres, Z. J.; Basile, A.; Haddleton, D. M.; Wilson, P.; Unwin, P. R. Surface Patterning of Polyacrylamide Gel using Scanning Electrochemical Cell Microscopy (SECCM). *Chem. Commun.* **2016**, *52*, 9929−9932.
(376) Takahashi, Y.; Kumatani, A.; Munakata, H.; Inomata, H.; Ito, K.; Ino, K.; Shiku, H.; Unwin, P. R.; Korchev, Y. E.; Kanamura, K.; et al. Nanoscale Visualization of Redox Activity at Lithium-Ion Battery Cathodes. *Nat. Commun.* **2014**, *5*, 5450.
(377) E, S. P.; Kang, M.; Wilson, P.; Meng, L.; Perry, D.; Basile, A.; Unwin, P. R. High Resolution Visualization of the Redox Activity of Li_2O_2 in Non-Aqueous Media: Conformal Layer vs. *Toroid Structure. Chem. Commun.* **2018**, *54*, 3053−3056.
(378) Dayeh, M.; Ghavidel, M. R. Z.; Mauzeroll, J.; Schougaard, S. B. Micropipette Contact Method to Investigate High-Energy Cathode Materials by using an Ionic Liquid. *ChemElectroChem.* **2019**, *6*, 195−201.
(379) Inomata, H.; Takahashi, Y.; Takamatsu, D.; Kumatani, A.; Ida, H.; Shiku, H.; Matsue, T. Visualization of Inhomogeneous Current Distribution on ZrO_2-Coated $LiCoO_2$ Thin-Film Electrodes using Scanning Electrochemical Cell Microscopy. *Chem. Commun.* **2019**, *55*, 545−548.
(380) Tao, B.; Yule, L. C.; Daviddi, E.; Bentley, C. L.; Unwin, P. R. Correlative Electrochemical Microscopy of Li-Ion (De)intercalation at a Series of Individual LiMn2 O4 Particles. *Angew. Chem., Int. Ed.* **2019**, *58*, 4606−4611.
(381) Takahashi, Y.; Yamashita, T.; Takamatsu, D.; Kumatani, A.; Fukuma, T. Nanoscale Kinetic Imaging of Lithium Ion Secondary Battery Materials using Scanning Electrochemical Cell Microscopy. *Chem. Commun.* **2020**, *56*, 9324−9327.
(382) Kumatani, A.; Takahashi, Y.; Miura, C.; Ida, H.; Inomata, H.; Shiku, H.; Munakata, H.; Kanamura, K.; Matsue, T. Scanning Electrochemical Cell Microscopy for Visualization and Local Electrochemical Activities of Lithium-Ion (De) Intercalation Process in Lithium-Ion Batteries Electrodes. *Surf. Interface Anal.* **2019**, *51*, 27−30.
(383) Martín-Yerga, D.; Kang, M.; Unwin, P. R. Scanning Electrochemical Cell Microscopy in a Glovebox: Structure-Activity Correlations in the Early Stages of Solid-Electrolyte Interphase Formation on Graphite. *ChemElectroChem.* **2021**, *8*, 4240−4251.
(384) Bentley, C. L.; Kang, M.; Unwin, P. R. Scanning Electrochemical Cell Microscopy (SECCM) in Aprotic Solvents: Practical Considerations and Applications. *Anal. Chem.* **2020**, *92*, 11673−11680.
(385) Gateman, S. M.; Georgescu, N. S.; Kim, M.-K.; Jung, I.-H.; Mauzeroll, J. Efficient Measurement of the Influence of Chemical Composition on Corrosion: Analysis of an Mg-Al Diffusion Couple Using Scanning Micropipette Contact Method. *J. Electrochem. Soc.* **2019**, *166*, C624−C630.
(386) Yule, L. C.; Bentley, C. L.; West, G.; Shollock, B. A.; Unwin, P. R. Scanning Electrochemical Cell Microscopy: A Versatile Method for Highly Localised Corrosion Related Measurements on Metal Surfaces. *Electrochim. Acta* **2019**, *298*, 80−88.
(387) Yule, L. C.; Shkirskiy, V.; Aarons, J.; West, G.; Shollock, B. A.; Bentley, C. L.; Unwin, P. R. Nanoscale Electrochemical Visualization of Grain-Dependent Anodic Iron Dissolution from Low Carbon Steel. *Electrochim. Acta* **2020**, *332*, 135267.
(388) Aaronson, B. D. B.; Byers, J. C.; Colburn, A. W.; McKelvey, K.; Unwin, P. R. Scanning Electrochemical Cell Microscopy Platform for Ultrasensitive Photoelectrochemical Imaging. *Anal. Chem.* **2015**, *87*, 4129−4133.
(389) Strange, L. E.; Yadav, J.; Garg, S.; Shinde, P. S.; Hill, J. W.; Hill, C. M.; Kung, P.; Pan, S. Investigating the Redox Properties of Two-Dimensional MoS_2 using Photoluminescence Spectroelectrochemistry and Scanning Electrochemical Cell Microscopy. *J. Phys. Chem. Lett.* **2020**, *11*, 3488−3494.
(390) Kim, J.; Gewirth, A. A. Mechanism of Oxygen Electroreduction on Gold Surfaces in Basic Media. *J. Phys. Chem. B* **2006**, *110*, 2565−2571.
(391) Yeager, E. Dioxygen Electrocatalysis: Mechanisms in Relation to Catalyst Structure. *J. Mol. Catal.* **1986**, *38*, 5−25.
(392) Vassilev, P.; Koper, M. T. M. Electrochemical Reduction of Oxygen on Gold Surfaces: A Density Functional Theory Study of Intermediates and Reaction Paths. *J. Phys. Chem. C* **2007**, *111*, 2607−2613.

https://doi.org/10.1021/acs.chemrev.2c00766
Chem. Rev. 2023, 123, 4972−5019

(393) Ge, X.; Sumboja, A.; Wuu, D.; An, T.; Li, B.; Goh, F. W. T.; Hor, T. S. A.; Zong, Y.; Liu, Z. Oxygen Reduction in Alkaline Media: From Mechanisms to Recent Advances of Catalysts. *ACS Catal.* **2015**, *5*, 4643−4667.
(394) Vielstich, W.; Lamm, A.; Gasteiger, H. A. *Handbook of Fuel Cells:Fundamentals Technology and Applications Technology and Applications. Pt. 2*; Wiley: Chichester, 2003.
(395) Greeley, J.; Markovic, N. M. The Road from Animal Electricity to Green Energy: Combining Experiment and Theory in Electrocatalysis. *Energy Environ. Sci.* **2012**, *5*, 9246.
(396) Anastasijević, N. A.; Vesović, V.; Adžić, R. R. Determination of the Kinetic Parameters of the Oxygen Reduction Reaction using the Rotating Ring-disk Electrode: Part I. Theory. *J. Electroanal. Chem.* **1987**, *229*, 305−316.
(397) Anastasijević, N. A.; Vesović, V.; Adžić, R. R. Determination of the Kinetic Parameters of the Oxygen Reduction Reaction using the Rotating Ring-disk Electrode: Part II. Applications. *J. Electroanal. Chem.* **1987**, *229*, 317−325.
(398) Zinola, C. F.; Arvia, A. J.; Estiu, G. L.; Castro, E. A. A Quantum Chemical Approach to the Influence of Platinum Surface Structure on the Oxygen Electroreduction Reaction. *J. Phys. Chem.* **1994**, *98*, 7566.
(399) Shen, Y.; Träuble, M.; Wittstock, G. Detection of Hydrogen Peroxide Produced During Electrochemical Oxygen Reduction using Scanning Electrochemical Microscopy. *Anal. Chem.* **2008**, *80*, 750−759.
(400) Fernández, J. L.; Walsh, D. A.; Bard, A. J. Thermodynamic Guidelines for the Design of Bimetallic Catalysts for Oxygen Electroreduction and Rapid Screening by Scanning Electrochemical Microscopy. M-Co (M: Pd, Ag, Au). *J. Am. Chem. Soc.* **2005**, *127*, 357−365.
(401) Wang, X.; Li, Z.; Qu, Y.; Yuan, T.; Wang, W.; Wu, Y.; Li, Y. Review of Metal Catalysts for Oxygen Reduction Reaction: From Nanoscale Engineering to Atomic Design. *Chem.* **2019**, *5*, 1486−1511.
(402) Liu, B.; Bard, A. J. Scanning Electrochemical Microscopy. 45. Study of the Kinetics of Oxygen Reduction on Platinum with Potential Programming of the Tip. *J. Phys. Chem. B* **2002**, *106*, 12801−12806.
(403) Sanchez-Sanchez, C. M.; Bard, A. J. Hydrogen Peroxide Production in the Oxygen Reduction Reaction at Different Electrocatalysts as Quantified by Scanning Electrochemical Microscopy. *Anal. Chem.* **2009**, *81*, 8094−8100.
(404) Sánchez-Sánchez, C. M.; Rodríguez-López, J.; Bard, A. J. Scanning Electrochemical Microscopy. 60. Quantitative Calibration of the SECM Substrate Generation/Tip Collection Mode and its use for the Study of the Oxygen Reduction Mechanism. *Anal. Chem.* **2008**, *80*, 3254−3260.
(405) Zhang, C.; Fan, F.-R. F.; Bard, A. J. Electrochemistry of Oxygen in Concentrated NaOH Solutions: Solubility, Diffusion Coefficients, and Superoxide Formation. *J. Am. Chem. Soc.* **2009**, *131*, 177−181.
(406) Shen, Y.; Träuble, M.; Wittstock, G. Electrodeposited Noble Metal Particles in Polyelectrolyte Multilayer Matrix as Electrocatalyst for Oxygen Reduction Studied using SECM. *Phys. Chem. Chem. Phys.* **2008**, *10*, 3635−3644.
(407) Noel, J.-M.; Kostopoulos, N.; Achaibou, C.; Fave, C.; Anxolabéhère-Mallart, E.; Kanoufi, F. Probing the Activity of Iron Peroxo Porphyrin Intermediates in the Reaction Layer during the Electrochemical Reductive Activation of O_2. *Angew. Chem., Int. Ed.* **2020**, *59*, 16376−16380.
(408) Bae, J. H.; Yu, Y.; Mirkin, M. V. Scanning Electrochemical Microscopy Study of Electron-Transfer Kinetics and Catalysis at Nanoporous Electrodes. *J. Phys. Chem. C* **2016**, *120*, 20651−20658.
(409) Barwe, S.; Andronescu, C.; Engels, R.; Conzuelo, F.; Seisel, S.; Wilde, P.; Chen, Y.-T.; Masa, J.; Schuhmann, W. Cobalt Metalloid and Polybenzoxazine Derived Composites for Bifunctional Oxygen Electrocatalysis. *Electrochim. Acta* **2019**, *297*, 1042−1051.
(410) Sklyar, O.; Ufheil, J.; Heinze, J.; Wittstock, G. Application of the Boundary Element Method Numerical Simulations for Characterization of Heptode Ultramicroelectrodes in SECM Experiments. *Electrochim. Acta* **2003**, *49*, 117−128.
(411) Nagaiah, T. C.; Maljusch, A.; Chen, X. X.; Bron, M.; Schuhmann, W. Visualization of the Local Catalytic Activity of Electrodeposited Pt-Ag Catalysts for Oxygen Reduction by means of SECM. *ChemPhysChem* **2009**, *10*, 2711−2718.
(412) Schwamborn, S.; Stoica, L.; Chen, X.; Xia, W.; Kundu, S.; Muhler, M.; Schuhmann, W. Patterned CNT Arrays for the Evaluation of Oxygen Reduction Activity by SECM. *ChemPhysChem* **2010**, *11*, 74−78.
(413) Kundu, S.; Nagaiah, T. C.; Xia, W.; Wang, Y.; Van Dommele, S.; Bitter, J. H.; Santa, M.; Grundmeier, G.; Bron, M.; Schuhmann, W.; et al. Electrocatalytic Activity and Stability of Nitrogen-Containing Carbon Nanotubes in the Oxygen Reduction Reaction. *J. Phys. Chem. C* **2009**, *113*, 14302−14310.
(414) Singh, V.; Tiwari, A.; Nagaiah, T. C. Facet-Controlled Morphology of Cobalt Disulfide Towards Enhanced Oxygen Reduction Reaction. *J. Mater. Chem. A* **2018**, *6*, 22545−22554.
(415) Lima, A.; Lima, A.; Meloni, G.; Santos, C.; Bertotti, M. Perovskite-Type Oxides $La_{0.6}M_{0.4}Ni_{0.6}Cu_{0.4}O_3$ (M = Ag, Ba, Ce) towards the Oxygen Reduction Reaction (ORR) in Alkaline Medium: Structural Aspects and Electrocatalytic Activity. *J. Braz. Chem. Soc.* **2021**, *32*, 665−674.
(416) Okunola, A.; Kowalewska, B.; Bron, M.; Kulesza, P. J.; Schuhmann, W. Electrocatalytic Reduction of Oxygen at Electropolymerized Films of Metalloporphyrins Deposited onto Multi-walled Carbon Nanotubes. *Electrochim. Acta* **2009**, *54*, 1954−1960.
(417) Nagaiah, T. C.; Schäfer, D.; Schuhmann, W.; Dimcheva, N. Electrochemically Deposited Pd-Pt and Pd-Au Codeposits on Graphite Electrodes for Electrocatalytic H_2O_2 Reduction. *Anal. Chem.* **2013**, *85*, 7897−7903.
(418) Seiffarth, G.; Steimecke, M.; Walther, T.; Kühhirt, M.; Rümmler, S.; Bron, M. Mixed Transition Metal Oxide Supported on Nitrogen Doped Carbon Nanotubes - A Simple Bifunctional Electrocatalyst Studied with Scanning Electrochemical Microscopy. *Electroanalysis* **2016**, *28*, 2335−2345.
(419) Dobrzeniecka, A.; Zeradjanin, A.; Masa, J.; Puschhof, A.; Stroka, J.; Kulesza, P. J.; Schuhmann, W. Application of SECM in Tracing of Hydrogen Peroxide at Multicomponent Non-Noble Electrocatalyst Films for the Oxygen Reduction Reaction. *Catal. Today* **2013**, *202*, 55−62.
(420) Silva, S. M.; Aguiar, L. F.; Carvalho, R. M. S.; Tanaka, A. A.; Damos, F. S.; Luz, R. C. S. A Glassy Carbon Electrode Modified with an Iron N_4-Macrocycle and Reduced Graphene Oxide for Voltammetric Sensing of Dissolved Oxygen. *Microchim. Acta* **2016**, *183*, 1251−1259.
(421) Schulte, W.; Liu, S.; Plettenberg, I.; Kuhri, S.; Lüke, W.; Lehnert, W.; Wittstock, G. Local Evaluation of Processed Membrane Electrode Assemblies by Scanning Electrochemical Microscopy. *J. Electrochem. Soc.* **2017**, *164*, F873−F878.
(422) Botz, A.; Clausmeyer, J.; Öhl, D.; Tarnev, T.; Franzen, D.; Turek, T.; Schuhmann, W. Local Activities of Hydroxide and Water Determine the Operation of Silver-Based Oxygen Depolarized Cathodes. *Angew. Chem., Int. Ed.* **2018**, *57*, 12285−12289.
(423) Kolagatla, S.; Subramanian, P.; Schechter, A. Simultaneous Mapping of Oxygen Reduction Activity and Hydrogen Peroxide Generation on Electrocatalytic Surfaces. *ChemSusChem* **2019**, *12*, 2708−2714.
(424) Hengstenberg, A.; Kranz, C.; Schuhmann, W. Facilitated Tip-Positioning and Applications of Non-Electrode Tips in Scanning Electrochemical Microscopy using a Sheer Force Based Constant-Distance Mode. *Chem.—Eur. J.* **2000**, *6*, 1547−1554.
(425) O'Connell, M. A.; Lewis, J. R.; Wain, A. J. Electrochemical Imaging of Hydrogen Peroxide Generation at Individual Gold Nanoparticles. *Chem. Commun.* **2015**, *51*, 10314−10317.

https://doi.org/10.1021/acs.chemrev.2c00766
Chem. Rev. 2023, 123, 4972−5019

(426) Cai, Z.-F.; Wang, X.; Wang, D.; Wan, L.-J. Cobalt-Porphyrin-Catalyzed Oxygen Reduction Reaction: A Scanning Tunneling Microscopy Study. *ChemElectroChem.* **2016**, *3*, 2048−2051.
(427) Pfisterer, J. H. K.; Liang, Y.; Schneider, O.; Bandarenka, A. S. Direct Instrumental Identification of Catalytically Active Surface Sites. *Nature* **2017**, *549*, 74−77.
(428) Haid, R. W.; Kluge, R. M.; Liang, Y.; Bandarenka, A. S. In Situ Quantification of the Local Electrocatalytic Activity via Electrochemical Scanning Tunneling Microscopy. *Small Methods* **2021**, *5*, No. 2000710.
(429) Yoshimoto, S.; Tada, A.; Suto, K.; Itaya, K. Adlayer Structures and Electrocatalytic Activity for O_2 of Metallophthalocyanines on Au(111): In Situ Scanning Tunneling Microscopy Study. *J. Phys. Chem. B* **2003**, *107*, 5836−5843.
(430) Yoshimoto, S.; Tada, A.; Itaya, K. In Situ Scanning Tunneling Microscopy Study of the Effect of Iron Octaethylporphyrin Adlayer on the Electrocatalytic Reduction of O_2 on Au(111). *J. Phys. Chem. B* **2004**, *108*, 5171−5174.
(431) Liang, Y.; McLaughlin, D.; Csoklich, C.; Schneider, O.; Bandarenka, A. S. The Nature of Active Centers Catalyzing Oxygen Electro-Reduction at Platinum Surfaces in Alkaline Media. *Energy Environ. Sci.* **2019**, *12*, 351−357.
(432) Chen, X.; Eckhard, K.; Zhou, M.; Bron, M.; Schuhmann, W. Electrocatalytic Activity of Spots of Electrodeposited Noble-Metal Catalysts on Carbon Nanotubes Modified Glassy Carbon. *Anal. Chem.* **2009**, *81*, 7597−7603.
(433) Chen, X.; Botz, A. J. R.; Masa, J.; Schuhmann, W. Characterisation of Bifunctional Electrocatalysts for Oxygen Reduction and Evolution by Means of SECM. *J. Solid State Electrochem.* **2016**, *20*, 1019−1027.
(434) Suen, N.-T.; Hung, S.-F.; Quan, Q.; Zhang, N.; Xu, Y.-J.; Chen, H. M. Electrocatalysis for the Oxygen Evolution Reaction: Recent Development and Future Perspectives. *Chem. Soc. Rev.* **2017**, *46*, 337−365.
(435) Liu, Y.; Zhou, D.; Deng, T.; He, G.; Chen, A.; Sun, X.; Yang, Y.; Miao, P. Research Progress of Oxygen Evolution Reaction Catalysts for Electrochemical Water Splitting. *ChemSusChem* **2021**, *14*, 5359−5383.
(436) Reier, T.; Nong, H. N.; Teschner, D.; Schlögl, R.; Strasser, P. Electrocatalytic Oxygen Evolution Reaction in Acidic Environments - Reaction Mechanisms and Catalysts. *Adv. Energy Mater.* **2017**, *7*, 1601275.
(437) Badreldin, A.; Abusrafa, A. E.; Abdel-Wahab, A. Oxygen-Deficient Cobalt-Based Oxides for Electrocatalytic Water Splitting. *ChemSusChem* **2021**, *14*, 10−32.
(438) Song, J.; Wei, C.; Huang, Z.-F.; Liu, C.; Zeng, L.; Wang, X.; Xu, Z. J. A Review on Fundamentals for Designing Oxygen Evolution Electrocatalysts. *Chem. Soc. Rev.* **2020**, *49*, 2196−2214.
(439) Li, J. Oxygen Evolution Reaction in Energy Conversion and Storage: Design Strategies Under and Beyond the Energy Scaling Relationship. *Nano-micro Lett.* **2022**, *14*, 112.
(440) Vazhayil, A.; Vazhayal, L.; Thomas, J.; Ashok C, S.; Thomas, N. A Comprehensive Review on the Recent Developments in Transition Metal-Based Electrocatalysts for Oxygen Evolution Reaction. *Appl. Surf. Sci.* **2021**, *6*, 100184.
(441) Jamesh, M.-I.; Sun, X. Recent Progress on Earth Abundant Electrocatalysts for Oxygen Evolution Reaction (OER) in Alkaline Medium to Achieve Efficient Water Splitting − A Review. *J. Power Sources* **2018**, *400*, 31−68.
(442) Chen, S.; Ma, L.; Huang, Z.; Liang, G.; Zhi, C. In Situ/Operando Analysis of Surface Reconstruction of Transition Metal-Based Oxygen Evolution Electrocatalysts. *Cell Reports Physical Science* **2022**, *3*, 100729.
(443) Galán-Mascarós, J. R. Water Oxidation at Electrodes Modified with Earth-Abundant Transition-Metal Catalysts. *ChemElectroChem.* **2015**, *2*, 37−50.
(444) Maljusch, A.; Ventosa, E.; Rincón, R. A.; Bandarenka, A. S.; Schuhmann, W. Revealing Onset Potentials using Electrochemical Microscopy to Assess the Catalytic Activity of Gas-Evolving Electrodes. *Electrochem. Commun.* **2014**, *38*, 142−145.
(445) Fushimi, K.; Okawa, T.; Seo, M. A Scanning Electrochemical Microscopic Observation of Heterogeneous Oxygen Evolution on a Polycrystalline Titanium during Anodic Oxidation. *Electrochemistry* **2000**, *68*, 950−954.
(446) Kang, J.; Yang, Y.; Jiang, F.; Shao, H. Study on the Anodic Reaction of Ni in an Alkaline Solution by Transient pH Detection Based on Scanning Electrochemical Microscopy (SECM). *Surf. Interface Anal.* **2007**, *39*, 877−884.
(447) Snook, G. A.; Duffy, N. W.; Pandolfo, A. G. Detection of Oxygen Evolution from Nickel Hydroxide Electrodes Using Scanning Electrochemical Microscopy. *J. Electrochem. Soc.* **2008**, *155*, A262.
(448) Botz, A. J.; Nebel, M.; Rincón, R. A.; Ventosa, E.; Schuhmann, W. Onset Potential Determination at Gas-Evolving Catalysts by Means of Constant-Distance Mode Positioning of Nanoelectrodes. *Electrochim. Acta* **2015**, *179*, 38−44.
(449) Zhang, T.; Wu, Y.; Yu, Y.; Li, Y.; Qin, G.; Li, S. High Throughput Screening Driven Discovery of $Mn_5Co_{10}Fe_{30}Ni_{55}O_x$ as Electrocatalyst for Water Oxidation and Electrospinning Synthesis. *Appl. Surf. Sci.* **2022**, *588*, 152959.
(450) Zeradjanin, A. R.; Ventosa, E.; Bondarenko, A. S.; Schuhmann, W. Evaluation of the Catalytic Performance of Gas-Evolving Electrodes Using Local Electrochemical Noise Measurements. *ChemSusChem* **2012**, *5*, 1905−1911.
(451) Sun, T.; Wang, D.; Mirkin, M. V.; Cheng, H.; Zheng, J.-C.; Richards, R. M.; Lin, F.; Xin, H. L. Direct High-Resolution Mapping of Electrocatalytic Activity of Semi-Two-Dimensional Catalysts with Single-Edge Sensitivity. *Proc. Natl. Acad. Sci. U.S.A.* **2019**, *116*, 11618−11623.
(452) Gao, X.; Chen, Y.; Sun, T.; Huang, J.; Zhang, W.; Wang, Q.; Cao, R. Karst Landform-Featured Monolithic Electrode for Water Electrolysis in Neutral Media. *Energy Environ. Sci.* **2020**, *13*, 174−182.
(453) Minguzzi, A.; Alpuche-Aviles, M. A.; Rodríguez López, J.; Rondinini, S.; Bard, A. J. Screening of Oxygen Evolution Electrocatalysts by Scanning Electrochemical Microscopy using a Shielded Tip Approach. *Anal. Chem.* **2008**, *80*, 4055−4064.
(454) Angulo, A.; van der Linde, P.; Gardeniers, H.; Modestino, M.; Fernández Rivas, D. Influence of Bubbles on the Energy Conversion Efficiency of Electrochemical Reactors. *Joule* **2020**, *4*, 555−579.
(455) Chen, X.; Maljusch, A.; Rincón, R. A.; Battistel, A.; Bandarenka, A. S.; Schuhmann, W. Local Visualization of Catalytic Activity at Gas Evolving Electrodes using Frequency-Dependent Scanning Electrochemical Microscopy. *Chem. Commun.* **2014**, *50*, 13250−13253.
(456) Konkena, B.; Masa, J.; Botz, A. J. R.; Sinev, I.; Xia, W.; Koßmann, J.; Drautz, R.; Muhler, M.; Schuhmann, W. Metallic $NiPS_3$@NiOOH Core−Shell Heterostructures as Highly Efficient and Stable Electrocatalyst for the Oxygen Evolution Reaction. *ACS Catal.* **2017**, *7*, 229−237.
(457) Chakrabarty, S.; Mukherjee, A.; Su, W.-N.; Basu, S. Improved Bi-Functional ORR and OER Catalytic Activity of Reduced Graphene Oxide Supported $ZnCo_2O_4$ Microsphere. *Int. J. Hydrog.* **2019**, *44*, 1565−1578.
(458) Lu, Z.; Yang, Q.; Pan, H.; Liu, Z.; Huang, X.; Chen, X.; Niu, L. Bifunctional Oxygen Electrocatalysis at Co-B,N,S-Graphene Composite Investigated by Scanning Electrochemical Microscopy at Variable Temperatures and its Application in Zn-Air Battery. *Electrochim. Acta* **2021**, *389*, 138751.
(459) Iffelsberger, C.; Raith, T.; Vatsyayan, P.; Vyskočil, V.; Matysik, F.-M. Detection and Imaging of Reactive Oxygen Species Associated with the Electrochemical Oxygen Evolution by Hydrodynamic Scanning Electrochemical Microscopy. *Electrochim. Acta* **2018**, *281*, 494−501.
(460) Counihan, M. J.; Setwipatanachai, W.; Rodríguez-López, J. Interrogating the Surface Intermediates and Water Oxidation Products of Boron-Doped Diamond Electrodes with Scanning Electrochemical Microscopy. *ChemElectroChem.* **2019**, *6*, 3507−3515.

https://doi.org/10.1021/acs.chemrev.2c00766
Chem. Rev. 2023, 123, 4972−5019

(461) Li, X.; Pan, S. Transparent Ultramicroelectrodes for Studying Interfacial Charge-Transfer Kinetics of Photoelectrochemical Water Oxidation at TiO_2 Nanorods with Scanning Electrochemical Microscopy. *Anal. Chem.* **2021**, *93*, 15886−15896.
(462) Steimecke, M.; Seiffarth, G.; Bron, M. In Situ Characterization of Ni and Ni/Fe Thin Film Electrodes for Oxygen Evolution in Alkaline Media by a Raman-Coupled Scanning Electrochemical Microscope Setup. *Anal. Chem.* **2017**, *89*, 10679−10686.
(463) Kluge, R. M.; Haid, R. W.; Bandarenka, A. S. Assessment of Active Areas for the Oxygen Evolution Reaction on an Amorphous Iridium Oxide Surface. *J. Catal.* **2021**, *396*, 14−22.
(464) Ahn, H. S.; Bard, A. J. Surface Interrogation Scanning Electrochemical Microscopy of $Ni_{(1-x)}Fe_{(x)}OOH$ ($0 < x < 0.27$) Oxygen Evolving Catalyst: Kinetics of the "fast" Iron Sites. *J. Am. Chem. Soc.* **2016**, *138*, 313−318.
(465) Arroyo-Currás, N.; Bard, A. J. Iridium Oxidation as Observed by Surface Interrogation Scanning Electrochemical Microscopy. *J. Phys. Chem. C* **2015**, *119*, 8147−8154.
(466) Jin, Z.; Bard, A. J. Surface Interrogation of Electrodeposited MnO_x and $CaMnO_3$ Perovskites by Scanning Electrochemical Microscopy: Probing Active Sites and Kinetics for the Oxygen Evolution Reaction. *Angew. Chem., Int. Ed.* **2021**, *60*, 794.
(467) Barforoush, J. M.; Jantz, D. T.; Seuferling, T. E.; Song, K. R.; Cummings, L. C.; Leonard, K. C. Microwave-assisted synthesis of a nanoamorphous (Ni 0.8,Fe 0.2) oxide oxygen-evolving electrocatalyst containing only "fast" sites. *J. Mater. Chem. A* **2017**, *5*, 11661−11670.
(468) Lee, J.; Ye, H.; Pan, S.; Bard, A. J. Screening of Photocatalysts by Scanning Electrochemical Microscopy. *Anal. Chem.* **2008**, *80*, 7445−7450.
(469) Ye, H.; Lee, J.; Jang, J. S.; Bard, A. J. Rapid Screening of $BiVO_4$ -Based Photocatalysts by Scanning Electrochemical Microscopy (SECM) and Studies of Their Photoelectrochemical Properties. *J. Phys. Chem. C* **2010**, *114*, 13322−13328.
(470) Ye, H.; Park, H. S.; Bard, A. J. Screening of Electrocatalysts for Photoelectrochemical Water Oxidation on W-Doped BiVO 4 Photocatalysts by Scanning Electrochemical Microscopy. *J. Phys. Chem. C* **2011**, *115*, 12464−12470.
(471) Sarkar, S.; Wang, X.; Hesari, M.; Chen, P.; Mirkin, M. V. Scanning Electrochemical and Photoelectrochemical Microscopy on Finder Grids: Toward Correlative Multitechnique Imaging of Surfaces. *Anal. Chem.* **2021**, *93*, 5377−5382.
(472) Askarova, G.; Hesari, M.; Wang, C.; Mirkin, M. V. Decoupling Through-Tip Illumination from Scanning in Nanoscale Photo-SECM. *Anal. Chem.* **2022**, *94*, 7169−7173.
(473) Iffelsberger, C.; Ng, S.; Pumera, M. Photoelectrolysis of TiO_2 is Highly Localized and the Selectivity is Affected by the Light. *Chem. Eng. J.* **2022**, *446*, 136995.
(474) Ju, M.; Cai, R.; Ren, J.; Chen, J.; Qi, L.; Long, X.; Yang, S. Conductive Polymer Intercalation Tunes Charge Transfer and Sorption-Desorption Properties of LDH Enabling Efficient Alkaline Water Oxidation. *ACS Appl. Mater. Interfaces* **2021**, *13*, 37063−37070.
(475) Stumm, C.; Bertram, M.; Kastenmeier, M.; Speck, F. D.; Sun, Z.; Rodríguez-Fernández, J.; Lauritsen, J. V.; Mayrhofer, K. J. J.; Cherevko, S.; Brummel, O.; et al. Structural Dynamics of Ultrathin Cobalt Oxide Nanoislands under Potential Control. *Adv. Funct. Mater.* **2021**, *31*, 2009923.
(476) Tilak, B. V.; Ramamurthy, A. C.; Conway, B. E. High Performance Electrode Materials for the Hydrogen Evolution Reaction from Alkaline Media. *Proc. Indian Acad. Sci. (Chem. Sci.)* **1986**, *97*, 359−393.
(477) Dubouis, N.; Grimaud, A. The Hydrogen Evolution Reaction: From Material to Interfacial Descriptors. *Chem. Sci.* **2019**, *10*, 9165−9181.
(478) Zhu, J.; Hu, L.; Zhao, P.; Lee, L. Y. S.; Wong, K.-Y. Recent Advances in Electrocatalytic Hydrogen Evolution Using Nanoparticles. *Chem. Rev.* **2020**, *120*, 851−918.
(479) Ferriday, T. B.; Middleton, P. H.; Kolhe, M. L. Review of the Hydrogen Evolution Reaction—A Basic Approach. *Energies* **2021**, *14*, 8535.
(480) Anantharaj, S.; Aravindan, V. Developments and Perspectives in 3d Transition-Metal-Based Electrocatalysts for Neutral and Near-Neutral Water Electrolysis. *Adv. Energy Mater.* **2020**, *10*, 1902666.
(481) Selzer, Y.; Turyan, I.; Mandler, D. Studying Heterogeneous Catalysis by the Scanning Electrochemical Microscope (SECM): The Reduction of Protons by Methyl Viologen Catalyzed by a Platinum Surface. *J. Phys. Chem. B* **1999**, *103*, 1509−1517.
(482) Zhang, J.; Lahtinen, R. M.; Kontturi, K.; Unwin, P. R.; Schiffrin, D. J. Electron Transfer Reactions at Gold Nanoparticles. *Chem. Commun.* **2001**, 1818−1819.
(483) Li, F.; Bertoncello, P.; Ciani, I.; Mantovani, G.; Unwin, P. R. Incorporation of Functionalized Palladium Nanoparticles within Ultrathin Nafion Films: A Nanostructured Composite for Electrolytic and Redox-Mediated Hydrogen Evolution. *Adv. Funct. Mater.* **2008**, *18*, 1685−1693.
(484) Li, F.; Ciani, I.; Bertoncello, P.; Unwin, P. R.; Zhao, J.; Bradbury, C. R.; Fermin, D. J. Scanning Electrochemical Microscopy of Redox-Mediated Hydrogen Evolution Catalyzed by Two-Dimensional Assemblies of Palladium Nanoparticles. *J. Phys. Chem. C* **2008**, *112*, 9686−9694.
(485) Li, H.; Du, M.; Mleczko, M. J.; Koh, A. L.; Nishi, Y.; Pop, E.; Bard, A. J.; Zheng, X. Kinetic Study of Hydrogen Evolution Reaction over Strained MoS_2 with Sulfur Vacancies Using Scanning Electrochemical Microscopy. *J. Am. Chem. Soc.* **2016**, *138*, 5123−5129.
(486) Zhou, J.; Zu, Y.; Bard, A. J Scanning Electrochemical Microscopy Part 39. The Proton/Hydrogen Mediator System and its Application to the Study of the Electrocatalysis of Hydrogen Oxidation. *J. Electroanal. Chem.* **2000**, *491*, 22−29.
(487) Zoski, C. G. Scanning Electrochemical Microscopy: Investigation of Hydrogen Oxidation at Polycrystalline Noble Metal Electrodes. *J. Phys. Chem. B* **2003**, *107*, 6401−6405.
(488) Bonazza, H. L.; Vega, L. D.; Fernández, J. L. Analysis of the Hydrogen Electrode Reaction Mechanism in Thin-Layer Cells. 2. Study of Hydrogen Evolution on Microelectrodes by Scanning Electrochemical Microscopy. *J. Electroanal. Chem.* **2014**, *713*, 9−16.
(489) Iffelsberger, C.; Wert, S.; Matysik, F.-M.; Pumera, M. Catalyst Formation and In Operando Monitoring of the Electrocatalytic Activity in Flow Reactors. *ACS Appl. Mater. Interfaces* **2021**, *13*, 35777−35784.
(490) Sun, T.; Yu, Y.; Zacher, B. J.; Mirkin, M. V. Scanning Electrochemical Microscopy of Individual Catalytic Nanoparticles. *Angew. Chem., Int. Ed.* **2014**, *53*, 14120−14123.
(491) Niu, H.-J.; Yan, Y.; Jiang, S.; Liu, T.; Sun, T.; Zhou, W.; Guo, L.; Li, J. Interfaces Decrease the Alkaline Hydrogen-Evolution Kinetics Energy Barrier on $NiCoP/Ti_3C_2T_x$ MXene. *ACS Nano* **2022**, *16*, 11049.
(492) Liberman, I.; Ifraemov, R.; Shimoni, R.; Hod, I. Localized Electrosynthesis and Subsequent Electrochemical Mapping of Catalytically Active Metal−Organic Frameworks. *Adv. Funct Materials* **2022**, *32*, 2112517.
(493) Kund, J.; Romer, J.; Oswald, E.; Gaus, A.-L.; Küllmer, M.; Turchanin, A.; Delius, M.; Kranz, C. Pd-Modified De-alloyed Au−Ni-Microelectrodes for In Situ and Operando Mapping of Hydrogen Evolution. *ChemElectroChem.* **2022**, *9*, No. e202200071.
(494) Visibile, A.; Baran, T.; Rondinini, S.; Minguzzi, A.; Vertova, A. Determining the Efficiency of Photoelectrode Materials by Coupling Cavity-Microelectrode Tips and Scanning Electrochemical Microscopy. *ChemElectroChem.* **2020**, *7*, 2440−2447.
(495) Jamali, S. S.; Moulton, S. E.; Tallman, D. E.; Weber, J.; Wallace, G. G. Electro-Oxidation and Reduction of H_2 on Platinum Studied by Scanning Electrochemical Microscopy for the Purpose of Local Detection of H_2 Evolution. *Surf. Interface Anal.* **2015**, *47*, 1187−1191.
(496) Iffelsberger, C.; Rojas, D.; Pumera, M. Photo-Responsive Doped 3D-Printed Copper Electrodes for Water Splitting: Refractory One-Pot Doping Dramatically Enhances the Performance. *J. Phys. Chem. C* **2022**, *126*, 9016−9026.

https://doi.org/10.1021/acs.chemrev.2c00766
Chem. Rev. 2023, 123, 4972−5019

(497) Hill, J. W.; Hill, C. M. Directly Mapping Photoelectrochemical Behavior within Individual Transition Metal Dichalcogenide Nanosheets. *Nano Lett.* **2019**, *19*, 5710−5716.
(498) Kosmala, T.; Baby, A.; Lunardon, M.; Perilli, D.; Liu, H.; Durante, C.; Di Valentin, C.; Agnoli, S.; Granozzi, G. Operando Visualization of the Hydrogen Evolution Reaction with Atomic-Scale Precision at Different Metal−Graphene Interfaces. *Nat. Catal.* **2021**, *4*, 850−859.
(499) Kluge, R. M.; Haid, R. W.; Stephens, I. E. L.; Calle-Vallejo, F.; Bandarenka, A. S. Monitoring the Active sites for the Hydrogen Evolution Reaction at Model Carbon Surfaces. *Phys. Chem. Chem. Phys.* **2021**, *23*, 10051−10058.
(500) Nitopi, S.; Bertheussen, E.; Scott, S. B.; Liu, X.; Engstfeld, A. K.; Horch, S.; Seger, B.; Stephens, I. E. L.; Chan, K.; Hahn, C.; et al. Progress and Perspectives of Electrochemical CO_2 Reduction on Copper in Aqueous Electrolyte. *Chem. Rev.* **2019**, *119*, 7610−7672.
(501) Pacala, S.; Socolow, R. Stabilization Wedges: Solving the Climate Problem for the Next 50 Years with Current Technologies. *Science* **2004**, *305*, 968−972.
(502) De Luna, P.; Hahn, C.; Higgins, D.; Jaffer, S. A.; Jaramillo, T. F.; Sargent, E. H. What Would it take for Renewably Powered Electrosynthesis to Displace Petrochemical Processes? *Science* **2019**, *364*, 364.
(503) Zhu, D. D.; Liu, J. L.; Qiao, S. Z. Recent Advances in Inorganic Heterogeneous Electrocatalysts for Reduction of Carbon Dioxide. *Adv. Mater.* **2016**, *28*, 3423−3452.
(504) Rasul, S.; Anjum, D. H.; Jedidi, A.; Minenkov, Y.; Cavallo, L.; Takanabe, K. A Highly Selective Copper−Indium Bimetallic Electrocatalyst for the Electrochemical Reduction of Aqueous CO_2 to CO. *Angew. Chem., Int. Ed.* **2015**, *127*, 2174−2178.
(505) Pei, Y.; Zhong, H.; Jin, F. A Brief Review of Electrocatalytic Reduction of CO_2—Materials, Reaction Conditions, and Devices. *Energy Sci. Eng.* **2021**, *9*, 1012−1032.
(506) Zheng, Y.; Vasileff, A.; Zhou, X.; Jiao, Y.; Jaroniec, M.; Qiao, S.-Z. Understanding the Roadmap for Electrochemical Reduction of CO_2 to Multi-Carbon Oxygenates and Hydrocarbons on Copper-Based Catalysts. *J. Am. Chem. Soc.* **2019**, *141*, 7646−7659.
(507) Kuhl, K. P.; Cave, E. R.; Abram, D. N.; Jaramillo, T. F. New Insights into the Electrochemical Reduction of Carbon Dioxide on Metallic Copper Surfaces. *Energy Environ. Sci.* **2012**, *5*, 7050.
(508) Hori, Y.; Kikuchi, K.; Suzuki, S. Production of CO and CH_4 In Electrochemical Reduction of CO_2 at Metal Electrodes in Aqueous Hydrogencarbonate Solution. *Chem. Lett.* **1985**, *14*, 1695−1698.
(509) Kuhl, K. P.; Hatsukade, T.; Cave, E. R.; Abram, D. N.; Kibsgaard, J.; Jaramillo, T. F. Electrocatalytic Conversion of Carbon Dioxide to Methane and Methanol on Transition Metal Surfaces. *J. Am. Chem. Soc.* **2014**, *136*, 14107−14113.
(510) Yang, H.-P.; Yue, Y.-N.; Qin, S.; Wang, H.; Lu, J.-X. Selective Electrochemical Reduction of CO_2 to Different Alcohol Products by an Organically Doped Alloy Catalyst. *Green Chem.* **2016**, *18*, 3216−3220.
(511) Appel, A. M.; Bercaw, J. E.; Bocarsly, A. B.; Dobbek, H.; DuBois, D. L.; Dupuis, M.; Ferry, J. G.; Fujita, E.; Hille, R.; Kenis, P. J. A.; et al. Frontiers, Opportunities, and Challenges in Biochemical and Chemical Catalysis of CO_2 Fixation. *Chem. Rev.* **2013**, *113*, 6621−6658.
(512) Hall, A. S.; Yoon, Y.; Wuttig, A.; Surendranath, Y. Mesostructure-Induced Selectivity in CO_2 Reduction Catalysis. *J. Am. Chem. Soc.* **2015**, *137*, 14834−14837.
(513) Rosen, B. A.; Salehi-Khojin, A.; Thorson, M. R.; Zhu, W.; Whipple, D. T.; Kenis, P. J. A.; Masel, R. I. Ionic Liquid-Mediated Selective Conversion of CO_2 to CO at Low Overpotentials. *Science* **2011**, *334*, 643−644.
(514) Liu, X.; Xiao, J.; Peng, H.; Hong, X.; Chan, K.; Nørskov, J. K. Understanding Trends in Electrochemical Carbon Dioxide Reduction Rates. *Nat. Commun.* **2017**, *8*, 15438.
(515) Todorova, T. K.; Schreiber, M. W.; Fontecave, M. Mechanistic Understanding of CO_2 Reduction Reaction (CO2RR) Toward Multicarbon Products by Heterogeneous Copper-Based Catalysts. *ACS Catal.* **2020**, *10*, 1754−1768.
(516) Sreekanth, N.; Phani, K. L. Selective Reduction of CO2 to Formate through Bicarbonate Reduction on Metal Electrodes: New Insights Gained from SG/TC Mode of SECM. *Chem. Commun.* **2014**, *50*, 11143−11146.
(517) Sreekanth, N.; Nazrulla, M. A.; Vineesh, T. V.; Sailaja, K.; Phani, K. L. Metal-free Boron-Doped Graphene for Selective Electroreduction of Carbon Dioxide to Formic acid/Formate. *Chem. Commun.* **2015**, *51*, 16061−16064.
(518) Narayanaru, S.; Chinnaiah, J.; Phani, K. L.; Scholz, F. pH dependent CO Adsorption and Roughness-Induced Selectivity of CO_2 Electroreduction on Gold Surfaces. *Electrochim. Acta* **2018**, *264*, 269−274.
(519) Monteiro, M. C. O.; Dattila, F.; Hagedoorn, B.; García-Muelas, R.; López, N.; Koper, M. T. M. Absence of CO_2 Electroreduction on Copper, Gold and Silver Electrodes without Metal Cations in Solution. *Nat. Catal.* **2021**, *4*, 654−662.
(520) Li, J.; Zhang, Z.; Hu, W. Insight into the Effect of Metal Cations in the Electrolyte on Performance for Electrocatalytic CO_2 Reduction Reaction. *Energy Environ. Mater.* **2022**, *5*, 1008−1009.
(521) Shaughnessy, C. I.; Jantz, D. T.; Leonard, K. C. Selective Electrochemical CO_2 Reduction to CO using in situ Reduced In_2O_3 nanocatalysts. *J. Mater. Chem. A* **2017**, *5*, 22743−22749.
(522) Mayer, F. D.; Hosseini-Benhangi, P.; Sánchez-Sánchez, C. M.; Asselin, E.; Gyenge, E. L. Scanning Electrochemical Microscopy Screening of CO_2 Electroreduction Activities and Product Selectivities of Catalyst Arrays. *Commun. Chem.* **2020**, *3*, 155.
(523) Kim, Y.; Jo, A.; Ha, Y.; Lee, Y.; Lee, D.; Lee, Y.; Lee, C. Highly Dispersive Gold Nanoparticles on Carbon Black for Oxygen and Carbon Dioxide Reduction. *Electroanalysis* **2018**, *30*, 2861−2868.
(524) Monteiro, M. C. O.; Jacobse, L.; Koper, M. T. M. Understanding the Voltammetry of Bulk CO Electrooxidation in Neutral Media through Combined SECM Measurements. *J. Phys. Chem. Lett.* **2020**, *11*, 9708−9713.
(525) Higgins, D.; Hahn, C.; Xiang, C.; Jaramillo, T. F.; Weber, A. Z. Gas-Diffusion Electrodes for Carbon Dioxide Reduction: A New Paradigm. *ACS Energy Lett.* **2019**, *4*, 317−324.
(526) Dieckhöfer, S.; Öhl, D.; Junqueira, J. R. C.; Quast, T.; Turek, T.; Schuhmann, W. Probing the Local Reaction Environment During High Turnover Carbon Dioxide Reduction with Ag-Based Gas Diffusion Electrodes. *Chemistry* **2021**, *27*, 5906−5912.
(527) Monteiro, M. C. O.; Dieckhöfer, S.; Bobrowski, T.; Quast, T.; Pavesi, D.; Koper, M. T. M.; Schuhmann, W. Probing the Local Activity of CO_2 Reduction on Gold Gas Diffusion Electrodes: Effect of the Catalyst Loading and CO_2 Pressure. *Chem. Sci.* **2021**, *12*, 15682−15690.
(528) Junqueira, J. R. C.; O'Mara, P. B.; Wilde, P.; Dieckhöfer, S.; Benedetti, T. M.; Andronescu, C.; Tilley, R. D.; Gooding, J. J.; Schuhmann, W. Combining Nanoconfinement in Ag Core/Porous Cu Shell Nanoparticles with Gas Diffusion Electrodes for Improved Electrocatalytic Carbon Dioxide Reduction. *ChemElectroChem.* **2021**, *8*, 4848−4853.
(529) Sikdar, N.; Junqueira, J. R. C.; Dieckhofer, S.; Quast, T.; Braun, M.; Song, Y.; Aiyappa, H. B.; Seisel, S.; Weidner, J.; Ohl, D.; et al. A Metal−Organic Framework derived CuxOyCz Catalyst for Electrochemical CO_2 Reduction and Impact of Local pH Change. *Angew. Chem., Int. Ed.* **2021**, *60*, 23427−23434.
(530) Kim, Y.-G.; Baricuatro, J. H.; Javier, A.; Gregoire, J. M.; Soriaga, M. P. The Evolution of the Polycrystalline Copper Surface, first to Cu(111) and then to Cu(100), at a fixed CO_2RR Potential: A Study by Operando EC-STM. *Langmuir* **2014**, *30*, 15053−15056.
(531) Schouten, K. J. P.; Qin, Z.; Pérez Gallent, E.; Koper, M. T. M. Two Pathways for the Formation of Ethylene in CO Reduction on Single-Crystal Copper Electrodes. *J. Am. Chem. Soc.* **2012**, *134*, 9864−9867.
(532) Phan, T. H.; Banjac, K.; Cometto, F. P.; Dattila, F.; García-Muelas, R.; Raaijman, S. J.; Ye, C.; Koper, M. T. M.; López, N.; Lingenfelder, M. Emergence of Potential-Controlled Cu-Nanocuboids

https://doi.org/10.1021/acs.chemrev.2c00766
Chem. Rev. 2023, 123, 4972−5019

and Graphene-Covered Cu-Nanocuboids under Operando CO_2 Electroreduction. *Nano Lett.* **2021**, *21*, 2059−2065.
(533) Lim, T.; Jung, G. Y.; Kim, J. H.; Park, S. O.; Park, J.; Kim, Y.-T.; Kang, S. J.; Jeong, H. Y.; Kwak, S. K.; Joo, S. H. Atomically Dispersed Pt-N_4 sites as Efficient and Selective Electrocatalysts for the Chlorine Evolution Reaction. *Nat. Commun.* **2020**, *11*, 412.
(534) Wang, Y.; Liu, Y.; Wiley, D.; Zhao, S.; Tang, Z. Recent Advances in Electrocatalytic Chloride Oxidation for Chlorine Gas Production. *J. Mater. Chem. A* **2021**, *9*, 18974−18993.
(535) Zeradjanin, A. R.; Schilling, T.; Seisel, S.; Bron, M.; Schuhmann, W. Visualization of Chlorine Evolution at Dimensionally Stable Anodes by Means of Scanning Electrochemical Microscopy. *Anal. Chem.* **2011**, *83*, 7645−7650.
(536) Zeradjanin, A. R.; Menzel, N.; Schuhmann, W.; Strasser, P. On the Faradaic Selectivity and the Role of Surface Inhomogeneity during the Chlorine Evolution Reaction on Ternary Ti-Ru-Ir Mixed Metal Oxide Electrocatalysts. *Phys. Chem. Chem. Phys.* **2014**, *16*, 13741−13747.
(537) Noël, J.-M.; Kanoufi, F. Probing the Reactive Intermediate Species Generated during Electrocatalysis by Scanning Electrochemical Microscopy. *Curr. Opin. Electrochem.* **2022**, *35*, 101071.
(538) Chang, J.; Bard, A. J. Detection of the Sn(III) Intermediate and the Mechanism of the Sn(IV)/Sn(II) Electroreduction Reaction in Bromide Media by Cyclic Voltammetry and Scanning Electrochemical Microscopy. *J. Am. Chem. Soc.* **2014**, *136*, 311−320.
(539) Kai, T.; Zhou, M.; Duan, Z.; Henkelman, G. A.; Bard, A. J. Detection of $CO_2^{\bullet-}$ in the Electrochemical Reduction of Carbon Dioxide in N,N-Dimethylformamide by Scanning Electrochemical Microscopy. *J. Am. Chem. Soc.* **2017**, *139*, 18552−18557.
(540) Wijayawardhana, C. A.; Wittstock, G.; Halsall, H. B.; Heineman, W. R. Spatially Addressed Deposition and Imaging of Biochemically Active Bead Microstructures by Scanning Electrochemical Microscopy. *Anal. Chem.* **2000**, *72*, 333−338.
(541) Maciejewska, M.; Schäfer, D.; Schuhmann, W. SECM Visualization of Spatial Variability of Enzyme-Polymer Spots. Part 2: Complex Interference Elimination by Means of Selection of Highest Sensitivity Sensor Substructures and Artificial Neural Networks. *Electroanalysis* **2006**, *18*, 1916−1928.
(542) Mauzeroll, J.; Buda, M.; Bard, A. J.; Prieto, F.; Rueda, M. Detection of Tl(I) Transport through a Gramicidin−Dioleoylphosphatidylcholine Monolayer Using the Substrate Generation−Tip Collection Mode of Scanning Electrochemical Microscopy. *Langmuir* **2002**, *18*, 9453−9461.
(543) Fernández, J. L.; Mano, N.; Heller, A.; Bard, A. J. Optimization Of "Wired" Enzyme O_2-Electroreduction Catalyst Compositions by Scanning Electrochemical Microscopy. *Angew. Chem., Int. Ed.* **2004**, *43*, 6355−6357.
(544) Dantas, L. M. F.; De Souza, A. P. R.; Castro, P. S.; Paixão, T. R. L. C.; Bertotti, M. SECM Studies on the Electrocatalytic Oxidation of Glycerol at Copper Electrodes in Alkaline Medium. *Electroanalysis* **2012**, *24*, 1778−1782.
(545) Perales-Rondón, J. V.; Herrero, E.; Solla-Gullón, J.; Sánchez-Sánchez, C. M.; Vivier, V. Oxygen Crossover Effect on Palladium and Platinum Based Electrocatalysts During Formic Acid Oxidation Studied by Scanning Electrochemical Microscopy. *J. Electroanal. Chem.* **2017**, *793*, 218−225.
(546) Komkova, M. A.; Holzinger, A.; Hartmann, A.; Khokhlov, A. R.; Kranz, C.; Karyakin, A. A.; Voronin, O. G. Ultramicrosensors Based on Transition Metal Hexacyanoferrates for Scanning Electrochemical Microscopy. *Beilstein J. Nanotechnol.* **2013**, *4*, 649−654.
(547) Ye, M.; Li, Y.; Wu, J.; Su, T.; Zhang, J.; Tang, J. SECM Screening of the Catalytic Activities of AuPd Bimetallic Patterns Fabricated by Electrochemical Wet-Stamping Technique. *J. Electroanal. Chem.* **2016**, *772*, 96−102.
(548) Tomlinson, L. I.; Patten, H. V.; Green, B. L.; Iacobini, J.; Meadows, K. E.; McKelvey, K.; Unwin, P. R.; Newton, M. E.; Macpherson, J. V. Intermittent-Contact Scanning Electrochemical Microscopy (IC-SECM) as a Quantitative Probe of Defects in Single Crystal Boron Doped Diamond Electrodes. *Electroanalysis* **2016**, *28*, 2297−2302.
(549) Kim, J.; Renault, C.; Nioradze, N.; Arroyo-Currás, N.; Leonard, K. C.; Bard, A. J. Electrocatalytic Activity of Individual Pt Nanoparticles Studied by Nanoscale Scanning Electrochemical Microscopy. *J. Am. Chem. Soc.* **2016**, *138*, 8560−8568.
(550) Miranda Vieira, M.; Lemineur, J.-F.; Médard, J.; Combellas, C.; Kanoufi, F.; Noël, J.-M. Operando Analysis of the Electrosynthesis of Ag_2O Nanocubes by Scanning Electrochemical Microscopy. *Electrochem. Commun.* **2021**, *124*, 106950.
(551) He, W.; Zhang, J.; Dieckhöfer, S.; Varhade, S.; Brix, A. C.; Lielpetere, A.; Seisel, S.; Junqueira, J. R. C.; Schuhmann, W. Splicing the Active Phases of Copper/Cobalt-Based Catalysts Achieves High-Rate Tandem Electroreduction of Nitrate to Ammonia. *Nat. Commun.* **2022**, *13*, 1129.
(552) Haram, S. K.; Bard, A. J. Scanning Electrochemical Microscopy. 42. Studies of the Kinetics and Photoelectrochemistry of Thin Film CdS/Electrolyte Interfaces. *J. Phys. Chem. B* **2001**, *105*, 8192−8195.
(553) Zhang, B.; Zhang, X.; Xiao, X.; Shen, Y. Photoelectrochemical Water Splitting System-A Study of Interfacial Charge Transfer with Scanning Electrochemical Microscopy. *ACS Appl. Mater. Interfaces* **2016**, *8*, 1606−1614.
(554) Yu, Z.; Huang, Q.; Jiang, X.; Lv, X.; Xiao, X.; Wang, M.; Shen, Y.; Wittstock, G. Effect of a Cocatalyst on a Photoanode in Water Splitting: A Study of Scanning Electrochemical Microscopy. *Anal. Chem.* **2021**, *93*, 12221−12229.

https://doi.org/10.1021/acs.chemrev.2c00766
Chem. Rev. 2023, 123, 4972−5019